# Bilayer Formation with Fluorinated Amphiphiles and Applications in Membrane Protein Studies

A dissertation by

**Pinky Raychaudhuri**


Submitted to the University of Oxford for the degree of

DOCTOR OF PHILOSOPHY

Major-Subject: Chemical Biology

Exeter College

June 2012

# Declaration

The work described in this thesis was carried out between October 2008 and March 2012, in the laboratory of Prof. Hagan Bayley at the Chemistry Research Laboratory of the University of Oxford. All the work described within this thesis is entirely my own unless otherwise stated in the text. This work has not been submitted previously for any other degree at the University of Oxford or any other university.

**Pinky Raychaudhuri**

June 2012

# Acknowledgements

This thesis is the culmination of a journey that I started in October 2008. I would like to thank all the people who stood by me and supported me in this endeavour. First and foremost, I offer my sincerest gratitude to Prof. Hagan Bayley for giving me the opportunity to work on such an interesting and challenging project. His guidance, support, and encouragement helped me to successfully overcome many hurdles and I have learned a lot from the time spent in this lab.

My first association with this lab started in the summer of 2007, when I came to work as a summer student for two months. The lovely time that I had spent in the lab combined with my love for the city of Oxford motivated me to return for a D.Phil. This dream was made possible by the Felix Scholarship and I will be eternally grateful to them for providing me with full funding for the duration of my study.

I would like to thank all members of the Bayley group, both past and present, who have contributed to making my time in the lab both fun and enjoyable. A big thanks to Lajos Hofler, Tanuj Sapra, Tivadar Mach, Andrew Heron, and Gabriel Villar for useful discussions. I would like to also thank Leon Harrington, Holger Gerlach, and Ellina Mikhailova for their help with molecular biology techniques. Last but not the least; I would also like to say thanks to Arpit, Mariam, Shiksha, Shovon, Sonali, and Sulzhan for making my time at Oxford enjoyable and memorable.

I would also like to thank my examiners, Prof. Martin Caffrey and Prof. Anthony Watts, for taking time out to read this thesis.

Finally, I would like to thank those closest to me: my mother, my father, Shane, Didi, Thama, Mom, and Dad. They have always stood by me and dealt with my long

absence from home with a smile. I feel blessed to have their love and endless support and I dedicate this thesis to them.

# THESIS ABSTRACT

**Bilayer Formation with Fluorinated Amphiphiles and Applications in Membrane Protein Studies.**

Pinky Raychaudhuri

Exeter College

Doctor of Philosophy

June 2012

## ABSTRACT

Every cell is enclosed by a membrane which gives structure to the cell and allows for the passage of nutrients and wastes into and out of the cell. Membranes are made up of amphiphilic lipid molecules, with one water-soluble end, and one hydrophobic end. Naturally occurring and synthetic membranes are made up of double-chained amphiphiles derived from hydrocarbons. Recently, a novel class of amphiphilic molecules derived from fluorocarbons have been reported. The properties of fluorinated amphiphiles are very different to that of hydrocarbon based amphiphiles. Fluorinated amphiphiles have been previously reported to be useful in the studies of membrane proteins. In this thesis, we explore some novel uses of fluorinated amphiphiles.

**Chapter one:** Provides a comprehensive review of the properties of fluorocarbon-based amphiphiles and discusses the existing uses of fluorinated amphiphiles in biochemical and biomedical research.

**Chapter two:** Describes some of the important materials and methods used in this thesis including a detailed description of the proteins used and the working principles behind the techniques used in the study.

**Chapter three:** Looks at the stability of pre-formed planar lipid bilayers in the presence of fluorinated amphiphiles (F-amphiphiles), and characterizes the behaviour of alpha-haemolysin and other proteins in liposomes and planar lipid bilayers in the presence of F-amphiphiles. We found that F-amphiphiles have an inhibitory effect on the insertion of protein into lipid bilayers, and this property has been exploited to control the number of proteins in the bilayer.

**Chapter four:** Using droplet interface bilayers, we investigate the electrical properties and behaviour of protein(s) in bilayers formed by F-amphiphiles. The results obtained with fluorinated bilayers are compared with results obtained in conventional DPhPC lipid bilayers. This is the first ever report to carry out such an investigation and it provides insights into the formation, stability and utility of fluorinated bilayers.

**Chapter five:** In Chapter five, we explore another aspect of droplet interface bilayers: the feasibility of using droplet interface bilayers to screen for membrane protein libraries. I have chosen to focus on certain fundamental aspects of the screening process that are sufficient to establish the feasibility of the method and to act as the proof of concept.

**Chapter six:** Summarizes all the important results in the thesis and discusses some possible future directions of this project.

# Abbreviations

| | |
|---|---|
| αHL | alpha-hemolysin |
| βCD | beta-cyclodextrin |
| BSA | bovine serum albumin |
| $C_6$FTAC | $C_6F_{13}C_2H_4$-S-poly[tris(hydroxymethyl)aminomethane] |
| CMC | critical micelle concentration |
| CTAB | cetyltrimethylammonium bromide |
| DIB | droplet interface bilayer |
| DPhPC | 1,2-diphytanoyl-sn-glycero-3-phosphocholine |
| DLPC | 1,2-dilauryl-sn-glycero-3-phosphocholine |
| EDTA | ethylenediaminetetraacetic acid |
| F-amphiphiles | fluorinated amphiphiles |
| FC | fluorocarbon |
| $F_6$FC | fos-Choline-8, Fluorinated |
| $F_6$OM | octyl Maltoside, Fluorinated |
| HC | hydrocarbon |
| IPTG | isopropyl β-D-thiogalactoside |
| I-V | current-voltage relationship |
| IVTT | coupled in vitro transcription and translation |
| LUV | large unilamellar vesicles |
| n | number of experiments |
| PAGE | polyacrylamide gel electrophoresis |

| | |
|---|---|
| PBS | phosphate buffered saline |
| PCR | polymerase chain reaction |
| rRBCm | rabbit red blood cell membrane |
| S.aureus | Staphylococcus aureus |
| s.d | standard deviation |
| SDS | sodium dodecyl sulphate |
| Tris | 2-amino-2-(hydroxymethyl)-1,3-propanediol |
| TBM | truncated barrel mutant |

# Table of contents

# Chapter 1

# General Introduction

Membranes are universal components of cells and are critical to the function of cells in all organisms. Its primary function is to protect the integrity of the interior of the cell. Another important function of membranes is to enable and regulate the transport of material between the inside and outside of a cell, with the help of special proteins embedded in the membrane. Both, the structure and function of lipid membranes, can be attributed to the special properties of the molecules which make up the membrane. Membranes are made up of amphipathic molecules called lipids. The most commonly found and studied amphiphilic molecules are derived from hydrocarbons (HC).

The work in this thesis transcends hydrocarbon based conventional amphiphiles (that make up the cellular lipid membrane), and studies bilayer formation with a new class of fluorinated amphiphilic molecules and characterizes the behaviour of proteins in these novel membranes.

## 1.1 Conventional amphiphiles

The word amphiphile comes from two Greek words. The prefix *amphi* means "double", and the root *philos* expresses friendship or affinity. Amphiphile is a general term that describes any molecule that has both hydrophilic (water loving) and hydrophobic (water

hating) parts in the same molecule (Figure 1.1). Examples of amphiphiles are phospholipids, fatty acids, alcohols, surfactants, block copolymers etc.

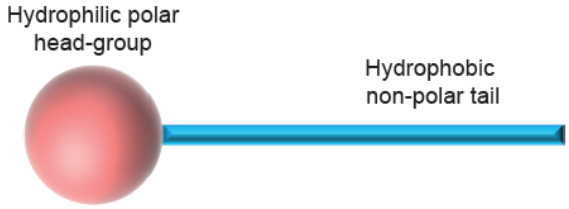


**Figure 1.1: Schematic of an amphiphilic molecule:** *Most amphiphiles have a hydrocarbon as the hydrophobic tail. Amphiphilic molecules such as phospholipids contain two hydrophobic tails and commonly found head-groups are phosphatidylcholine, glycerol, ethanolamine. Amphiphilic molecules such as surfactants usually contain a single hydrophobic tail, but can also contain two-three hydrophobic tails which may be linear or branched.*

Surfactants and lipids are the most common types of amphiphiles. They are classified according to the type of hydrophilic head group as ionic (cationic and anionic), zwitterionic and non-ionic. The hydrophobic chain may be a hydrocarbon (conventional surfactants), a fluorocarbon (FC), or a mixed hydrocarbon (HC) / fluorocarbon (FC) group (hybrid surfactants). Silicone surfactants have siloxane as the hydrophobic tail. Surfactants can have more than one hydrophobic tail which may be linear or branched. In the following part of this chapter, we concentrate on the properties of conventional hydrogenated amphiphiles and how they compare to the class of fluorinated amphiphiles, which is the main focus of this thesis.

Because of its dual affinity, an amphiphilic molecule exhibits a strong tendency to migrate to surfaces (air/water) and interfaces (oil/water), and orientate themselves favourably. The accumulation of amphiphilic molecules at the interface weakens the

hydrogen bonds holding the water molecules together at the surface, thereby reducing the surface tension of water. For example, one of the most widely utilized surfactant in biochemical studies, sodium dodecyl sulphate (4 mM) reduces the surface tension of water from 72 dynes $cm^{-1}$ to about 53 dynes $cm^{-1}$ at 25°C [1].

The dual chemical nature of amphiphiles gives rise to another interesting property of spontaneous self-assembly in water to form a variety of structures such as micelles, vesicles, bilayers etc [2]. The simplest form of self-assembly for single chain amphiphiles are micelles [3]. These aggregate structures are dynamic (continuously broken down and reformed) and exist in equilibrium with the free surfactant or lipid monomer in solution [4].

The concept of packing parameter proposed by J. Israelachvili allows a simple and intuitive insight into the self-assembled aggregates of amphiphiles in water (Figure 1.3) [2]. The packing parameter P is defined as:

$$P = v / l.a_o$$

where $v$ and $l$ are the volume and length of the surfactant hydrophobic tail respectively and $a_o$ is the optimal surface area per amphiphile (Figure 1.2). The concept of optimal surface area per amphiphile ($a_o$) is based on the principle of opposing forces: the hydrophobic interactions which act to pack the molecules closer together to avoid exposing hydrophobic tails at the surface, and the repulsive energy between head-groups which increases as molecules are pushed closer together. The surface energy of the aggregate is minimized when the amphiphilic molecules occupy the optimal area (Figure 1.2).

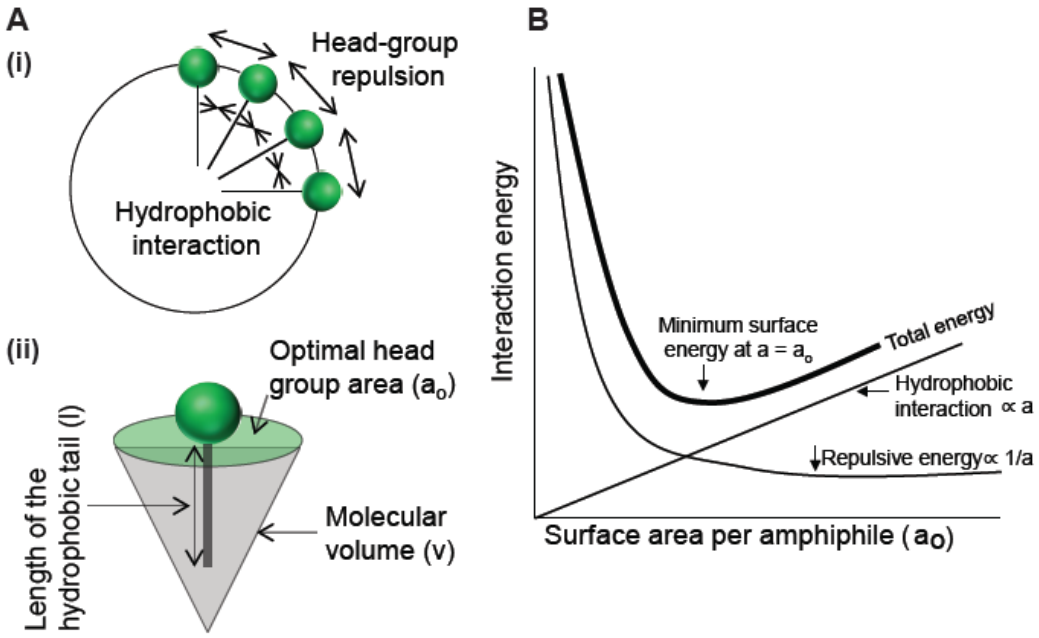


**Figure 1.2: Concept of optimal area per amphiphile:** *(A) (i) The repulsive force between head-groups tends to push the amphiphiles apart. However, if the amphiphiles are too far apart, it results in water penetration in the hydrophobic core which is not favourable. Thus the hydrophobic effect (attractive force) tends to push the amphiphiles together. (ii) The balance between these two opposing forces results in an optimum head-group spacing of the amphiphiles. (B) At the optimum area per amphiphile, the total free energy of the aggregate structure is at the minimum.*

Single-tailed amphiphiles with a large head-group area have packing parameter P < 1/3 and will form spherical micelles. Ionic surfactants such as sodium dodecyl sulphate (SDS / NaDS) generally forms spherical micelles in solution at low salt concentrations [5, 6]. Single-tailed amphiphiles with a small head-group area (1/3 < P < 1/2) will form elongated or cylindrical micelles. Non-ionic surfactants and ionic surfactants such as SDS and CTAB in high salt are known to form elongated micelles [5, 6]. Double-tailed amphiphiles with a large head-group area (phosphatidylcholine lipids,

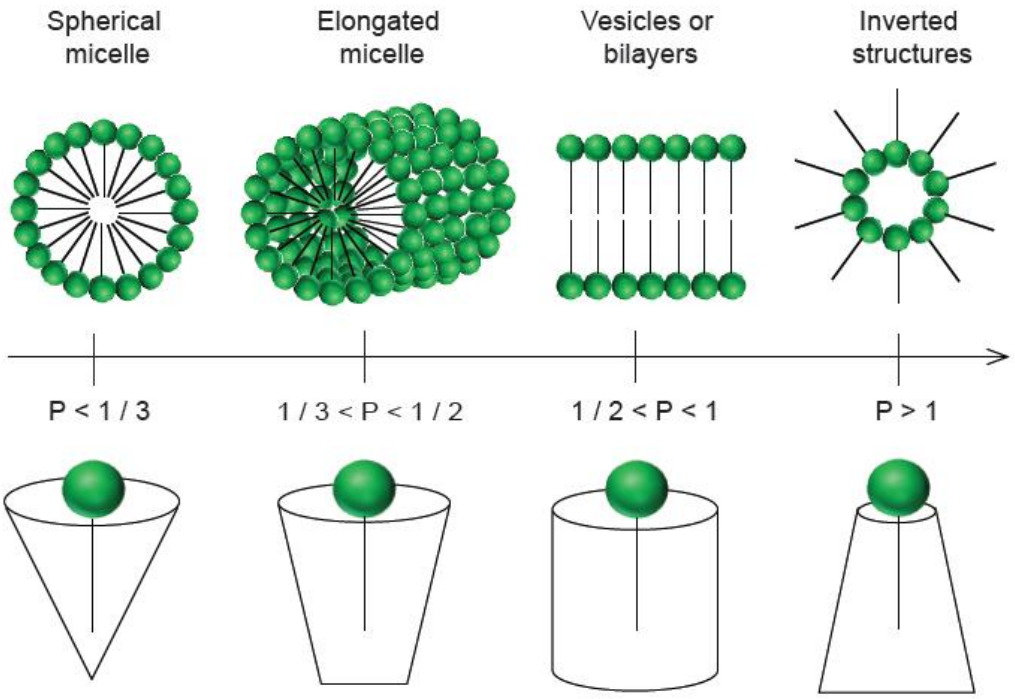


**Figure 1.3: Concept of amphiphile packing parameter:** *The preferred aggregate structure as a function of the amphiphile's molecular shape and packing parameter*.

phosphatidylserine lipids, phosphatidylinositol lipids etc) have a packing parameter approaching unity and tend to self-assemble into planar bilayers and vesicles [2]. Amphiphiles with packing parameter greater than unity form inverted micelles (Hexagonal ($H_{II}$) phase). Examples of such amphiphiles include non-lamellar lipids such as DOPE which can form the hexagonal $H_{II}$ phase, poly (cis) unsaturated chains, and phosphatidic acid in presence of calcium.

The molecular packing parameter also indicates that changes in aggregate morphology can be brought about by changes in the solution conditions [7, 8]. For a given surfactant, both the volume (*v)* and length of the hydrophobic chain (*l)* are defined by the nature of the molecule and are fixed. However, as $a_o$ is influenced

directly by the head-group interactions, it can vary depending on the solution conditions. For example, adding salt to a solution of an ionic surfactant such as SDS decreases $a_o$ due to a decrease in ionic repulsions. This increases the value of packing parameter and therefore, the spherical micelle is transformed into a rod-like one under these conditions. At higher concentrations, the simpler aggregate structures further self-assemble into arrangements with long-range order. Spherical micelles will assemble into cubic-packed structures, cylindrical micelles will assemble into hexagonal-packed structures and membranes will stack generating lamellar structures [9].

Micelle formation thermodynamics is based on the Gibbs-Helmoltz equation ($\Delta G_m = \Delta H_m - T\Delta S_m$), where $\Delta G_m$, $\Delta H_m$, and $\Delta S_m$ are the free energy, enthalpy, and entropy of micellization respectively. The enthalpies and entropies of micellization are determined experimentally from the variation of CMC with temperature. Experimental results suggest that at room temperature (298K), micelle formation involves a small enthalpy change, whereas $T\Delta S$ is large and positive [10]. For example, the values for the enthalpy, entropy, and free energy of micellization for SDS at 298K in water as determined by calorimetry were -1.42 $kJ.mol^{-1}$, 50.30 $J.mol^{-1}K^{-1}$, and -16.40 $kJ.mol^{-1}$ and respectively [10].

The increase in entropy resulting in positive $\Delta S$ is the driving force for the formation of micelles. The increase in the entropy of water on micelle formation arises from the hydrophobic effect (the tendency for oil and water to segregate) [3]. In order to accommodate the hydrophobic tail of the free surfactant, the hydrogen-bonded structure of bulk water must be distorted. A nonpolar hydrocarbon cannot form hydrogen bonds

with water and thus water molecules in the immediate vicinity of a hydrocarbon are constrained in the possible orientations that it can assume. The water molecules around a hydrophobic chain are more ordered which is unfavourable as it results in a decrease in conformational entropy. When all the hydrocarbon chains are hidden inside micelles, the structure of bulk water is largely restored leading to an increase in the conformational entropy. So the hydrophobic effect is an entropy-driven process that seeks to minimize the free energy of a system by minimizing the interface between hydrophobic molecules and water. The increase in the conformational entropy of water more than compensates for the negative aggregation entropy of the surfactants themselves (surfactants are becoming more ordered on micelle formation).

Due to their interesting surface properties and self –associating tendencies, amphiphiles have found wide-spread use in industries, healthcare, and academia [11]. Their importance in practical applications has triggered the development of novel amphiphilic molecules such as fluorinated amphiphiles.

## 1.2 Fluorinated amphiphiles

A fluorinated amphiphile (F-amphiphile) comprises a polar head-group and a hydrophobic tail that features a partially or fully fluorinated chain. Like conventional amphiphilic molecules, F-amphiphiles can also be classified by the nature of the head-group as: (i) non-ionic (ii) ionic and (iii) zwitterionic. Depending on the nature of the hydrophobic tail, F-amphiphiles can be classified as: (i) perfluorinated (ii) hemifluorinated and (iii) semifluorinated (Figure 1.4). Perfluorinated amphiphiles

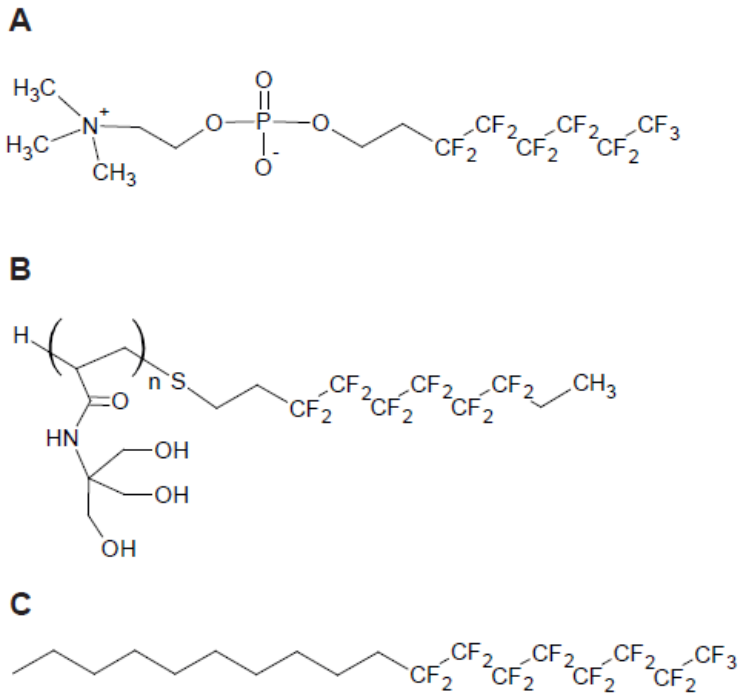


**Figure 1.4: Types of fluorinated amphiphiles:** *(A) A perfluorinated amphiphile with the zwitterionic phosophocholine headgroup. (B) A hemifluorinated amphiphile with an ethyl cap at the end of the fluorinated tail. (C) A semifluorinated alkane ($H_{10}F_8$).*

contain fully fluorinated hydrophobic tails. To facilitate its synthesis, such amphiphiles often contain a "spacer" group ($C_2H_4$) between the head-group and the fluorinated tail. A previous study has shown that the two methylene groups of the spacer do not affect the properties of the perfluorinated amphiphile [12]. Hemifluorinated amphiphiles consist of a hydrogenated tip (ethyl, propyl) grafted at the end of the fluorinated tail. Unlike the spacer group between the head-group and the fluorinated tail, the presence of a hydrogenated tip at the end of a fluorocarbon chain has been shown to affect the properties of the amphiphile [13, 14]. A hemifluorinated amphiphile with an ethyl tip

(terminal $–CH_3$) at the end of the fluorinated chain was shown to have a higher CMC than its fully perfluorinated analogue (terminal $–CF_3$) [15].

Semifluorinated molecules do not conform to the conventional structure of an amphiphilic molecule. Semifluorinated alkanes have a characteristic linear molecular structure consisting of a hydrocarbon segment linked to a fluorocarbon segment (the structural formula of is $F(CF_2)_n(CH_2)_mH$). Although, semifluorinated molecules lack a polar head-group it has been shown to act as an amphiphile as it can accumulate at interfaces and form micelles [16]. The work described in this thesis focuses on perfluorinated amphiphiles.

The introduction of fluorine in the hydrophobic tail of an amphiphile imparts very different properties to the amphiphile when compared to a conventional hydrocarbon-based amphiphile. The unusual properties of F-amphiphiles arise from the larger size of fluorine compared to hydrogen and its unique properties such as its high electronegativity, and very low polarizability.

Perfluorinated amphiphiles are remarkably stable. The carbon-fluorine bond is among the strongest of known covalent bonds. The average C-F bond energy is 485 $kJ.mol^{-1}$ and the dissociation energy increases as the number of fluorine atoms bound to the same carbon atom in the given molecule increases (460, 497, 526, 545 $kJ.mol^{-1}$ for $H_3CF$, $H_2CF_2$, $HCF_3$, and $CF_4$, respectively). Carbon-fluorine bonds are on average, more stable than carbon-hydrogen bonds (415 $kJ.mol^{-1}$) by approximately 75 $kJ.mol^{-1}$ [17]. Fluorinated amphiphiles are stable to acids, alkali, oxidation, reduction, and even at relatively high temperatures (in excess of 200°C) [16]. Fluorine has a dense electron

cloud due to its very high electronegativity, which acts as a repellent sheath of electrons that protects the perfluorinated moiety against the approach of other chemicals and reagents. This renders perfluoroalkyl chains inert. Their outstanding thermal and chemical stability permits applications under conditions which would be too harsh for conventional hydrocarbon based surfactants. Some examples are mentioned later on.

The Van der Waals radius of fluorine (1.47Å) is 20% larger than that of hydrogen (1.20Å) [18]. However, the volumes of $CF_2$ (38Å$^3$) and a terminal $CF_3$ group (92 Å$^3$) are significantly larger than the volumes of a $CH_2$ (27 Å$^3$) and a terminal $CH_3$

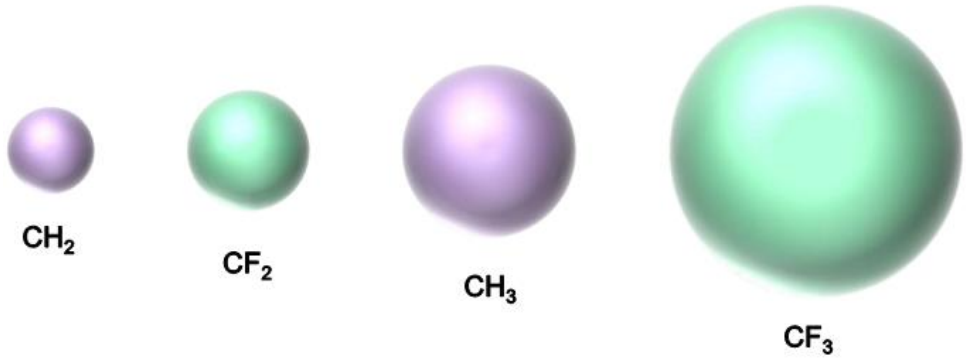


**Figure 1.5: Comparison of the volumes occupied by hydrogen and fluorine containing groups:** *The volumes of $CF_2$ (38Å$^3$) and a terminal $CF_3$ group (92 Å$^3$) are significantly larger than a methyl $CH_2$ group (27 Å$^3$) and a terminal $CH_3$ group (54 Å$^3$) in the corresponding alkane.*

group (54 Å$^3$) in the corresponding alkane [19, 20] (Figure 1.5). Thus, fluorinated chains occupy a larger volume when compared to their hydrogenated counterparts [21] . A consequence of the difluoromethyl and trifluoromethyl groups being much larger than their hydrogenated counterparts is the greater rigidity of fluorocarbon chains. This is reflected in the gauche / trans energy difference of 2.0 kJ.mol$^{-1}$ and 4.6 kJ.mol$^{-1}$ for

hydrocarbon and fluorocarbon chains, respectively [21, 22]. This high trans−gauche energy barrier prevents configurational isomerization of the fluorinated chain. For these reasons, fluorocarbons have been reported to adopt the all-trans helical conformation unlike hydrocarbons which adopt the all-trans planar conformation (Figure 1.6) [22, 23].

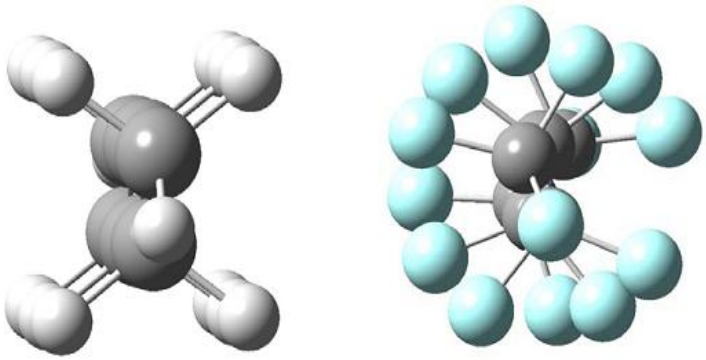

**Figure 1.6**: **Chain conformations adopted by hydrocarbons and fluorocarbons:** *Left: All-trans planar conformation adopted by the hydrocarbon $C_6H_{14}$ with dihedral angles of 180° (end view) Right: All-trans helical conformation adopted by the fluorocarbon $C_6F_{14}$ with dihedral angles of ~ 17° from the all-trans (end view). Figure reproduced from Fournier et al. [24].*

The helical conformation of fluorocarbons was first deduced by Bunn and Howells in 1954 from X-ray diffraction photos of crystals of polytetrafluoroethylene (PTFE) [23]. Since then there have been studies which have looked at the conformations ofshorter length fluorocarbons. The F–F repulsions on alternate carbons in perfluoropropane ($C_3F_8$) are not sufficient to cause a twist in the structure whereas helical structures are observed for longer chains beginning with perfluorobutane ($C_4F_{10}$) [24].

Although both fluorocarbons and hydrocarbons are non-polar, they are known to be immiscible [25]. This segregation phenomenon arises from the low polarizability of fluorine which results in very weak Van der Waals interactions [26]. Van der Waals interaction is an attractive force between two atoms caused when the fluctuating dipole of one atom induces a dipole in the other atom. The average charge distribution in an atom is spherically symmetric i.e zero dipole moment. However, at any moment of time there may be a non-zero dipole moment caused by fluctuations of the electronic charge distribution. According to electrostatics, this non-zero dipole moment produces an electric field, which induces a dipole moment on the other atom. The energy of the interaction of the two dipoles is proportional to the product of the dipole moments and inversely proportional to the cube of the distance between the atoms. Since fluorine is not very polarizable, its electron cloud does not distort very easily. As a result, the cohesive dispersion forces between two hydrocarbon molecules are greater than between two fluorocarbon molecules or between a fluorocarbon and a hydrocarbon molecule (because hydrocarbons are more polarizable than fluorocarbons) [26]. Thus, fluorocarbons are excluded from the hydrocarbons. The incompatibility of the two compounds is reflected in the large positive heat of mixing (endothermic) of a fluorocarbon and a hydrocarbon. There exists a linear dependence of enthalpy of mixing ($\Delta H_{mix}$) on the number of carbon atoms in the two components. For example, the $\Delta H_{mix}$ for a $C_4F_{10}/C_4H_{10}$ mix was determined to be 1750 $J.mol^{-1}$ which increased to 2600 $J.mol^{-1}$ for $C_7F_{16}/C_7H_{16}$ mixtures [25].

Although, it is well established that segregation does occur when FC and HC are present simultaneously, the exact nature of segregation remains an open question. Mukerjee and Yang first proposed the idea of the co-existence of two separate types of aggregates (fluorocarbon-rich and hydrocarbon-rich) in a mixed solution of H-amphiphiles and F-amphiphiles [27] ((Figure 1.7). Evidence for this has been obtained using a variety of techniques: fluorescence quenching [28-32], gel filtration [33], ultracentrifugation [34], NMR [35, 36], surface tensiometry [37] and electrical conductivity [38, 39]. However, other reports [40-42] have questioned the co-existence of two types of aggregates and have instead proposed the existence of only one kind of mixed "aggregate" with a non-homogeneous distribution of fluorocarbon and hydrocarbon components (micro-phase separated micelles) (Figure 1.7).

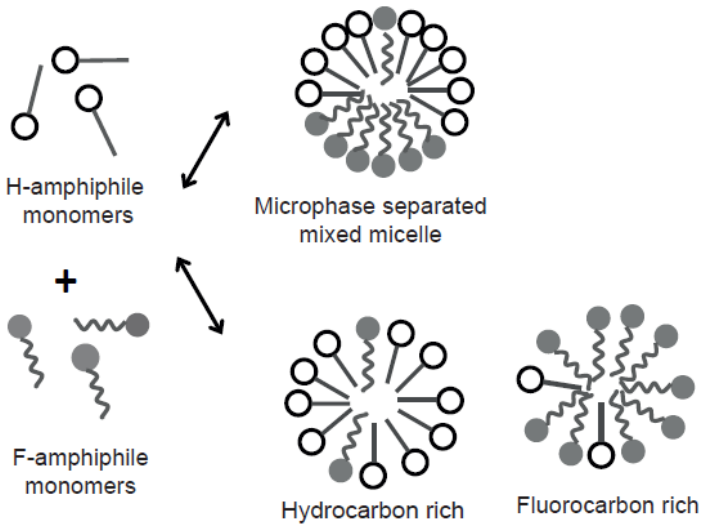


**Figure 1.7: Schematic representation of the different species existing in the mixtures of hydrogenated and fluorinated amphiphiles in solution.** *It is not clear if there exists one kind of micelle with micro-phase separated F-rich and H-rich domains or if there exists two kinds of micelles (i.e hydrocarbon rich micelles and fluorocarbon rich micelles) (adapted from Peyre 2007 [43]).*

The mutual phobicity of fluorocarbons and hydrocarbons gives rise to a very important property of fluorinated amphiphiles: fluorinated amphiphiles are poor solubilizing agents for lipid membranes. This property has been exploited in many membrane protein studies and will be discussed in greater detail in chapter three.

The energy needed to transfer one $CH_2$ group from a hydrocarbon to a fluorocarbon phase (1.4 $kJ.mol^{-1}$) is only one third of the energy required to transfer a $CH_2$ group from a hydrocarbon to water (3.7 $kJ.mol^{-1}$). This implies that the tendency of fluorocarbons and hydrocarbons to segregate (lipophobic) is weaker than the tendency of hydrocarbons to avoid water (hydrophobic). Thus, the lipophobic effect of fluorinated amphiphiles is estimated to be one third in magnitude of the hydrophobic effect [44].

The large surface area presented by fluorinated chains results in enhanced hydrophobicity of F-amphiphiles when compared to their hydrogenated counterparts [45]. Thus F-amphiphiles have an increased tendency to collect at interfaces and self-assemble in water. Due to weak intermolecular forces between fluorinated chains, F-amphiphiles are superior in their ability to lower the surface tension of water when compared to hydrocarbon based amphiphiles. F-amphiphiles can decrease the surface tension of water down to values (15-20 mN $m^{-1}$) that cannot be reached by H-amphiphiles (30-40 mN $m^{-1}$) [16]. F-amphiphiles are very effective in reducing the huge fluorocarbon/water interfacial tension (over 50mN $m^{-1}$) to values as low as 1 mN $m^{-1}$ [46]. Unlike H-amphiphiles, fluorinated amphiphiles are also capable of reducing the surface tension in acids, alkali and in non-aqueous systems such as organic solvents

(m-xylene, methanol) [47]. Various fluorinated surfactants have been shown to lower the surface tension of 10% potassium hydroxide, 25% sulfuric acid and 37% hydrochloric acid and 70% nitric acid to below 25mN/m. The ability of fluorinated surfactants to lower surface tension in acids and alkali arises from the extreme chemical stability mentioned before. The remarkable surface activity of fluorinated surfactants in organic liquids is because the fluorocarbon tail of F-amphiphiles apart from being hydrophobic is also lipophobic (oil hating).

Owing to their increased hydrophobic character, F-amphiphiles have lower critical micellization concentrations (CMC) when compared to their hydrogenated analogues. For example, the CMC of sodium perfluorooctanoate ($C_7F_{15}COO^-Na^+$: 30mM) [48, 49] is about an order of magnitude smaller than that of sodium octanoate ($C_7H_{15}COO^-Na^+$: 400mM) [50]. In most cases, the cmc values for fluorosurfactants are roughly equivalent to those of hydrocarbon surfactants with a 50% longer chain [12]. Unlike single-tailed H-amphiphiles which usually form spherical micelles in dilute solutions, most single-tailed F-amphiphiles have a very strong tendency to spontaneously form complex aggregate structures in solution although there are reports of few F-amphiphiles forming spherical micelles in solution. Metal salts of fluorinated acids [51, 52] and cationic perfluorinated surfactants of pyridinium chloride [19] formed spherical micelles. Fluorinated amphiphiles bearing two or three glucose moieties in the head-group formed spherical micelles whereas those with a single glucosyl head-group formed very large cylindrical aggregates [14]. Similar cylindrical aggregate structures were observed in solutions of F-amphiphiles with lactose and

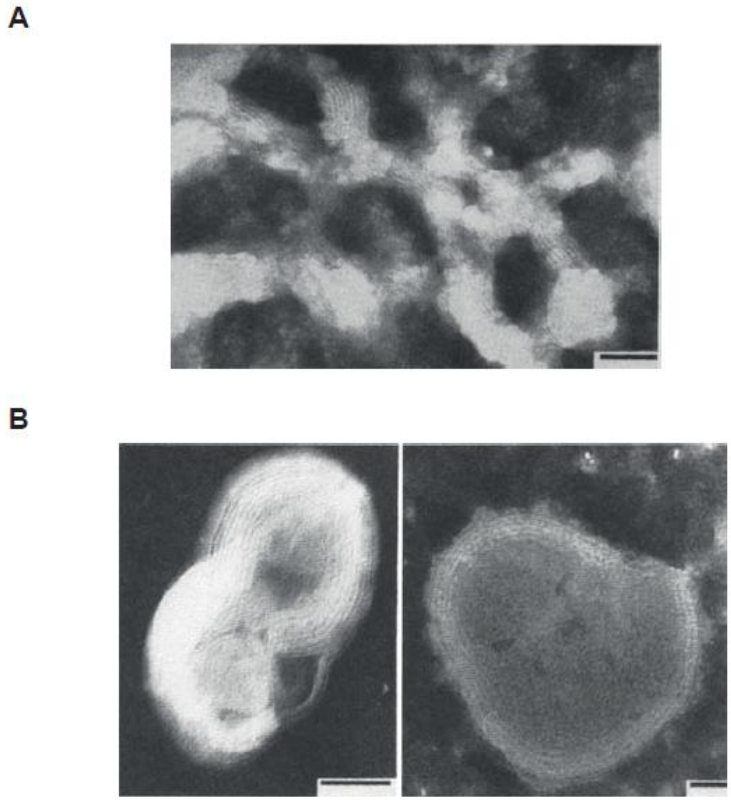


**Figure 1.8**: **Lamellar aggregates formed by F-amphiphiles:** *Transmission electron microscopy images of lamellar and vesicular structures formed by the single-tailed F-amphiphile ($C_8F_{17}C_2H_4OP(O)_2^-OC_2H_4N^+(CH_3)_3$) in aqueous solution: (A) uniformly stacked bilayers formed by hand shaking at 25°C (3% w/v) (B) isolated multilayered vesicles obtained in dilute solutions after gentle shaking at room temperature (0.5% w/v). Scale bar: 50µm. Figures reproduced from Krafft et al. [56].*

maltose head-groups and in solutions of ammonium perfluorooctanoate [53-55]. Vesicles and lamellar aggregates were observed in solutions of diethylammonium perfluorononanoate [52] perfluoroheptanoic acid, non-ionic perfluoroalkylpolyethoxylated amides [51], and perfluorononanoic acid ($C_8F_{17}COOH$) [19]. Single-chain perfluoroalkylated phosphocholines form various organized systems significantly different in morphology, including stacked bilayers, vesicles, globules, and

long fibres depending on the conditions of preparation (Figure 1.8) [56, 57]. The unusual behaviour of single tailed F-amphiphiles to form lamellar aggregates can be explained in terms of the value of Israelachvili packing parameter. For example, the packing parameter of the single-tailed F-ampiphile $C_8F_{17}C_2H_4OP(O)_2^-OC_2H_4N^+(CH_3)_3$ has been calculated to be 0.7 which favours lamellar structure [58]. It has been proposed that the larger cross-section of the F-alkylated chain endows these amphiphiles with truncated-cone geometry, hence favouring the formation of lamellar phases and vesicles.

Tadros et al. determined the micellization parameters for a range of non-ionic, anionic and cationic Monflor industrial fluorinated surfactants and report higher values of enthalpies and entropies of micellization when compared to hydrocarbon amphiphiles [59]. The table below summarizes and compares micellization parameters for an F-amphiphile and an H-amphiphile like SDS.

| Property at 25C | Fluorinated surfactants such as Monflor51 and Monflor31 | Hydrogen surfactants such as SDS |
|---|---|---|
| Enthalpy ΔH | 42kJ.mol$^{-1}$ | -1.42 kJ.mol$^{-1}$ |
| Entropy ΔS | 84kJ.mol$^{-1}$ | 15 kJ.mol$^{-1}$ |
| Free energy ΔG | 40kJ.mol$^{-1}$ | -16.40 kJ.mol$^{-1}$ |

**Table 1.1: Comparison of micellization parameters at 25°C for fluorinated and hydrocarbon surfactants.** *These values have been reproduced from Tadros et al. [59].*

As mentioned above, the possible orientations of water around a non-polar solute decreases and this results in a shell of highly ordered water molecules in the vicinity of the non-polar molecule. The number of water molecules in the highly ordered shell is proportional to the surface area of the hydrophobic solute. Due to the larger size of fluorine, fluorocarbons have larger molecular volume compared to hydrocarbons. Thus when compared to hydrocarbons, fluorocarbons induce greater ordering of water around itself. Thus, on micellization, the transfer of the fluorocarbon chain from the aqueous environment is accompanied with destruction of a larger number of this structured water and hence a larger enthalpy and entropy of micellization.

## 1.3 Applications of F-amphiphiles

Like conventional hydrocarbon based amphiphiles, F- amphiphiles have varied application in industry, medicine, physics, chemistry, and biology [60]. In keeping with the scope of this thesis, applications of F-amphiphiles in medicine and biology will be mentioned here. Most pharmaceutical and biological applications of F-amphiphiles are based on the limited miscibility of fluorocarbons and hydrocarbons and the strong tendency of F-amphiphiles to form aggregate structures.

The most promising use of F-amphiphiles in medicine is as microcontainers for drug delivery. Fluorinated vesicles have been formed from a variety of single, double and triple chain amphiphiles, as well as from combinations with standard phosphoplipids and mixed hydrocarbon –fluorocarbon diblocks [61]. Many of these liposomes were stable enough to withstand sterilization at 121°C. The high

hydrophobicity of fluorocarbons in the liposome membrane is expected to reduce membrane permeability and hinder the release of non-fluorinated encapsulated materials. This was confirmed by release experiments of entrapped hydrophilic, lipophilic and amphipathic drugs and dyes (carboxyfluorescein) from vesicles made of various F-amphiphiles [62, 63]. Since fluorinated amphiphiles are capable of self-assembling spontaneously to form vesicles, (often just after gentle hand shaking at room temperature), they might be useful for the encapsulation of fragile materials such as proteins or DNA. However, despite having desirable properties, the use of F-amphiphile vesicles in pharmaceuticals is limited due to little information regarding their toxicity and pharmacology.

Recently, attention has focused on two-dimensional crystallization of membrane proteins using Langmuir monolayers. A water soluble ligand of the protein of interest is chemically anchored to a lipid moiety. The resulting amphiphilic molecule when deposited at the air-water interface spreads into a monolayer, displaying all the ligands into the aqueous medium. When introducing the protein into the subphase, molecular recognition between the macromolecule and the immobilised ligand leads to in-plane concentration of the polypeptide. However, this technique has proved difficult when dealing with a protein (eg: retinoid receptors) the ligand of which is hydrophobic. In this case, the anchoring of the ligand onto a lipid moiety and its spreading at the air-water interface resulted in the insertion of the hydrophobic ligand in between the lipid fatty chains. This prevented the molecular recognition process with the protein and the 2D crystallisation of the retinoid receptor.

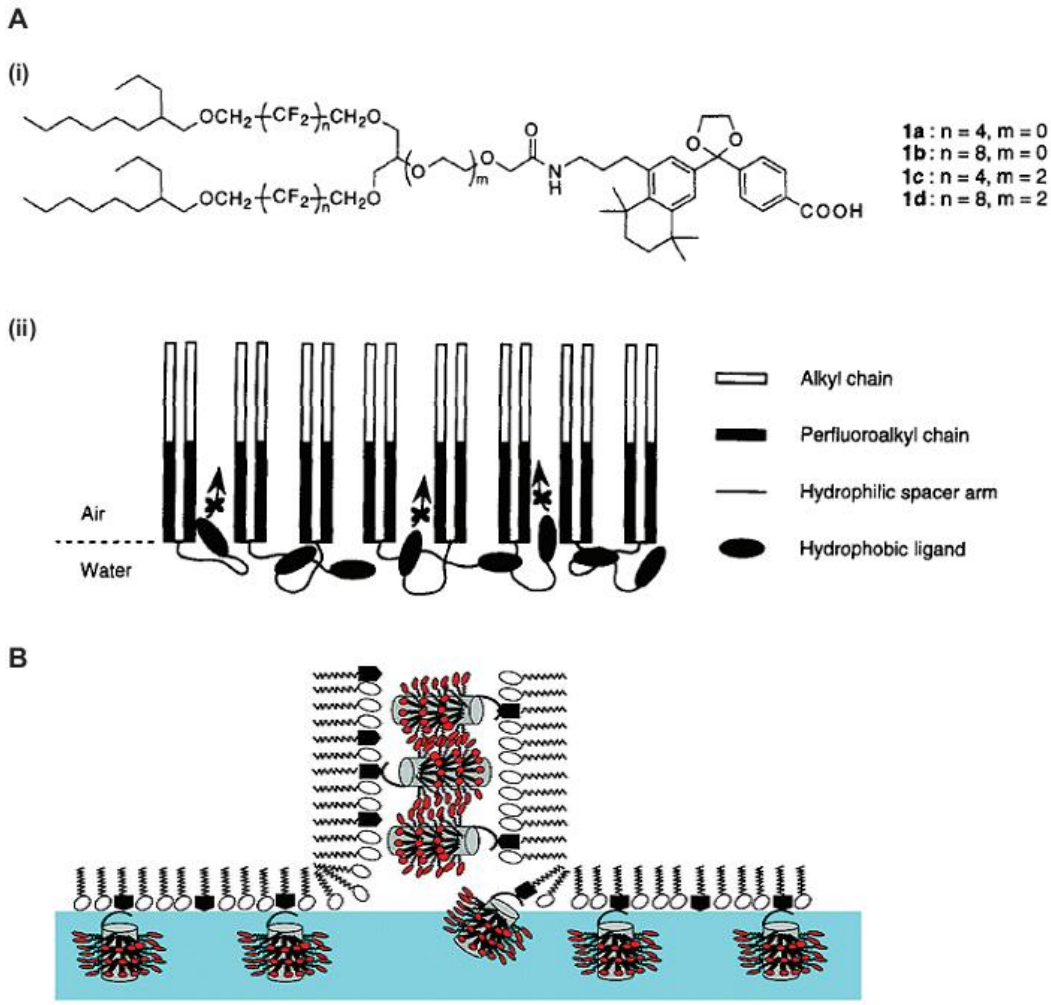


**Figure 1.9: Uses of fluorinated monolayers in recrystallization of membrane protein.** *(A) Lipids were designed (i) which, when derivatised with a hydrophobic ligand, are able to facilitate the 2D crystallization of proteins such as retinoid receptors. When attempting to recrystallize proteins with hydrophobic ligands, it often results in insertion of the hydrophobic ligand in between the lipid fatty acid chains. However, insertion of the ligand in between the lipid chains is not thermodynamically favoured when the lipid chains have been modified with a fluorinated segment. The ligand is then confined at the interface thus remaining accessible to the protein receptor in solution (ii) Figure reproduced from Held et al [64] . (B) Schematic to show the formation of 2D crystals of detergent solubilized tOmpA protein between two monolayers of derivatized fluorinated lipids spread at the air/water interface. Figure reproduced from Petkova et al. [65].*

To overcome this difficulty, lipids were designed which were derivatised with a hydrophobic fluorinated segment [64]. The fluorinated moiety forces the ligand to stay exposed on the aqueous side of the monolayer as the insertion of the ligand in between the chains is not thermodynamically favoured. Thus it remained accessible to its receptor in solution and facilitated 2D crystal formation of retinoid receptors (Figure 1.9A).Another study proposed the use of newton black films formed from fluorinated amphiphiles as a matrix for growing 2D membrane protein crystals in the plane of the film (Figure 1.9B) [65]. Monolayers made from hemifluorinated amphiphiles with a fluorinated chain linked to a tricarboxylic acid polar head which is able to complex a Ni atom (Phenyl-HF-NTANi) also hold interesting promises for forming 2D membrane protein crystals [66].

The non-cytolytic property of F-amphiphiles arising from the poor miscibility of hydrocarbons and fluorocarbons has recently been exploited in membrane protein studies. Although unable to solubilise membranes, F-amphiphiles have been shown to efficiently keep membrane proteins such as cytochrome $b_6f$ and bacteriorhodpsin water soluble after the proteins have been initially solubilized using a classical detergent [54, 67-71]. Recently, F-amphiphiles have been shown to prevent the aggregation of the pore-forming fragment of diphtheria toxin at low pH, thereby making it available for insertion into liposomes [72, 73]. In 2007, Park et al. demonstrated the utility of fluorinated and hemifluorinated amphiphiles to express membrane proteins in cell-free systems followed by their reconstitution into liposomes [15].

## 1.4 Overview of thesis

Based on previous reports which have studied the properties and uses of fluorinated amphiphiles in biomedical research, the main aim of my thesis is to explore the potential of F-amphiphiles in studying membrane proteins. Fluorinated amphiphiles have been suggested as an alternative to detergents for stabilizing membrane proteins in solution [15]. To expand on this work, I investigated the effect of F-amphiphiles on the insertion of membrane proteins in pre-formed DPhPC bilayers. Experiments described in chapter three look at the stability of pre-formed bilayers and characterize the behaviour of alpha-hemolysin protein in liposomes and planar lipid bilayers in presence of F-amphiphiles. The main finding from this work was that F-amphiphiles did not destabilize a pre-formed DPhPC bilayer, but stopped the insertion of membrane protein into a DPhPC bilayer. We speculate that this inhibitory effect of F-amphiphiles on protein insertion into membranes could be due to the sequestration of protein into aggregates formed by fluorinated amphiphiles. This observation has proved to be an effective tool to control the number of proteins in the lipid bilayer.

The next set of experiments is a novel piece of research based on previous reports which suggest that fluorinated amphiphiles form stable lamellar aggregates in solution [56, 57, 74]. Using droplet interface bilayers, we report for the first time the formation of stable free-standing fluorinated bilayers. The properties of these fluorinated bilayers were characterized and we also looked at the behaviour of proteins in such bilayers. The main finding from this work was that the physical properties of

fluorinated bilayers were significantly different from a DPhPC bilayer, although protein behaviour in the two bilayers seemed comparable. These studies are of academic interest and the use of F-amphiphiles provides insights into how the chemical nature and structure of the amphiphile determines properties of the bilayer. Most studies with bilayers are done using hydrocarbon amphiphiles and this study highlights the similarities and differences between a conventional lipid bilayer and a fluorinated bilayer. We hope that this study will open up more avenues for research based on fluorinated amphiphiles.

In the final set of experiments, we study another aspect of droplet interface bilayers. Recently, there has been a lot of focus on using microfluidics and other high throughput screening methods to screen for drugs and other small molecule blockers against ion channels and other membrane proteins. Previous work from the Bayley lab has shown the use of droplet interface bilayers to screen for blockers of a potassium channel [75]. We attempt to assess the feasibility of using droplet interface bilayers as a screening platform for libraries of membrane proteins. The alpha-hemolysin heptamer protein has been engineered for a number of biotechnology and nanotechnology applications [76, 77]. However, studies with engineered pores have been slow because each mutant needs to be generated and screened individually for its activity. Developing a high-throughput screen for membrane proteins using droplets would act to significantly hasten the screening process.

I conclude this thesis with an overall summary of the important results and possible future avenues based on research discussed in this thesis.

## 1.5 Bibliography

[1] K. J. Mysels, "Surface-tension of solutions of pure sodium dodecyl-sulfate," *Langmuir*, vol. 2, pp. 423-428, Jul-Aug 1986.

[2] J. N. Israelachvili, D. J. Mitchell, and B. W. Ninham, "Theory of self-assembly of hydrocarbon amphiphiles into micelles and bilayers," *Journal of the Chemical Society-Faraday Transactions Ii*, vol. 72, pp. 1525-1568, 1976.

[3] L. Maibaum, A. R. Dinner, and D. Chandler, "Micelle formation and the hydrophobic effect," *Journal of Physical Chemistry B,* vol. 108, pp. 6778-6781, May 27 2004.

[4] A. Patist, S. G. Oh, R. Leung, and S. D.O., "Kinetics of micellization: its significance to technological processes," *Colloids and Surfaces A: Physicochem. Eng. Aspects,* vol. 176, pp. 3-16, 2001.

[5] A. Coello, F. Meijide, M. A. Mougan, E. R. Nunez, and J. V. Tato, "Spherical and rod sds micelles," *Journal of Chemical Education,* vol. 72, pp. 73-75, Jan 1995.

[6] T. Imae, R. Kamiya, and S. Ikeda, "Formation of spherical and rod-like micelles of cetyltrimethylammonium bromide in aqueous nabr solutions," *Journal of Colloid and Interface Science,* vol. 108, pp. 215-225, 1985.

[7] Y. Yan, W. Xiong, X. Li, T. Lu, J. Huang, Z. Li, *et al.*, "Molecular packing parameter in bolaamphiphile solutions: Adjustment of aggregate morphology by

modifying the solution conditions," *Journal of Physical Chemistry B,* vol. 111, pp. 2225-2230, Mar 8 2007.

[8] S. Ikeda, "Sphere rod transition of surfactant micelles and size distribution of rodlike micelles," *Journal of Physical Chemistry,* vol. 88, pp. 2144-2149, 1984.

[9] G. Battaglia and A. J. Ryan, "The evolution of vesicles from bulk lamellar gels," *Nature Materials,* vol. 4, pp. 869-876, Nov 2005.

[10] P. L. O. Volpe and E. A. Silva, "Calorimetric study of sds micelle formation in water and in nacl solution at 298-K," *Thermochimica Acta,* vol. 257, pp. 59-66, Jun 1995.

[11] L. L. Schramm, E. N. Stasiuk, and D. G. Marangoni, "Surfactants and their applications," *Annu. Rep. Prog. Chem., Sect. C,* vol. 99, pp. 3-48, 2003.

[12] V. M. Sadtler, F. Giulieri, M. P. Krafft, and J. G. Riess, "Micellization and adsorption of fluorinated amphiphiles: Questioning the 1CF(2)approximate to 1.5CH(2) rule," *Chemistry-a European Journal,* vol. 4, pp. 1952-1956, Oct 1998.

[13] M. Abla, G. Durand, and B. Pucci, "Propyl-Ended Hemifluorinated Surfactants: Synthesis and Self-Assembling Properties," *Journal of Organic Chemistry,* vol. 76, pp. 2084-2093, Apr 2011.

[14] C. Breyton, F. Gabel, M. Abla, Y. Pierre, F. Lebaupain, G. Durand, *et al.*, "Micellar and biochemical properties of (hemi)fluorinated surfactants are controlled by the size of the polar head.," *Biophys J,* vol. 97, pp. 1077-86, Aug 2009.

[15] K. Park, C. Berrier, F. Lebaupain, B. Pucci, J. Popot, A. Ghazi, *et al.*, "Fluorinated and hemifluorinated surfactants as alternatives to detergents for membrane protein cell-free synthesis.," *Biochem J,* vol. 403, pp. 183-7, Apr 2007.

[16] K. Erik, *Fluorinated surfactants and repellents*: CRC press, 2001.

[17] M. P. Krafft and J. G. Riess, "Highly fluorinated amphiphiles and colloidal systems, and their applications in the biomedical field. A contribution," *Biochimie,* vol. 80, pp. 489-514, May-Jun 1998.

[18] A. BONDI, "VAN DER WAALS VOLUMES + RADII," *Journal of Physical Chemistry,* vol. 68, pp. 441-&, 1964 1964.

[19] K. Wang, G. Karlsson, M. Almgren, and T. Asakawa, "Aggregation behavior of cationic fluorosurfactants in water and salt solutions. A cryoTEM survey," *Journal of Physical Chemistry B,* vol. 103, pp. 9237-9246, Oct 1999.

[20] M. P. Krafft, "Fluorocarbons and fluorinated amphiphiles in drug delivery and biomedical research," *Advanced Drug Delivery Reviews,* vol. 47, pp. 209-228, Apr 2001.

[21] M. Krafft, "Fluorocarbons and fluorinated amphiphiles in drug delivery and biomedical research," *Advanced Drug Delivery Reviews,* vol. 47, pp. 209-228, APR 25 2001 2001.

[22] H. Saito, W. Shinoda, and M. Mikami, "Enhanced hydrophobicity of fluorinated lipid bilayer: A molecular dynamics study," *Journal of Physical Chemistry B,* vol. 112, pp. 11305-11309, Sep 2008.

[23] C. W. Bunn and E. R. Howells, "Structures of molecules and crystals of fluorocarbons," *Nature*, vol. 174, pp. 549-551, 1954.

[24] J. A. Fournier and R. K. Bohn, "Microwave spectroscopy and structures of two conformers of 1H-heptafluoropropane," *Dalton Transactions*, vol. 39, pp. 4575-4578, 2010.

[25] P. Lonostro, "Phase-separation properties of fluorocarbons, hydrocarbons and their copolymers," *Advances in Colloid and Interface Science*, vol. 56, pp. 245-287, Mar 1995.

[26] B. C. Buer, J. L. Meagher, J. A. Stuckey, and E. N. G. Marsh, "Structural basis for the enhanced stability of highly fluorinated proteins," *Proceedings of the National Academy of Sciences of the United States of America*, vol. 109, pp. 4810-4815, Mar 2012.

[27] P. Mukerjee and A. Y. S. Yang, "Nonideality of mixing of micelles of fluorocarbon and hydrocarbon surfactants and evidence of partial miscibility from differential conductance data," *Journal of Physical Chemistry*, vol. 80, pp. 1388-1390, 1976.

[28] T. Asakawa, H. Hisamatsu, and S. Miyagishi, "Experimental verification of demixing micelles composed of fluorocarbon and hydrocarbon surfactants via the fluorescence-quenching method," *Langmuir*, vol. 12, pp. 1204-1207, Mar 1996.

[29] T. Asakawa, A. Saruta, and S. Miyagishi, "Distribution of fluorocarbon quencher among micelles via pyrene fluorescence probe method," *Colloid and Polymer Science*, vol. 275, pp. 958-963, Oct 1997.

[30] M. Almgren, K. Wang, and T. Asakawa, "Fluorescence quenching studies of micellization and solubilization in fluorocarbon-hydrocarbon surfactant mixtures," *Langmuir*, vol. 13, pp. 4535-4544, Aug 1997.

[31] T. Asakawa and S. Miyagishi, "Demicellization of sodium perfluorooctanoate and dodecyl sulfate mixtures revealed by pyrene fluorescence quenching," *Langmuir*, vol. 15, pp. 3464-3468, May 1999.

[32] T. Asakawa, S. Ishino, P. Hansson, M. Almgren, A. Ohta, and S. Miyagishi, "Appearance of pure fluorocarbon micelles surveyed by fluorescence quenching of amphiphilic quinoline derivatives in fluorocarbon and hydrocarbon surfactant mixtures," *Langmuir*, vol. 20, pp. 6998-7003, Aug 2004.

[33] T. Asakawa, S. Miyagishi, and M. Nishida, "Coexistence of two kinds of mixed micelles revealed by gel filtration," *Langmuir*, vol. 3, pp. 821-827, 1987.

[34] F. H. Haegel and H. Hoffmann, "Selective incorporation of dyes with fluorocarbon and hydrocarbon chains into coexisting micellar phases of sodium perfluorooctanoate and dimethyl tetradecyl aminoixde," *Progress in Colloid and Polymer Science*, vol. 76, pp. 132-139, 1988.

[35] P. Barthelemy, V. Tomao, J. Selb, Y. Chaudier, and B. Pucci, "Fluorocarbon - Hydrocarbon nonionic surfactants mixtures: A study of their miscibility," *Langmuir*, vol. 18, pp. 2557-2563, Apr 2002.

[36] T. Asakawa, T. Imae, S. Ikeda, S. Miyagishi, and M. Nishida, "H-1-NMR self-diffusion study for mixed micelles of fluorocarbon and hydrocarbon surfactants," *Langmuir*, vol. 7, pp. 262-266, Feb 1991.

[37] M. BenGhoulam, N. Moatadid, A. Graciaa, G. Marion, and J. Lachaise, "Hydrocarbon/fluorocarbon mixed micelle diagram from surface tensiometry," *Langmuir,* vol. 12, pp. 5048-5051, Oct 1996.

[38] J. A. Zhang, A. X. Song, Z. B. Li, G. Y. Xu, and J. C. Hao, "Phase Behaviors and Self-Assembly Properties of Two Catanionic Surfactant Systems: C(8)F(17)COOH/TTAOH/H(2)O and C(8)H(17)COOH/TTAOH/H(2)O," *Journal of Physical Chemistry B,* vol. 114, pp. 13128-13135, Oct 2010.

[39] Y. Moroi and H. Furuya, "Micellization of sodium perfluorodecanoate sodium 1-decanesulfonate mixture in aqueous solution," *Journal of Colloid and Interface Science,* vol. 180, pp. 296-298, Jun 1996.

[40] S. J. Burkitt, R. H. Ottewill, J. B. Hayter, and B. T. Ingram, "Small-angle neutron-scattering studies on micellar systems .2. mixed systems of ammonium decanoate and ammonium perfluoro-octanoate," *Colloid and Polymer Science,* vol. 265, pp. 628-636, Jul 1987.

[41] M. Abe, T. Yamaguchi, Y. Shibata, H. Uchiyama, N. Yoshino, K. Ogino*, et al.*, "Solution properties of mixed fluorocarbon hydrocarbon surfactant systems," *Colloids and Surfaces,* vol. 67, pp. 29-35, Nov 1992.

[42] M. Kadi, P. Hansson, M. Almgren, M. Bergstrom, and V. M. Garamus, "Mixed micelles of fluorocarbon and hydrocarbon surfactants. A small angle neutron scattering study," *Langmuir,* vol. 20, pp. 3933-3939, May 2004.

[43] V. Peyre, "Segregation phenomena in micelles from mixtures of fluorinated and hydrogenated surfactants," *Current Opinion in Colloid & Interface Science,* vol. 14, pp. 305-314, Oct 2009.

[44] M. P. Krafft and M. Goldmann, "Monolayers made from fluorinated amphiphiles," *Current Opinion in Colloid & Interface Science,* vol. 8, pp. 243-250, Aug 2003.

[45] V. Dalvi and P. Rossky, "Molecular origins of fluorocarbon hydrophobicity," *Proceedings of the National Academy of Sciences of the United States of America,* vol. 107, pp. 13603-13607, AUG 3 2010 2010.

[46] J. G. Riess, "Highly fluorinated systems for oxygen-transport, diagnosis and drug-delivery," *Colloids and Surfaces a-Physicochemical and Engineering Aspects,* vol. 84, pp. 33-48, Apr 1994.

[47] C. Rodriguez, H. Kunieda, Y. Noguchi, and T. Nakaya, "Surface-tension properties of novel phosphocholine-based fluorinated surfactants," *Journal of Colloid and Interface Science,* vol. 242, pp. 255-258, Oct 2001.

[48] J. L. Lopez-Fontan, F. Sarmiento, and P. C. Schulz, "The aggregation of sodium perfluorooctanoate in water," *Colloid and Polymer Science,* vol. 283, pp. 862-871, May 2005.

[49] A. Gonzalez-Perez, J. M. Ruso, G. Prieto, and F. Sarmiento, "The self-aggregation of sodium perfluorooctanoate in aqueous solution at different temperatures," *Journal of Surfactants and Detergents,* vol. 7, pp. 387-395, Oct 2004.

[50] T. Zemb, M. Drifford, M. Hayoun, and A. Jehanno, "Light-scattering study of solutions of sodium octanoate micelles," *Journal of Physical Chemistry,* vol. 87, pp. 4524-4528, 1983.

[51] W. Guo, T. Brown, and B. Fung, "Micelles and aggregates of fluorinated surfactants," *Journal of Physical Chemistry,* vol. 95, pp. 1829-1836, FEB 21 1991 1991.

[52] H. Hoffmann, J. Kalus, and H. Thurn, "Small-angle neutron-scattering measurements on micellar solutions of perfluor detergents," *Colloid and Polymer Science,* vol. 261, pp. 1043-1049, 1983.

[53] S. J. Burkitt, R. H. Ottewill, J. B. Hayter, and B. T. Ingram, "Small-angle neutron-scattering studies on micellar systems .1. ammonium octanoate, ammonium decanoate and ammonium perfluoroocatanoate," *Colloid and Polymer Science,* vol. 265, pp. 619-627, Jul 1987.

[54] F. Lebaupain, A. G. Salvay, B. Olivier, G. Durand, A. S. Fabiano, N. Michel, *et al.*, "Lactobionamide surfactants with hydrogenated, perfluorinated or hemifluorinated tails: Physical-chemical and biochemical characterization," *Langmuir,* vol. 22, pp. 8881-8890, Oct 2006.

[55] A. Polidori, M. Presset, F. Lebaupain, B. Ameduri, J. L. Popot, C. Breyton, *et al.*, "Fluorinated and hemifluorinated surfactants derived from maltose: Synthesis and application to handling membrane proteins in aqueous solution," *Bioorganic & Medicinal Chemistry Letters,* vol. 16, pp. 5827-5831, Nov 2006.

[56] M. P. Krafft, F. Giulieri, and J. G. Riess, "Can single-chain perfluoroalkylated amphiphiles alone form vesicles and other organized supramolecular systems," *Angewandte Chemie-International Edition in English,* vol. 32, pp. 741-743, May 1993.

[57] F. Giulieri, M. P. Krafft, and J. G. Riess, "Stable flexible fibers and rigid tubules made from single-chain perfluoroalkylated amphiphiles," *Angewandte Chemie-International Edition in English,* vol. 33, pp. 1514-1515, Aug 1994.

[58] F. Giulieri and M.-P. Krafft, "Can the formation of vesicles from single-chain perfluoroalkylated amphiphiles be predicted?," *Colloids and Surfaces A: Physiochemical and Engineering Aspects,* vol. 84, pp. 121-127, 1994.

[59] T. F. Tadros, "Thermodynamics of micellization of fluorocarbon surfactants," *Journal of Colloid and Interface Science,* vol. 74, pp. 196-200, 1980.

[60] E. Kissa, *Fluorinated Surfactants: Synthesis, Properties, Applications.* vol. 50. New York: Marcel Dekker Inc., 1994.

[61] J. Riess, "Fluorinated vesicles.," *J Drug Target,* vol. 2, pp. 455-68, 1994.

[62] F. Frezard, C. Santaella, P. Vierling, and J. G. Riess, "Fluorinated phospholipid-based vesicles as potential-drug carriers - encapsulation/sustaining of drugs and stability in human serum," *Artificial Cells Blood Substitutes and Immobilization Biotechnology,* vol. 22, pp. 1403-1408, 1994.

[63] C. Gadras, C. Santaella, and P. Vierling, "Improved stability of highly fluorinated phospholipid-based vesicles in the presence of bile salts," *Journal of Controlled Release,* vol. 57, pp. 29-34, Jan 1999.

[64] P. Held, F. Lach, L. Lebeau, and C. Mioskowski, "Synthesis and preliminary evaluation of a new class of fluorinated amphiphiles designed for in-plane immobilisation of biological macromolecules," *Tetrahedron Letters,* vol. 38, pp. 1937-1940, Mar 1997.

[65] V. Petkova, J. J. Benattar, M. Zoonens, F. Zito, J. L. Popot, A. Polidori, *et al.*, "Free-standing films of fluorinated surfactants as 2D matrices for organizing detergent-solubilized membrane proteins," *Langmuir,* vol. 23, pp. 4303-4309, Apr 2007.

[66] J. Dauvergne, A. Polidori, C. Venien-Bryan, and B. Pucci, "Synthesis of a hemifluorinated amphiphile designed for self-assembly and two-dimensional crystallization of membrane protein," *Tetrahedron Letters,* vol. 49, pp. 2247-2250, Mar 2008.

[67] Y. Chaudier, F. Zito, P. Barthelemy, D. Stroebel, B. Ameduri, J. L. Popot, *et al.*, "Synthesis and preliminary biochemical assessment of ethyl-terminated perfluoroalkylamine oxide surfactants," *Bioorganic & Medicinal Chemistry Letters,* vol. 12, pp. 1587-1590, Jun 2002.

[68] A. Polidori, M. Presset, F. Lebaupain, B. Ameduri, J. Popot, C. Breyton, *et al.*, "Fluorinated and hemifluorinated surfactants derived from maltose: synthesis and application to handling membrane proteins in aqueous solution.," *Bioorg Med Chem Lett,* vol. 16, pp. 5827-31, Nov 2006.

[69] P. Barthelemy, B. Ameduri, E. Chabaud, J. L. Popot, and B. Pucci, "Synthesis and preliminary assessments of ethyl-terminated perfluoroalkyl nonionic surfactants derived from tris(hydroxymethyl)acrylamidomethane," *Organic Letters,* vol. 1, pp. 1689-1692, Dec 1999.

[70] A. Maher, D. Gregory, B. Cecile, R. Simon, E. Christine, and P. Bernard, "A diglucosylated fluorinated surfactant to handle integral membrane proteins in

aqueous solution.," *Journal of fluorine chemistry,* vol. 134, pp. 63-71, February 2012.

[71] C. Breyton, E. Chabaud, Y. Chaudier, B. Pucci, and J. L. Popot, "Hemifluorinated surfactants: a non-dissociating environment for handling membrane proteins in aqueous solutions?," *Febs Letters,* vol. 564, pp. 312-318, Apr 2004.

[72] S. Palchevskyy, Y. Posokhov, B. Olivier, J. Popot, B. Pucci, and A. Ladokhin, "Chaperoning of insertion of membrane proteins into lipid bilayers by hemifluorinated surfactants: application to diphtheria toxin.," *Biochemistry,* vol. 45, pp. 2629-35, Feb 2006.

[73] M. Rodnin, Y. Posokhov, C. Contino-Pépin, J. Brettmann, A. Kyrychenko, S. Palchevskyy, *et al.,* "Interactions of fluorinated surfactants with diphtheria toxin T-domain: testing new media for studies of membrane proteins.," *Biophys J,* vol. 94, pp. 4348-57, Jun 2008.

[74] M. P. Krafft, F. Giulieri, and J. G. Riess, "Supramolecular assemblies from single-chain perfluoroalkylated phosphorylated amphiphiles," *Colloids and Surfaces a-Physicochemical and Engineering Aspects,* vol. 84, pp. 113-119, Apr 1994.

[75] R. Syeda, M. A. Holden, W. L. Hwang, and H. Bayley, "Screening Blockers Against a Potassium Channel with a Droplet Interface Bilayer Array," *Journal of the American Chemical Society,* vol. 130, pp. 15543-15548, Nov 2008.

[76] O. Braha, B. Walker, S. Cheley, J. J. Kasianowicz, L. Z. Song, J. E. Gouaux, *et al.*, "Designed protein pores as components for biosensors," *Chemistry & Biology*, vol. 4, pp. 497-505, Jul 1997.

[77] G. Maglia, A. J. Heron, W. L. Hwang, M. A. Holden, E. Mikhailova, Q. H. Li, *et al.*, "Droplet networks with incorporated protein diodes show collective properties," *Nature Nanotechnology*, vol. 4, pp. 437-440, Jul 2009.

# Chapter 2

# Materials and methods

## 2.1 Overview of the alpha-hemolysin pore

### 2.1.1 Full length alpha-hemolysin

The protein that has been used for most of the experiments described here is the full-length pore-forming α-hemolysin (αHL) toxin from the bacterium *Staphylococcus aureus.* It is secreted as a water-soluble monomer (33.2 kDa) comprising 293 amino acid residues [1]. Seven monomers assemble on target membranes (erythrocyte membranes, planar lipid bilayers, liposomes etc.) to form a water-filled heptameric pore [2, 3]. However, not all target cells are equally susceptible to attack by αHL. For example, lysis of rabbit red blood cells requires only approximately 1 nM αHL, whereas human erythrocytes and synthetic membranes require > 1 μM αHL to show similar activity [4]. On pore formation, the bilayer becomes permeable to ions, water and low molecular weight molecules of less than 2 kDa.

While the αHL monomer has not been crystallized; a high-resolution (1.9Å) structure of the detergent-solublized homo-heptamer pore was determined by X-ray crystallography by Song et al. in 1996 [5]. The α-hemolysin protomer is made up of 16 β-strands and consists of the β-sandwich, the amino latch (first 20 residues of the N-

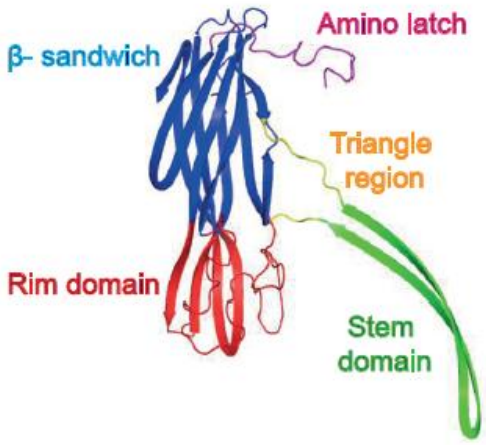


**Figure 2.1**: **α-Hemolysin Protomer Structure.** *A single protomer abstracted from the α-hemolysin heptamer is shown in ribbon representation.*

terminal), the rim domain and the stem domain (Figure 2.1). The stem domains (an anti-parallel β-hairpin) one from each protomer form the barrel of the αHL pore, which spans the width of the lipid membrane. Seven β-sandwiches and the amino latches from each protomer make up the cap domain in the fully assembled heptamer pore. The rim domain, which is directly linked to the cap domain, lies below the cap domain and is formed from three β-strands. The rim domain lies close to the surface of the lipid bilayer. In co-crystals of the αHL heptamer with diheptanoyl phosphatidylcholine, interactions of the lipid with aromatic residues present at the bottom surface of the rim domain were observed [5]. The triangle region connects the stem domain to the β-sandwich and participates in inter-protomer interactions with neighbouring triangle and rim domains.

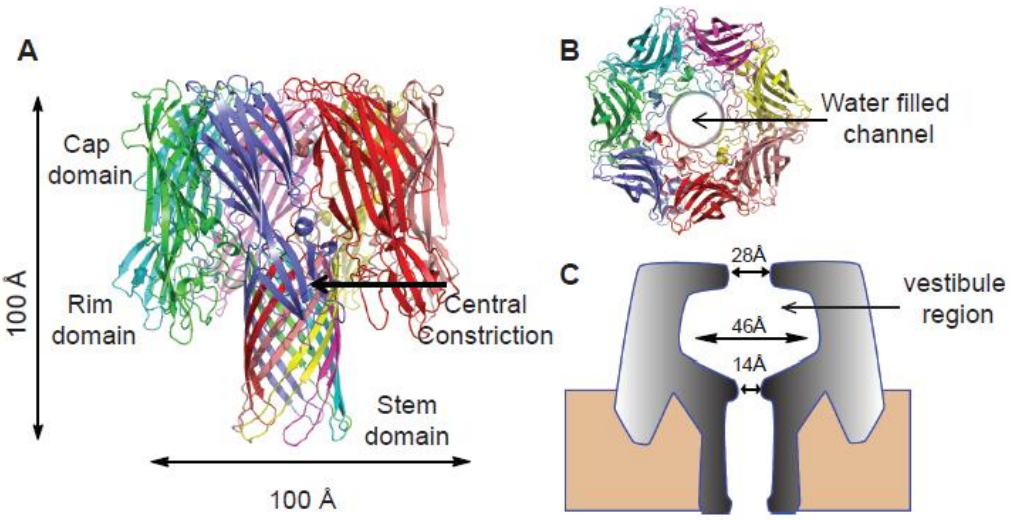


**Figure 2.2: α-hemolysin heptamer structure.** *(A) Ribbon representation of the αHL heptamer. Each protomer is in a different color. The cap, rim, and stem domains are labeled. (B) View of the αHL pore along the axis of symmetry. The water filled channel in the middle of the pore is visible. (C) The diameter of the pore is not constant along the length of the pore. At the entrance of the cap domain, the diameter is 28Å, which increases to 46Å in the vestibule region (inside the cap domain), and then decreases to 14Å in the central constriction region.*

The fully assembled αHL heptamer pore (232.4 kDa) is mushroom-shaped, and is 100Å in length and 100Å wide. It can be divided into the cap, rim and stem domains (Figure 2.2A). The stem domain measures 52 Å in height and thus is capable of spanning a lipid bilayer. The diameter of the barrel is not constant along the length of the pore (Figure 2.2C). The diameter at the entrance of the cap domain is 28Å, which increases to 46Å in the vestibule region (inside the cap domain), and then decreases to 14Å in the central constriction region (at the beginning of the stem domain). The presence of the constriction where the stem domain begins is responsible for the size limit of the transport of macromolecules through the pore.

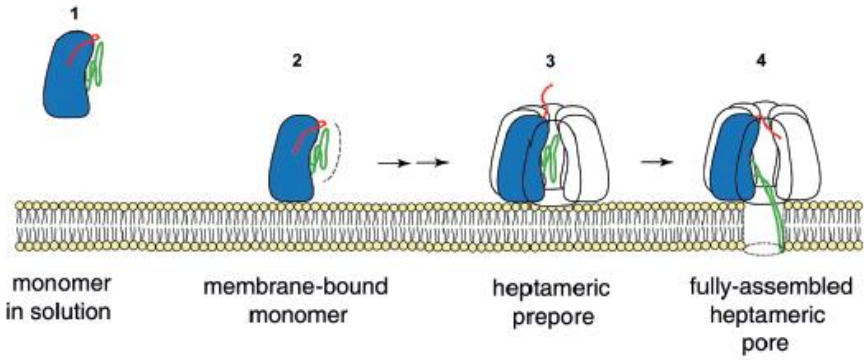


**Figure 2.3: Proposed model for the assembly of αHL.** *The N terminus is shown in magenta, and the pre-stem domain is shown in green. Stage 1: Water-soluble monomer: both the N terminus and the pre-stem region are protease-sensitive. Stage 2: Membrane-bound monomer: the N terminus remains protease-sensitive at this stage, but the pre-stem region becomes protease-resistant (indicated by the dashed line). Stage 3: Prepore: the N terminus remains protease-sensitive. One possibility is that it is exposed to the aqueous phase, as depicted. Stage 4: Functional pore: latch formation makes the entire pore protease-resistant. Image reproduced with permission from Jayasinghe et al. [6].*

Heptamer formation from the monomer occurs in three steps (Figure 2.3) [7, 8]. In the first step, α-hemolysin monomers bind to the surface of a lipid bilayer, either mediated by specific receptors or spontaneously. In the second step, monomers diffuse on the membrane surface, which results in their coming together to form the inactive pre-pore. In the third step, which is irreversible, the pre-pore undergoes a conformational change whereby it spontaneously inserts a membrane-spanning β-barrel domain into the lipid bilayer forming the aqueous channel. Recent studies using simultaneous fluorescence and electrophysiology measurements have shown that assembly from the monomer to the complete heptamer is extremely rapid, occurring in less than 5 milliseconds after a lag phase [9]. Assembled oligomers were stable after formation and their lateral

diffusion in the bilayer was found to be slower than the monomers (the diffusion coefficient of the monomer is known to be 23.4±6.4 $\mu m^{-2}s^{-1}$.

### 2.1.2 Truncated alpha-hemolysin

As part of on-going efforts to improve DNA sequencing using nanopores, mutants of αHL were made by David Stoddart, where the beta-barrel was truncated [10]. As mentioned above, the β-barrel of the full length αHL protein which spans the lipid membrane contains 14 antiparallel β-strands and measures 52Å in length. Each protomer contributes two adjacent β-strands (connected by a turn sequence) to the trans-membrane barrel of the heptamer.

Of special interest to this thesis is the truncated barrel mutant in which a total of 8 amino acids were deleted. Amino acids Y118 - T125 were deleted from the "down" strand and amino acids V140 - G133 were deleted from the "up" strand by PCR mutagenesis (Figure 2.4A). However, the turn sequence connecting the two strands was left untouched. In addition to this, the charged residues of glutamic acid (E111) and lysine (K147) present at the central constriction were mutated to neutral asparagines (NN). This mutant will hereafter be referred to as TBMΔ8NN. Molecular dynamic simulations of TBMΔ8NN (carried out by J. Klingelhoefer) showed that the trans-membrane β-barrel of the truncated protein was shorter than the β-barrel of the full length protein by 18.5Å (Figure 2.4B).

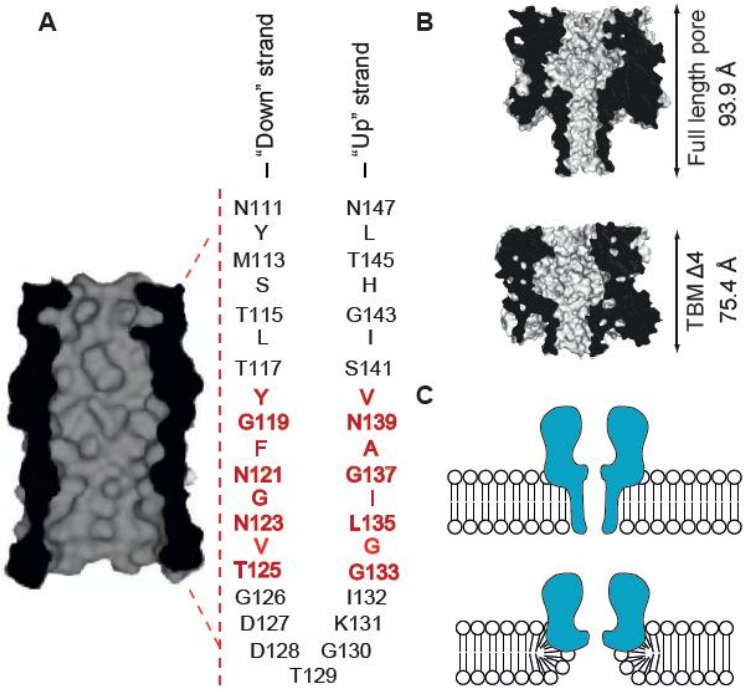


**Figure 2.4: Structure of the truncated barrel mutant (TBMΔ8NN).** *(A) The beta barrel which spans the lipid bilayer is a 14 stranded, antiparallel β barrel. Shown here is the pair of adjacent β strands contributed by each protomer to the barrel. The truncated barrel mutant was formed by deleting the amino acids shown in red by PCR mutagenesis. Also, two mutations (E111N and K147N) were made at the entrance to the barrel. (B) Molecular dynamics simulations (performed by J. Klingelhoefer) of the mutated protein. The barrel of the truncated protein is shorter by 18.5Å when compared to the full length protein. (C) The proposed conformation of TBMΔ8NN protein in the lipid bilayer. While the full length αHL pore (upper panel) is able to span the entire length of the bilayer, in the case of TBMΔ8NN, the lipid bilayer forms a part of the ion conductive pathway (lower panel). This figure has been adapted from David Stoddart's thesis [10].*

Surprisingly, TBMΔ8NN showed activity in planar lipid bilayers, although it was unable to lyse rabbit erythrocytes. In bilayers made from DPhPC (1, 2-diphytanoyl-sn-glycero-3-phosphocholine), the pores formed from TBMΔ8NN proteins were typically short-lived, exhibiting "burst-like" behaviour. Longer-lived stable pores from

TBMΔ8NN were obtained in DPhPC bilayers doped with shorter chain lipids like DLPC (1, 2-dilauroyl-sn-glycero-3-phosphocholine). To explain the fact that the open pore lifetime of TBMΔ8NN is lengthened (from seconds to minutes) by adding a short chain DLPC lipid to the bilayer, the authors proposed bilayer deformation such as local thinning or leaflet curvature which is facilitated by the presence of the short chain DLPC lipid (Figure 2.4C).

## 2.2 Overview of techniques

### 2.2.1 Single channel recording

#### 2.2.1.1 Planar lipid bilayers

All single channel recordings mentioned in Chapter three were done in planar lipid bilayers. Planar lipid bilayers were prepared by the Montal–Mueller technique [11]. The custom-built set-up consisted of two chambers (1 mL each), separated by a hydrophobic film (a 25 μm Teflon film) which contained an aperture approximately 100 μm in diameter (Figure 2.5A). This set-up allows for easy access to both chambers for the purposes of adding reagents or solution perfusion. The aperture was pre-treated with a solution of hexadecane (10% (v/v) in pentane) to leave a hydrophobic coating, which helped the bilayer to form. Aqueous buffer was added to both chambers below the level of the aperture (~500 μL) and lipids (10mg $mL^{-1}$ in pentane) were added to the buffer surface. As the pentane evaporates, a lipid monolayer self-assembles at the air-water interface on either side of the Teflon film with the heads oriented toward the

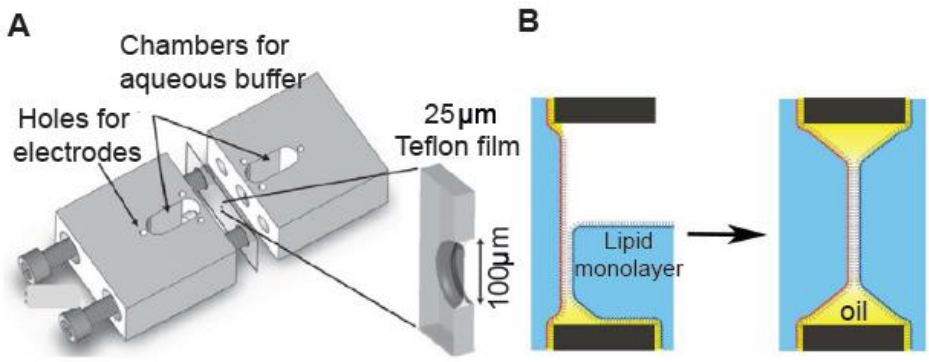


**Figure 2.5: Planar bilayer formation.** *(A) Custom-built apparatus with two chambers (1mL) separated by a 25µm Teflon film which contains the aperture across which the bilayer is formed. The Teflon film is clamped between the two chambers which are held together by screws. The apparatus is sealed with silicone glue to ensure water-tightness. (B) The bilayer is formed at the aperture by the sequential raising and lowering of the lipid monolayers formed on either side of the aperture.*

water and the tails oriented in the air. More buffer (~500µL) was added to raise the solution level above the aperture. As the solution level passed over the aperture, the hydrophobic tails of the lipid on each side of the aperture came together resulting in the formation of a lipid bilayer at the aperture (Figure 2.5B). The electrolyte solutions in the two chambers were accessed with Ag/AgCl electrodes. Detergent-solubilised protein was inserted into the bilayer by addition into the chamber, followed by stirring until protein insertion occurred.

### 2.2.1.2 Droplet interface bilayers

All electrical recordings in chapter four were done using droplet interface bilayers (DIBs), a technique developed in our laboratory [12]. Droplet interface bilayers form between aqueous droplets in oil that have a lipid monolayer coating.

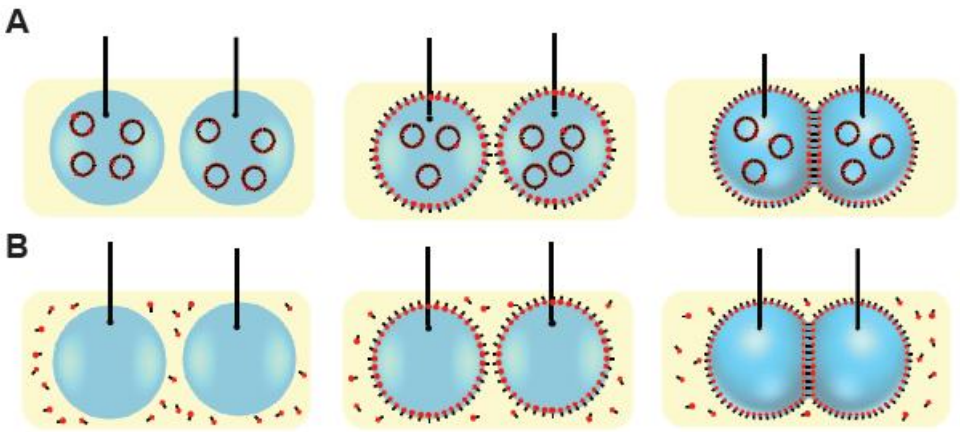


**Figure 2.6: Formation of droplet interface bilayers.** *(A) "lipid-in" DIB formation. Aqueous droplets, containing lipid vesicles are pipetted under an oil phase (yellow). Liposome fusion at the oil–water interface results in monolayer formation. (B) "lipid-out"DIB formation. Aqueous droplets submerged in an oil–lipid mixture acquire a lipid monolayer. In both cases, bilayer formation occurs at the interface when two monolayer coated droplets are brought into contact.*

DIBs can be formed in two ways. In the "lipid-in" technique, the lipid is present as vesicles in the internal aqueous phase, which spreads at the oil-water interface resulting in monolayer formation around the aqueous droplets (Figure 2.6A). In the "lipid-out" technique, the lipids are dissolved in the oil phase and diffuse to the oil-water interface resulting in monolayer formation around each droplet (Figure 2.6B). Specific capacitance measurements of droplet interface bilayers (0.65μF/cm$^2$) fall in the expected range for bilayer capacitance (0.2μF/cm2 to 1μF/cm2) [13]. Hence it is believed that each droplet is only coated by a lipid monolayer (not multilayer formation) which forms a bilayer when brought together. When one of the droplets contains, detergent-solubilised protein, protein insertion occurs in the bilayer.

### 2.2.1.3 Data acquisition and analysis

In both planar bilayers and droplet interface bilayers, the formation of bilayer was monitored by measuring the membrane capacitance. The membrane capacitance (C) is measured by applying a potential in the form of a triangular wave where the rate of change in voltage (dV/dt) is 1 V/s. The input waveform was calibrated by using a model bilayer cell (MCB-1U, Molecular Devices). The current through a capacitor (ic) is given by the equation: $i_c = dV/dt \times C$. In our set-ups, dV/dt is set to be equal to one, therefore, the measured current is directly equal to the membrane capacitance and the output waveform is a square wave (Figure 2.7).

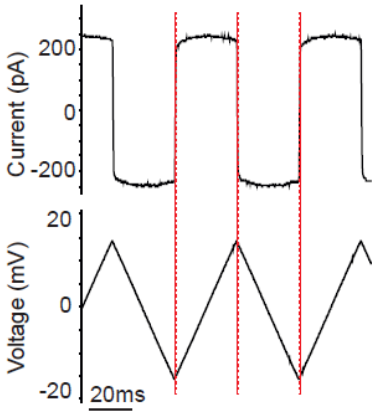


**Figure 2.7: Measuring bilayer capacitance.** *A triangular-wave voltage input (lower) applied across a capacitor produces a square-wave current output (upper). Bilayer capacitance is half the peak-to-peak magnitude of the square-wave current output ($i_c$).*

The lipid bilayer acts as an insulator (impermeable to ions) and in the absence of protein negligible current (<1 pA) flows across the bilayer. The insertion of a trans-membrane pore such as αHL in the bilayer, results in a step-wise change in the current

(Figure 2.8). The amplitude of this current step depends on both the electrolyte concentration and the applied potential. On application of +100mV in 1M KCL, 10mM Tris, pH 7.0 buffer, the insertion of a single αHL channel results in a 100pA current. According to standard convention, the side to which the protein is added (cis) is grounded and the applied potential is that at the trans side. Therefore, a positive current represents a net flux of cations flowing from the trans to the cis side (Figure 2.8).

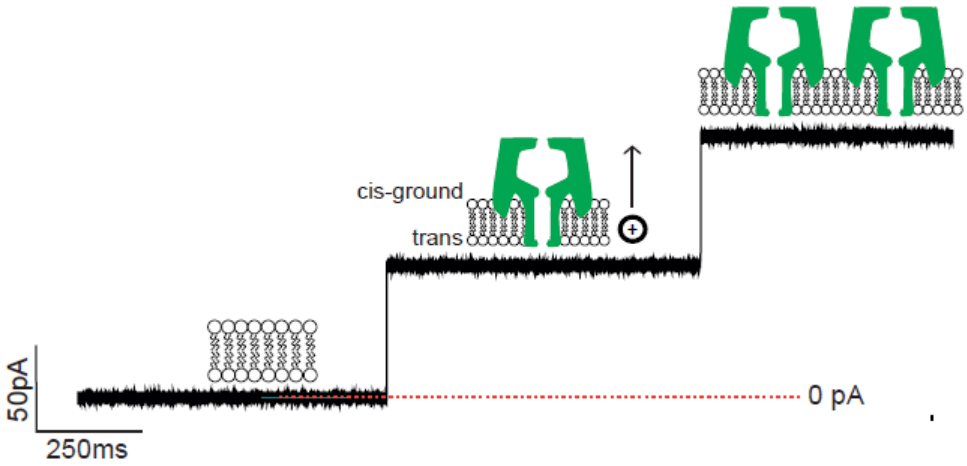


**Figure 2.8:** *Current increase on pore insertion in the bilayer. In the absence of protein, no current flows across the bilayer as it is impermeable to ions. The insertion of αHL protein(s) in the bilayer results in an ionic current can flow across the bilayer. The insertion of protein in the bilayer is characterized by a step-wise change in the current measurement. A positive current represents a net flux of cations flowing from the trans to the cis side*

Electrical currents were recorded using Ag/AgCl electrodes connected to an Axopatch 200B patch-clamp amplifier (Axon Instruments, Foster City, CA). Currents were filtered at 1 kHz with a built-in 4-pole low-pass Bessel Filter, sampled at 10 kHz and then digitized with a DigiData 1320 A/D converter (Axon Instruments). Data were

analysed using pClamp 9.2 software (Axon). The entire set-up for bilayer recordings (chamber, amplifying headstage and micromanipulator) were enclosed in a Faraday cage, to shield against electrical noise.

### 2.2.2 Light scattering hemolytic assay

Light scattering is a powerful tool for the measurement of cell lysis kinetics. The advantage of light scattering assays is that they are non-destructive and can be automated to minimize intervention by the experimenter. Light scattering from intact erythrocytes arises from the difference in refractive index (caused by intracellular hemoglobin) of the red blood cells and the surrounding media [14]. For red blood cells, the refractive-index of hemoglobin is 1.40 compared to 1.33 for the surrounding medium which is aqueous buffer.

Monomers of αHL lyse rabbit erythrocytes by forming a pore on the erythrocyte membranes. This pore results in rapid efflux of ions and small molecules from the erythrocytes. Osmotic swelling of erythrocytes occurs due to the movement of water into the erythrocyte cells. Consequently, the refractive index of the cytoplasm is comparable to the refractive index of the external aqueous medium. Thus ghost erythrocytes (post hemolytic residues of red blood cells) scatter very little light by comparison to intact erythrocytes. This results in a decrease in the optical density of the cell suspension. Osmotic swelling of erythrocytes finally results in its rupture.

Lysis of the erythrocytes is followed by monitoring the decrease in light scattered at a chosen wavelength (usually 595 nm) (Figure 2.9). Hemolytic lysis

experiments are carried out at concentrations (1% v/v) where the blood cells are sparsely distributed in order to avoid multiple scattering effects and relatively long wavelengths are used (595nm) as it lies outside the absorption band of most cytoplasmic components.

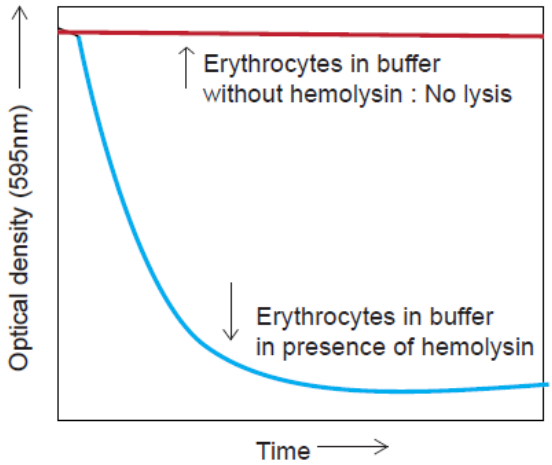


**Figure 2.9: Schematic showing the decrease of optical density (595nm) on lysis of rabbit erythrocytes.** *The rate of haemolysis is determined by measuring the change in optical density of erythrocytes at 575 nm as a measure of time using a spectrophotometer.*

### 2.2.3 Surface tension measurements

Drop shape analysis has been routinely used to accurately (± 0.01 $mN.m^{-1}$) measure tension at the interface of two immiscible liquids. In a typical experiment (Figure 2.10A), the interfacial tension between the two fluids is determined by creating a drop of one fluid (in this case hexadecane) at the tip of an inverted needle submerged in a cuvette filled with the solution of interest (in this case an aqueous solution of DPhPC or F-amphiphiles). After formation of the drop, the interfacial tension is determined by

analyzing the shape of the drop (in a captured video image). In this case, the computer is set to calculate the interfacial tension from the drop shape 12 times every second.

The shape of the drop depends on the balance between gravity (tends to elongate the drop) and interfacial tension (tends to round the drop). Adsorption of amphiphilic molecules from the bulk solution onto the freshly formed drop interface results in a decrease in the interfacial tension. As this minimizes the surface energy, it leads to an increase in the interfacial area with time (the drop becomes more elongated).

The drop shape is analysed by fitting it to the Laplace equation which states that the pressure difference across a curved interface is described by:

$$\frac{\Delta P}{\gamma} = (1/R_1 + 1/R_2) \qquad (2.1)$$

where $R_1$ and $R_2$ are the principal radii of curvature at any point on the drop, $\Delta P$ is the pressure difference across the curved interface, and $\gamma$ is the interfacial tension.

For a static drop of a known fluid in mechanical equilibrium with the surrounding fluid system, the interfacial tension and gravity are the only forces shaping the drop. In this situation, the pressure difference ($\Delta P$) (hydrostatic pressure arising from the density difference ($\Delta\rho$) of the two bulk phases) is a linear function of the height of the drop (z):

$$\Delta P = \Delta P_0 + \Delta\rho g z \qquad (2.2)$$

where $\Delta P_0$ ($=\frac{2\gamma}{a}$) is the pressure difference at the apex of the drop (x=0, z=0), the radius of curvature is "a", $\Delta\rho$ is the difference in the density of, g is the acceleration due

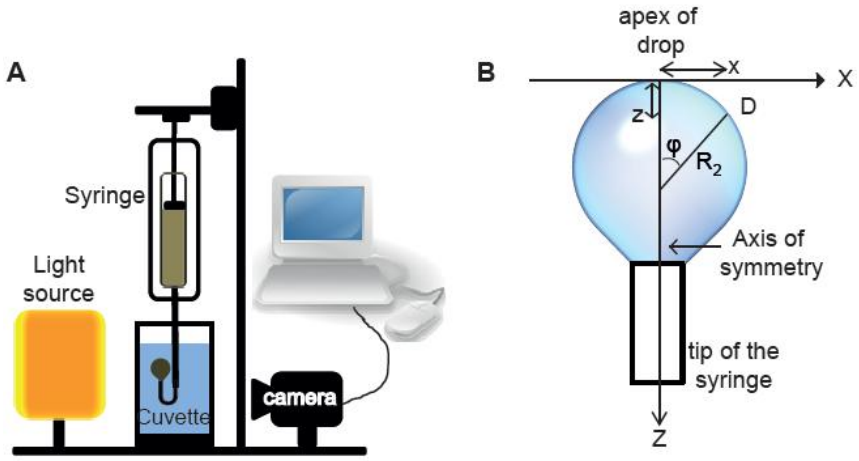


**Figure 2.10: Drop shape analysis for determination of surface tension.** *(A) diagram of the experimental set-up. (B) principle of the analysis of the profile of a drop using the Laplace equation.*

to gravity, and z is the vertical height measured from the apex of the drop (Figure 2.10B).

By combining equation 2.1 and 2.2, the Laplace equation can be rewritten as:

$$\gamma(1/R_1 + 1/R_2) = (2\gamma/a) + \Delta\rho g z \qquad (2.3)$$

The Laplace equation was solved by Bashforth and Adams [15] and it relates the drop profile to the interfacial tension through an equation given by:

$$2 + B(z/a) = (a/R_1) + \sin\phi/(x/a) \qquad (2.4)$$

where x and z are the co-ordinates at any point on the drop, a is the radius of curvature at the drop apex, φ is the angle between the axis of symmetry and a normal drawn to the surface at a given point (say D), and $B = \frac{a^2 g \Delta\rho}{\gamma}$ (Figure 2.10B).

## 2.3 Experimental methods

*Note: The pH for all buffers used in this thesis was set with all ingredients of the buffer present. Unless specified otherwise, all experiments were carried out at room temperature.*

### 2.3.1 Protein Purification.

**2.3.1.1 Full length alpha –hemolysin** (expressed and purified by Ms. Qiuhong Li)

Heptameric WT αHL from *Staphylococcus aureus* (Wood 46 strain) in SDS buffer [20 mM sodium phosphate, 150 mM NaCl, and 0.3% (w/v) SDS (pH 8.0)], for liposome assays and planar bilayer recordings, was obtained as previously reported [16]. Monomeric WT αHL, used for liposome assays and planar bilayer recordings, was also obtained from *S. aureus* by a modification of a previously reported protocol [16]. After elution from the S-Sepharose FF XK-16 cation exchange column, the peak fractions containing the monomer were collected and concentrated to approximately 3 mg/mL by using ultracentrifugal filter devices with a 10 kDa cut-off (model 4321, Amicon) spun at 2900*g*. The protein concentration was determined from the absorbance at 280 nm (the $OD_{280}$ of a 1.0 mg/mL solution is 1.95). The monomer was purified further by chromatography on a Superdex 200 HiLoad gel filtration column (model 17107101, GE Healthcare), which was equilibrated and run with 10 mM Tris-HCl and 150 mM NaCl (pH 8.0), at a flow rate of 1 mL/min. The peak fractions were located by sodium dodecyl sulphate−polyacrylamide gel electrophoresis (SDS−PAGE), pooled, and concentrated to 1 mg/mL. The yield of the ~95% pure monomer, as judged by SDS−PAGE, was ~10 mg/L of culture.

The monomeric WT-αHL used in the hemolytic assay was expressed in an *Escherichia coli* in vitro transcription and translation (IVTT) system (*E. coli* T7 S30 Extract System for Circular DNA, Promega) for 1 h at 37 °C with the complete amino acid mix. The solution was spun at 25000*g* for 15 min at 4 °C, and the supernatant containing the αHL monomers was retained.

**2.3.1.2. Truncated barrel mutant of αHL** (expressed and purified by Mr. David Stoddart)

The αHL truncated barrel mutant used for studies with asymmetric fluorinated bilayers was generated by PCR mutagenesis (a detailed protocol can be found in David's thesis [10]). The protein was expressed in the presence of methionine [$^{35}$S] and rabbit red blood cell membranes (rRBCM) in a cell free *E. coli in vitro* transcription and translation (IVTT) system (*E. coli* T7 S30 Extract System for circular DNA, Cat. #L1130, Promega) for 1 h at 37°C. $^{35}$S was used to radiolabel the protein because: (i) it is a low-energy beta-emitting radioisotope and is safe to be used in the lab (ii) most IVTT kits are compatible with the $^{35}$S (iii) most proteins contain methionine and therefore the expressed proteins can be visualized by autoradiography. The membrane suspension was centrifuged at 25,000 X g and the pellet containing the heptamers was recovered. Expressed protein was analysed by SDS-PAGE and visualised by exposure to a photographic film. The band corresponding to the truncated heptamer was cut from the gel and rehydrated in 10mM Tris.HCl, 1mM EDTA pH 8.0 (400 µl) followed by centrifugation through a cellulose micro spin column (25,000 X g for 10 minutes at RT)

to remove the polyacrylamide. The concentration of heptamer, after purification, was typically ~ 1 ng $\mu l^{-1}$. Aliquots of the purified protein were stored at -80°C.

**2.3.1.3 MspA pore** (expressed and purified by Ms. Ellina Mikhailova)

The MspA (NNNRRK) mutant (GeneScript) was expressed in the IVTT system (50 μL) for 2h at 37 °C in the presence of rRBCM (2 μL, 2 mg protein/mL) and methionine [$^{35}$S]. The membranes were recovered by centrifugation and solubilized in sample buffer. The proteins were then separated in an 8% SDS−polyacrylamide gel. The gel was dried without being heated onto paper (Whatman 3M) under a vacuum, and the MspA oligomer band was located by autoradiography. After rehydration in buffer [300 μL of 25 mM Tris-HCl (pH 8.0)], the paper was removed. The gel was crushed using a pestle and the slurry filtered through a QIAshredder column (Qiagen) by centrifugation at 25000 X *g* for 10 min.

**2.3.1.4 Tetrameric potassium channel Kcv** (expressed and purified by Ms. Amy Mason)

The tetrameric potassium channel, Kcv, used for single-channel recording experiments in presence of F-amphiphiles was obtained after IVTT in the presence of methionine [$^{35}$S] as previously described [17, 18].

**2.3.2 Dye Leakage Assay**.

A 100 mM stock solution of 5(6)-carboxyfluorescein (CF, Sigma-Aldrich) was made in 150 mM NaCl, 2.7 mM KCl, 10 mM $Na_2HPO_4$, and 2 mM $KH_2PO_4$ (pH 7.4). The pH

of the dye solution was re-adjusted to pH 7.4 with NaOH. Liposomes containing CF were made by extrusion. Soybean lecithin (20 mg, Calbiochem) was dissolved in chloroform (1 mL) in a round-bottom flask. The lipid was dried under $N_2$ to form a thin uniform layer and further dehydrated in a vacuum desiccator for 2-3 h. The lipid was then rehydrated by resuspension in a CF solution that had been diluted 50% with water (total volume of 300 μL) to give a final dye concentration of 50 mM. The flask was vortexed for a few minutes to ensure complete resuspension of the lipids, followed by five freeze-thaw cycles (liquid nitrogen/ 37 °C water bath). The suspension was then extruded 23 times through a 0.1 μm polycarbonate filter by using a mini-extruder (Avanti Polar Lipids) to yield large, unilamellar vesicles (LUV). Free CF was removed from the LUV suspension by size exclusion chromatography on a manually packed Sephadex G50 (Sigma Aldrich) column (1 cm X 20 cm), equilibrated and eluted with 300 mM NaCl, 2.7 mM KCl, 10 mM $Na_2HPO_4$, and 2 mM $KH_2PO_4$ (pH 7.4) (buffer X). Before dye release experiments, the freshly prepared liposome stock was diluted 50-fold in buffer X so that the maximal released CF fluorescence was within the range of the fluorimeter. The release of CF, which is self-quenched within the liposomes, was assessed from the increase in fluorescence emission at 520 nm (excitation at 492 nm). At the end of each run, Triton X-100 was added to the cuvette (final concentration of 0.1%) to determine the maximal CF fluorescence.

To determine the effects of the F-amphiphiles, αHL was added to buffer X containing the diluted LUV and the F-amphiphile at the required concentration. The final volume in the cuvette was 1 mL, and the amount of heptamer or monomer was 20

or 5 μg, respectively. The data were analysed with Origin software.

The amount of released CF as a percentage of the total, at time t is given by:

$$R(t) = 100X[I(t) - I(0)]/[I(\infty) - I(0)] \quad (2.5)$$

where the fluorescence intensity at time t is I(t), the initial fluorescence of the liposomes is I(0), and the fluorescence after Triton X-100 addition is I(∞).

### 2.3.3 Single-Channel Recordings.

The apparatus for planar lipid bilayer recording consisted of two compartments separated by a Teflon septum containing an aperture with a diameter of 100 μm. The aperture was pre-treated with a solution of hexadecane in pentane (10%, v/v). To form a bilayer, buffer was added to both compartments at a level below the aperture, and 1,2-diphytanoyl-sn-glycero-3-phosphocholine (DPhPC, Avanti Polar Lipids) in pentane (10 mg/mL) was added to each surface. The pentane evaporates to leave a lipid monolayer at the air-water interface. Sequential lowering and raising of the levels of the buffer solutions fold the two monolayers together to form a vertical lipid bilayer (21). The formation and quality of the bilayers were monitored by capacitance measurements. Currents were recorded under voltage-clamp conditions with Ag/AgCl electrodes.

#### 2.3.3.1 Single-Channel Recordings with F-Amphiphiles.

Control experiments without F-amphiphiles were initiated by the addition of the αHL heptamer or monomer (final concentration of 30 ng/mL), MspA (final concentration of 40 ng/mL), or Kcv (final concentration of 4 ng/mL) to the cis compartment (ground), the contents of which were stirred until insertion of a single channel occurred.

Experiments for examination of the inhibitory effects of F-amphiphiles on the insertion of WT αHL, MspA, or Kcv were initiated by the addition of protein to the cis compartment, which contained (1000 – V) μL of electrolyte, where V is the volume of the F-amphiphile later added to the cis side after channel insertion had occurred. The contents of the cis compartment were stirred briefly after the addition of the F-amphiphile solution. To compensate for the addition of the F-amphiphile solution, an equal volume of water was added to the trans compartment. The low-pass Bessel filter of the amplifier was set at 1 kHz.Data were acquired at a sampling rate of 10 kHz. The data points for the I-V curves, for the WT αHL heptamer, MspA, and Kcv are the mean values from three separate single-channel experiments. The current values obtained in the presence of 10 mM $F_6FC$ (cis) were normalized to the current values obtained in the absence of $F_6FC$ to take into account the reduction in the ionic strength of the recording buffer caused by the addition of the F-amphiphile.

**2.3.3.2 Single-Channel Recordings in β-Cyclodextrin (βCD) Binding Studies.**

The recording buffer contained 1 M NaCl and 10 mM $Na_2HPO_4$ (adjusted to pH 7.5 with aqueous HCl). The experiments were initiated by the addition of ~30 ng of the WT αHL heptamer to the cis compartment with stirring until a channel was inserted. βCD (40 μM) was added to the trans compartment. The internal low-pass Bessel filter of the amplifier was set at 5 kHz, and the acquisition rate was 20 kHz. $\tau_{on}$ and $\tau_{off}$ values for binding of βCD to the WT αHL pore, at (±40 mV, were obtained from dwell-time histograms fitted to single exponentials with Clampfit. To determine kinetic

constants for the association and dissociation of βCD in the presence of the F-amphiphiles, we averaged data from three single-channel experiments.

### 2.3.4 Hemolytic Assay in the Presence of F-amphiphiles.

WT αHL monomer (5 μL of IVTT protein), incubated for 10 min with either 10mM $F_6FC$, 5mM $F_6OM$, or 2mM $C_6$-FTAC in a final volume of 10 μL, was diluted into MBSA [10mM MOPS and 150mM NaCl (pH 7.4) containing 1 mg/mL bovine serum albumin] in the first well of a microtiter plate (final volume of 100 μL). The protein was then subjected to serial 2-fold dilution in MBSA over the remaining 11 wells of the plate row (final volumes of 50 μL). An equal volume of 1% (v/v) washed rabbit erythrocytes (rRBCM) in MBSA was then added to each well, beginning with the most diluted lane. Hemolysis was followed for 1.5 h at 24°C by monitoring the decrease in light scattering at 595 nm with a Bio-Rad microplate reader (model 3550-UV) running MicroplateManager version 4.0.

### 2.3.5 Surface tension measurements with F-amphiphiles

Fluorinated fos-choline ($F_6FC$, purity > 99%) was obtained from Anatrace (cat. F300F). Stock solutions (100mM) were made in water. Stock solutions were diluted as required (1 mM or 10 mM) in water unless stated otherwise. Hexadecane (anhydrous, ≥99%) was purchased from Sigma-Aldrich Co. (cat. 296317). Both $F_6FC$ and hexadecane were used as received. Each experiment was initiated by forming a drop (5μl) of hexadecane in the cuvette containing a solution of F-amphiphile $F_6FC$ in milliQ water (5mL). A video camera continuously monitored the shape of the bubble, from which the surface

tension values were calculated. The surface tension was monitored until the monolayer surface reached equilibrium (i.e surface tension changes by less than 0.1 mN/m over a period of 30 minutes). Between runs, the cuvette was cleaned thoroughly (3 X 1 litre washes) and the syringe needle was cleaned to remove any residual F-amphiphile.

### 2.3.6 Fluorinated droplet interface bilayers

Two types of fluorinated bilayers were studied: (i) symmetric $F_6FC$ bilayers where both leaflets of the bilayer were composed of $F_6FC$ and (ii) asymmetric DPhPC-$F_6FC$ bilayers one leaflet of which was composed exclusively of the single chain F-amphiphile $F_6FC$ and the other of the double chain hydrocarbon lipid DPhPC. Both types of bilayer were formed using the "lipid-in" method of forming droplet interface bilayers.

#### 2.3.6.1 Sample preparation

Liposomes of DPhPC were prepared by extrusion as follows: 25 mg of 1, 2-Diphytanoyl-*sn*-glycero-3-phosphocholine (DPhPC, Avanti Polar Lipids, Alabaster, AL) was dissolved in pentane (2.5 mL) (Sigma Aldrich, Dorset, UK) and dried under a stream of nitrogen in a glass vial. The lipid was dried further under vacuum in a desiccator for 1-2 hours and then rehydrated (by vortexing) with buffer (1M KCL, 10mM Tris, pH 7.0) to give a final concentration of 10mM. DPhPC liposomes were prepared by extrusion (Mini-Extruder, Avanti Polar Lipids, Alabaster, AL) of the lipid suspension through two 0.1 μm polycarbonate membrane filters. The extruded

liposomes were divided into aliquots of 0.5 mL and stored at 4°C. Fluorinated fos-choline ($F_6FC$) was obtained from Anatrace. Stock solutions (100mM) were made and stored at 4°C. Stock solutions were diluted as required (1mM or 10mM) in 1M KCl, 10mM Tris, pH 7.0.

### 2.3.6.2 Electrical recording

Droplet interface bilayers were formed as previously described by Holden et al. in 2007 [12, 19]. The experimental chamber was filled with the oil phase hexadecane (~400µl). Two Ag/AgCl wire electrodes were mounted onto two separate micromanipulators to enable independent positioning of the droplets. The tip of the Ag/AgCl electrodes were coated with 5 %( w/v) low-melt agarose which served as a hydrophilic anchor from which droplets could be hung. Typically, ~250 nL droplets of the desired solution were manually deposited onto the electrodes by bringing the tip of a pipette under the oil very close to the electrode and carefully extruding the droplet out of the pipette tip. For symmetric DPhPC bilayers, a 1 mM DPhPC vesicle solution in 1M KCl 10mM Tris, pH 7.0 buffer solution was hung on both electrodes. For asymmetric DPhPC-$F_6FC$ bilayers, 1mM DPhPC vesicle solution in 1M KCl, 10mM Tris, pH7.0 was hung on one electrode, while $F_6FC$ in 1M KCl, 10mM Tris, pH 7.0 (either 1mM or 10mM depending on the experiment) was hung on the other electrode. For symmetric $F_6FC$ bilayers, $F_6FC$ in 1M KCl, 10mM Tris, pH 7 (10mM unless specified otherwise) was hung on both electrodes. The droplets on the electrode were allowed to incubate in the oil at room

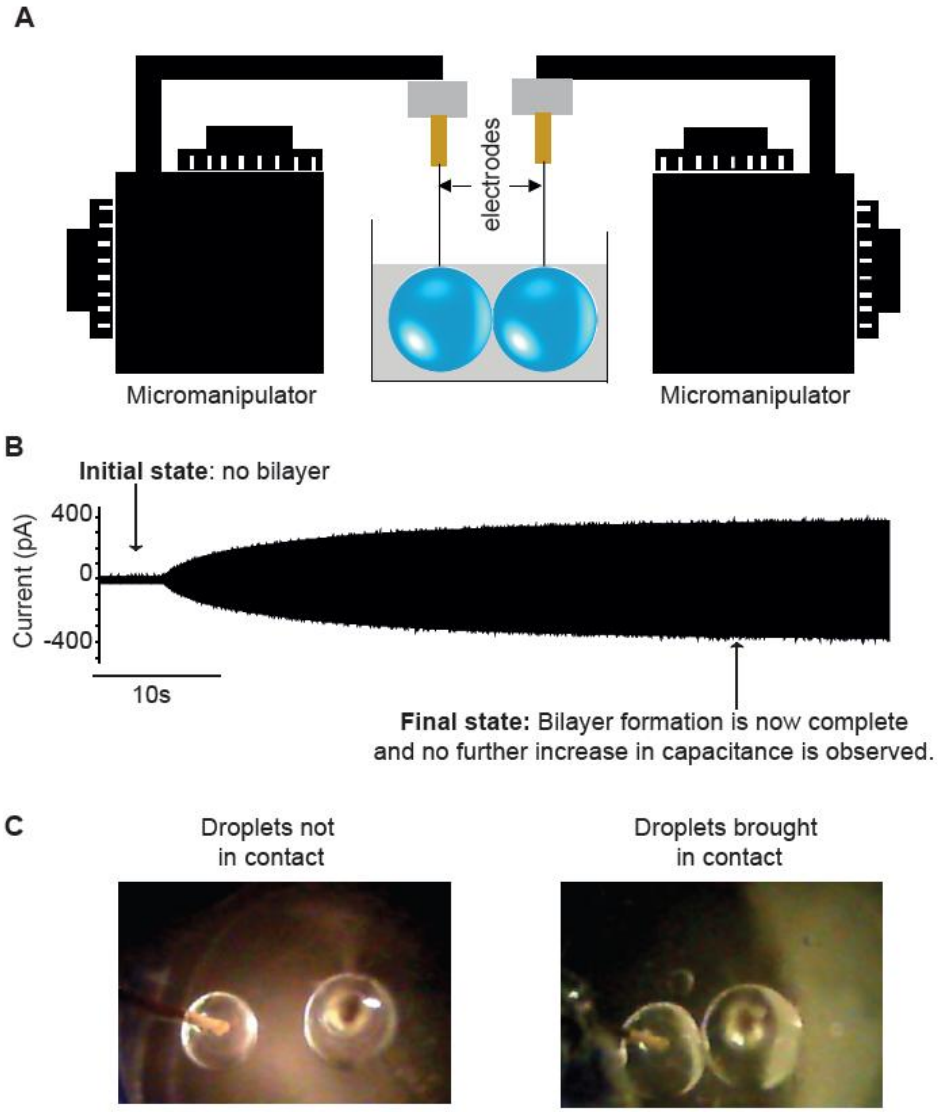


**Figure 2.11:** *Formation of Droplet Interface Bilayers (DIBs). (A) The set-up used for the formation of DIBs. A chamber is filled with hexadecane oil (grey). The droplets were suspended from two Ag/AgCl electrodes which were attached to independent micromanipulators. After an incubation period (few minutes to hours) which allows a lipid monolayer to self –assemble at the droplet-oil interphase, the droplets are brought into contact to form droplet interface bilayers (DIBs). (B) Bilayer formation was observed by measuring the square-wave current response to an applied triangular-wave potential input. Bilayers usually take 30-40 seconds to form. (C) Bright field images of two aqueous droplets in an oil-lipid medium suspended by Ag/AgCl electrodes demonstrating the initial (droplets were separated) and final state (droplets brought into contact) of the droplets.*

temperature until the droplets had acquired a densely packed well-ordered lipid monolayer (this process was termed stabilization). When two stabilized droplets were brought together using the micromanipulator, bilayer formation occurred spontaneously which was observed as an increase in capacitance (determined by applying a triangular voltage wave) (Figure 2.11).

**2.3.6.3 Data analysis**

Even when the droplets are not connected, there exists a background capacitance ($C_o$) which arises from the residual capacitance in the acquisition electronics and device components (Figure 2.11B). On bilayer formation the measured capacitance is the total capacitance ($C_T$) which is the sum of the background capacitance ($C_o$) and the area-dependent bilayer membrane capacitance ($C_M$) (i.e. $C_T = C_o + C_M$). For all protein measurements, the droplet containing the protein (supplemented with either DPhPC or F-amphiphile) was connected to the grounded end of the patch-clamp head-stage. The opposing electrode with the protein-free buffer droplet was connected to the working end of the head-stage. The internal low-pass Bessel filter of the amplifier was set at 1 kHz, and the acquisition rate was 10 kHz.

Apart from studying the behaviour of the protein (I-V curve) in DPhPC and fluorinated bilayers, I also tried to compare the open-pore noise in the two bilayers. Noise in single-channel recording experiments can arise from a variety of sources: (i) noise originating in the acquisition electronics (ii) noise from the resistance of the solutions and electrodes and, (iii) noise from the protein [20]. The largest source of

noise is from the protein pore itself and it arises from extremely fast fluctuations in conformation and charge states inside a pore [21, 22].

In order to be able to estimate the noise arising from the protein, the system noise (electronics and solution) was subtracted from the total noise. The noise was determined from the standard deviation (σ) of the Gaussian fit to the current histograms at the respective voltage. In the absence of an applied potential (zero mV) the fluctuations/noise in the current recording provide an estimate of the system noise ($\sigma^{0mV}$). However, at an applied potential of +100 mV (trans is positive, relative to the grounded cis), a current flows through the pore and the noise in the current ($\sigma^{+100mV}$) recording contains contributions from both the noise of the pore and the noise of the system (total noise). The open-pore noise was calculated from the equation 2.6 given below:

$$\text{"Open-pore" noise} = \sqrt{\text{Total noise}\,(\sigma^{+100mV}) - \text{System noise}\,(\sigma^{0mV})} \qquad (2.6)$$

## 2.4 Bibliography

[1] S. Bhakdi and J. Tranumjensen, "Alpha-toxin of staphylococcus-aureus," *Microbiological Reviews*, vol. 55, pp. 733-751, Dec 1991.

[2] J. E. Gouaux, O. Braha, M. R. Hobaugh, L. Z. Song, S. Cheley, C. Shustak, *et al.*, "Subunit stoichiometry of staphylococcal alpha-hemolysin in crystals and on membranes - a heptameric transmembrane pore," *PNAS*, vol. 91, pp. 12828-12831, Dec 1994.

[3] O. V. Krasilnikov, P. G. Merzlyak, L. N. Yuldasheva, C. G. Rodrigues, S. Bhakdi, and A. Valeva, "Electrophysiological evidence for heptameric stoichiometry of ion channels formed by Staphylococcus aureus alpha-toxin in planar lipid bilayers," *Molecular Microbiology*, vol. 37, pp. 1372-1378, Sep 2000.

[4] A. Hildebrand, M. Pohl, and S. Bhakdi, "Staphylococcus-aureus alpha-toxin - dual mechanism of binding to target-cells," *JBC*, vol. 266, pp. 17195-17200, Sep 1991.

[5] L. Z. Song, M. R. Hobaugh, C. Shustak, S. Cheley, H. Bayley, and J. E. Gouaux, "Structure of staphylococcal alpha-hemolysin, a heptameric transmembrane pore," *Science*, vol. 274, pp. 1859-1866, Dec 1996.

[6] L. Jayasinghe, G. Miles, and H. Bayley, "Role of the amino latch of staphylococcal alpha-hemolysin in pore formation - A co-operative interaction

between the N terminus and position 217," *JBC,* vol. 281, pp. 2195-2204, Jan 2006.

[7] M. Montoya and E. Gouaux, "beta-barrel membrane protein folding and structure viewed through the lens of alpha-hemolysin," *Biochimica Et Biophysica Acta-Biomembranes,* vol. 1609, pp. 19-27, Jan 2003.

[8] H. Bayley, "Membrane-protein structure Piercing insights," *Nature,* vol. 459, pp. 651-652, Jun 2009.

[9] J. R. Thompson, B. Cronin, H. Bayley, and M. I. Wallace, "Rapid Assembly of a Multimeric Membrane Protein Pore," *Biophys. J.,* vol. 101, pp. 2679-2683, Dec 2011.

[10] D. Stoddart, "Progress Towards Ultra-rapid DNA Sequencing with Protein Nanopores," PhD, Chemistry Research Laboratory, University of oxford, Oxford, 2011.

[11] M. Montal and P. Mueller, "Formation of bimolecular membranes from lipid monolayers and a study of their electrical properties," *PNAS,* vol. 69, pp. 3561-3566, 1972.

[12] M. A. Holden, D. Needham, and H. Bayley, "Functional bionetworks from nanoliter water droplets," *JACS,* vol. 129, pp. 8650-8655, Jul 2007.

[13] L. C. M. Gross, A. J. Heron, S. C. Baca, and M. I. Wallace, "Determining Membrane Capacitance by Dynamic Control of Droplet Interface Bilayer Area," *Langmuir,* vol. 27, pp. 14335-14342, Dec 2011.

[14] D. P. Valenzeno and J. W. Trank, "Measurement of cell-lysis by light-scattering," *Photochemistry and Photobiology,* vol. 42, pp. 335-339, 1985.

[15] B. Francis and J. C. Adams, *an attempt to test the theories of capillary action.* London: Cambridge University Press, 1882.

[16] G. Maglia, M. Henricus, R. Wyss, Q. H. Li, S. Cheley, and H. Bayley, "DNA Strands from Denatured Duplexes are Translocated through Engineered Protein Nanopores at Alkaline pH," *Nano Letters,* vol. 9, pp. 3831-3836, Nov 2009.

[17] A. Mason, "Single-channel characterisation of potassium channels with high temperature studies.," PhD, Chemistry Research Laboratory, University of Oxford, Oxford, 2008.

[18] A. J. Heron, J. R. Thompson, A. E. Mason, and M. I. Wallace, "Direct detection of membrane channels from gels using water-in-oil droplet bilayers," *JACS,* vol. 129, pp. 16042-16047, Dec 2007.

[19] B. Cronin, A. Heron, M. A. Holden, W. L. Hwang, R. Syeda, and H. Bayley, "Droplet interface bilayers," *Molecular biosystems,* vol. 4, pp. 1191-208, 2008.

[20] G. Maglia, A. Heron, J., D. Stoddart, D. Japrung, and H. Bayley, "Analysis of single nucleic acid molecules with protein nanopores," *Methods Enzymol,* vol. 475, pp. 591-623, 2010.

[21] Y. E. Korchev, C. L. Bashford, G. M. Alder, P. Y. Apel, D. T. Edmonds, A. A. Lev*, et al.,* "A novel explanation for fluctuations of ion current through narrow pores," *Faseb Journal,* vol. 11, pp. 600-608, Jun 1997.

[22] S. M. Bezrukov and J. J. Kasianowicz, "Current noise reveals protonation kinetics and number of ionizable sites in an open protein ion channel," *Physical Review Letters*, vol. 70, pp. 2352-2355, Apr 1993.

# Chapter 3

# Effect of fluorinated amphiphiles on protein insertion in pre-formed bilayers.

**Declaration 1**

The work in this chapter is also described in the manuscript:

"Fluorinated Amphiphiles Control the Insertion of α-Hemolysin Pores into Lipid Bilayers." Pinky Raychaudhuri, Qiuhong Li, Amy Mason, Ellina Mikhailova, Andrew J. Heron, and Hagan Bayley. Biochemistry, 2011, 50 (10), pp 1599–1606.

*Author contributions:* P.R. performed all experiments (single channel recordings, fluorescence assays, and haemolytic assays); E.M, A.H, Q.L, and A.M performed the mutant and protein preparations; P.R. analysed data; and P.R. and H.B. wrote the paper.

**Declaration 2**

The work in this chapter has also been patented:

Name of patent: Method using fluorinated amphiphiles
Inventors: Bayley Hagan, Raychaudhuri Pinky
Year of patent: 2012
Country of patent: United Kingdom
International publication number: WO 2012/095660 A2
Date of filing: 11.01.2012
International publication date: 19.07.2012

# CHAPTER 3

## 3.1 Introduction

### 3.1.1 F-amphiphiles as alternatives to detergents for membrane protein studies

Proteins which span the lipid membrane can be solubilized by reagents that destroy the lipid bilayer with subsequent protein release. A special class of amphiphilic molecules called surfactants (Eg: SDS, Triton X) have been extensively used for the solubilisation and purification of membrane proteins. Sadly, such strong surfactants often unfold (denature) the membrane proteins, thereby rendering them inactive and unusable for functional studies.

In the search for new amphiphilic molecules which are not denaturing, fluorinated amphiphiles seem like a good alternative [1]. Unlike conventional hydrogen amphiphiles (H-amphiphiles), F-amphiphiles have been previously reported to not solubilize lipid membranes above their reported CMC due to the mutual immiscibility of fluorocarbons and hydrocarbons [2]. This property opened up interesting possibilities for the use of F-amphiphiles in investigations of membrane proteins.

The first effort in this direction by Shepherd et al. reported that ammonium perfluorooctanoate (APFO) was capable of solubilizing proteins from a wide range of membranes, but the solubilised proteins showed a strong tendency to aggregate [3]. Since APFO was highly charged, it had high solubility in water and it was possible to reach very high concentrations of the fluorinated detergent (40-80g/L) and at such high concentrations the membranes were compromised and the proteins were denatured. Subsequently many milder fluorinated amphiphiles were synthesized, which could no

longer solubilize membranes. However, after solubilisation of native membranes using a classical detergent, a variety of perfluorinated and hemifluorinated amphiphiles could substitute the latter to keep membrane proteins water-soluble [4-7]].

Recently, both perfluorinated and hemifluorinated amphiphiles have been shown to prevent the aggregation of the pore-forming fragment of diphtheria toxin at low pH, thereby making it available for insertion into liposomes [8, 9]. In 2007, Park et al. demonstrated that F-amphiphiles were compatible with the in-vitro protein synthesis, folding, and oligomerization of the pentameric mechanosensitive channel MscL [10]. It was also the first report to suggest that F-amphiphiles facilitate direct and rapid incorporation of functional MscL into liposomes. On reconstitution into liposomes, it was reported to have activities similar to MscL synthesised either *in vitro* in presence of Triton X-100 or *in vivo.* Recent reports have extended this work to show that the compatibility of F-amphiphiles with cell free synthesis could be extended to other proteins such as a trans-membrane protease, the bacterial Leader peptidase (Lep) and to other F-amphiphiles such as (H)F-Lac and (H)F-Diglu [11, 12].

Another study with fluorinated amphiphiles looked at the effect of F-amphiphiles on the insertion of Annexin B12 (ANX) into liposomes [13]. The insertion of ANX into membranes is reversible and the presence of F-amphiphiles caused a gradual decrease in ANX partitioning into the membranes. The study reports that since F-amphiphiles do not partition into or disrupt a bilayer even at high concentrations (above CMC) or even when present in overwhelming excess over lipid, they can be used to distribute membrane proteins between the lipid bilayer and the aqueous phase.

Based on this study, we wanted to study the insertion of tightly-binding membrane proteins into a lipid bilayer in presence of varying concentrations of F-amphiphiles.

### 3.1.2 Chapter overview

The work in this chapter adds significantly to the scope of previously reported work on F-amphiphiles and the results from this chapter provided the base and motivation for the work carried out in chapter four. We study the effect of F-amphiphiles on the membrane insertion of proteins which bind tightly to bilayers (unlike ANX which inserts reversibly). First, I study the insertion of both the *wild type* alpha-hemolysin (wtαHL) monomer and heptamer into pre-formed liposomes and planar lipid bilayers. The results show that the addition of F-amphiphile stops the insertion of new alpha-hemolysin channels in bilayers while not affecting the channels already inserted in the bilayer. Similar observations were made with other mutants of αHL, and other proteins such as MspA and Kcv. Finally, I speculate on some plausible mechanisms of action.

The following three F-amphiphiles were investigated for their suitability in membrane protein studies (i) $C_6$-FTAC ($C_6F_{13}C_2H_4$-*S*-poly [tris(hydroxymethyl)aminomethane]) [10]. $C_6$-FTAC was chosen because its effects on protein insertion into lipid bilayers have been it has been reported before [13]. It was found to reduce partitioning of ANX into lipid bilayers. $C_6$-FTAC was a kind gift from Prof. Bernard Pucci (Avignon, France) and was synthesized in his laboratory by radical polymerization in the presence of perfluoroalkanethiols as a transfer reagent [14]. The two other F-amphiphiles used in this study although commercially available, have not

been studied before: (ii) $F_6FC$ (Fos-Choline-8, Fluorinated from Affymetrix, Inc.) and (iii) $F_6OM$ (Octyl Maltoside, Fluorinated from Affymetrix, Inc.). Their structures are given below (Figure 3.1).

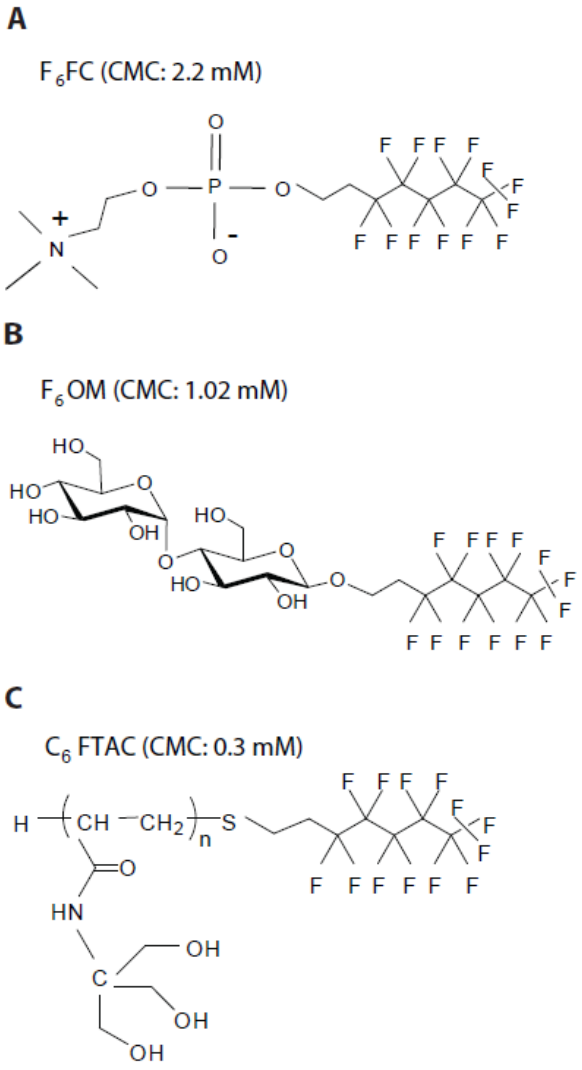


**Figure 3.1:** *Chemical structures and CMC values of the F-amphiphiles used in this study.*

## 3.2 Results and Discussion

### 3.2.1 Effects of F-Amphiphiles on lipid membranes

Unlike routinely used hydrocarbon based detergents in membrane protein studies, $C_6$-FTAC has been previously reported to be non-hemolyzing and not solubilize pre-formed liposomes even at concentrations above its CMC [10]. As discussed in chapter one, this interesting property of F-amphiphiles arises from the immiscibility of fluorocarbons and hydrocarbons, because of which F-amphiphiles do not partition into lipid bilayers. However, effects of the commercially available $F_6$FC and $F_6$OM on lipid bilayers have not been previously evaluated. Their effects on lipid membranes were investigated in two different systems. I tested for the hemolyzing ability (ability to lyse red blood cells) of $F_6$FC and $F_6$OM. In addition, I also studied the stability of pre-formed planar DPhPC lipid bilayers in presence of varying concentrations of $F_6$FC, $F_6$OM, and $C_6$FTAC.

The hemolyzing activity of F-amphiphiles was tested using a hemolytic assay. The absence of a decrease in the scattering of the erythrocytes at 595nm (for details see chapter 2, section 2.2.2) suggested that both $F_6$FC and $F_6$OM (even at 25 times the reported CMC) lacked lytic activity towards 1% (v/v) rRBC over the timescales tested (Figure 3.2). This result agrees well with previous studies which have reported the non-hemolytic property of F-amphiphiles for a number of structurally diverse fluorinated amphiphiles [15].

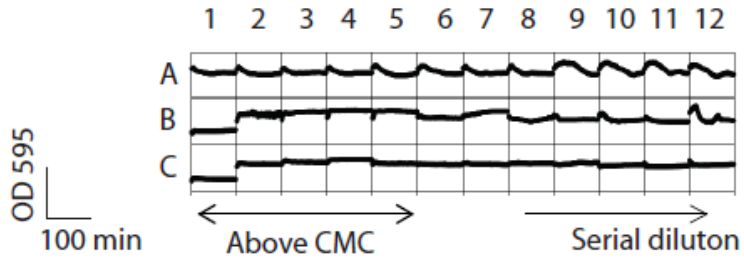


**Figure 3.2*:* Hemolytic assay to study the hemolytic effect of $F_6FC$ and $F_6OM$ on 1% rRBC.** *Lane A: MBSA buffer control. Lane B: $F_6FC$ incubated with rRBCs. Lane C: $F_6OM$ incubated with rRBCs. The final concentrations of $F_6FC$ and $F_6OM$ were 50mM and 20mM in wells B1 and C1 respectively. The F-amphiphiles samples were then subjected to 2-fold serial dilution in MBSA buffer over the 11 remaining wells (final volume of 50 μL per well), followed by the addition of washed 1% (v/v) rRBCs (50 μL) to each well.*

Next, the stability of *pre-formed* planar DPhPC lipid bilayers was tested in the presence of $F_6FC$, $F_6OM$ and $C_6$-FTAC at three final concentrations: (i) above CMC (ii) at CMC (iii) below CMC. Most experiments (eg: single strand DNA sequencing) carried out with the αHL pore in our lab are done at potentials in excess of 150mV [16] and for this reason bilayer stability in presence of F-amphiphiles was assessed at 150mV. In control experiments, in the absence of F-amphiphiles, bilayers stayed stable (i.e low leak current (≤ 1pA) and bilayers did not rupture during the course of the experiment) at applied potentials of 150mV for more than 30 minutes and could reform easily if broken (Figure 3.3A). At all the three concentrations of $F_6FC$ tested, the bilayer was stable at 150mV for more than 30 minutes (Figure 3.3A). A similar observation was made for all three concentrations of $C_6$F-TAC tested. In contrast, at all three concentrations tested, the addition of $F_6OM$ to bilayers led to an immediate increase in the bilayer capacitance (Figure 3.3.B), followed by the bilayers becoming leaky

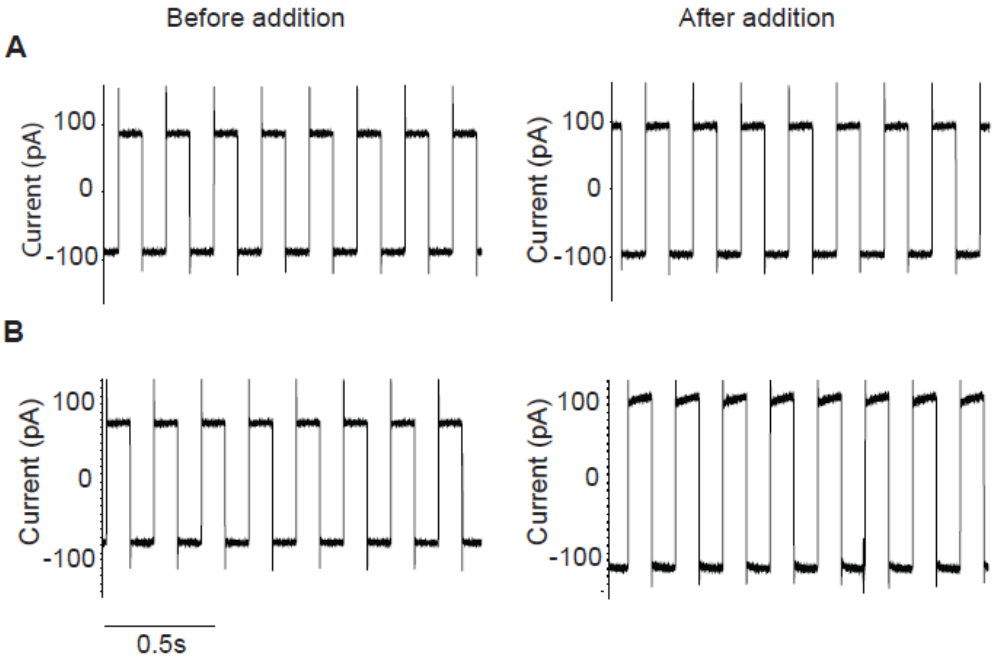


**Figure 3.3*:* Bilayer capacitance and stability in presence of F-amphiphiles.** *(A) Representative bilayer trace in presence of $F_6FC$ or $C_6FTAC$. As can be seen, there is no change in bilayer capacitance and the bilayers are also stable (B) Representative bilayer trace in presence of $F_6OM$. The bilayer capacitance increases from 75pF to 100pF on addition of $F_6OM$ and the bilayers are also leaky. Buffer used was 1M KCL, 10mM Tris, pH 7 and the applied potential was 150mV.*

which never survived beyond a couple of minutes and sometimes broke even in the absence of any applied potential. As $F_6OM$ always rendered preformed bilayers unstable, protein studies in planar bilayers were confined to $F_6FC$ and $C_6$-FTAC.

However, it was observed that in case of all three F-amphiphiles tested (irrespective of concentration) the bilayer once broken, was extremely difficult to reform. In few cases when it did reform, it broke soon after.

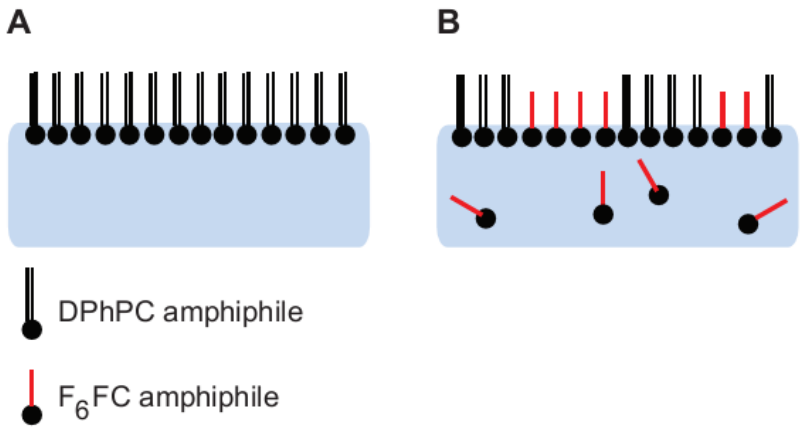


**Figure 3.4: Competing monolayer and bilayer formation in presence of F-amphiphiles:** *(A) In the absence of F-amphiphiles, a 100% DPhPC monolayer forms at the air-water interface in the two chambers on either side of the teflon film. These monolayers are then sequentially raised (by adding more buffer) to form a bilayer across the aperture in the Teflon film. (B) In the presence of F-amphiphiles, we speculate that the F-amphiphiles compete with DPhPC amphiphiles to form monolayers at the air-water interface and bilayers at the aperture on the Teflon film. This can explain why a DPhPC bilayer cannot be formed in presence of F-amphiphiles, although F-amphiphiles do not disrupt a pre-formed DPhPC bilayer.*

This observation seemed to suggest that although F-amphiphiles did not disrupt a pre-formed DPhPC bilayer, it interfered with bilayer formation. Planar lipid bilayers are formed by bringing together the lipid monolayers formed at the air-water interface on either side of the Teflon film. It is likely that F-amphiphiles interfere in bilayer formation by competing with DPhPC at the air-water interface for monolayer formation resulting in a mixed monolayer (Figure 3.4). Such competitive adsorption of amphiphiles at the air-water interface has been previously reported for mixed fluorocarbon-hydrocarbon systems [17].

### 3.2.2 Effect of F-amphiphile on insertion of wt-alpha hemolysin in liposomes

Alpha-hemolysin is a β-barrel pore forming toxin secreted by *Staphylococcus aureus* as a water-soluble monomer comprising 293 residues [18]. The 33.2 kDa, monomers first oligomerize to form a heptameric pre-pore on the bilayer surface. The pre-pore then undergoes a conformational reorganization, forming a β-barrel during insertion into the bilayer [19, 20]. On the other hand preformed αHL heptamers with bound detergent have been reported to insert directly into lipid bilayers [21]. The trans-membrane pore causes permeabilization of the bilayer to ions, water and is capable of transporting molecules as large as 2-4kDa.

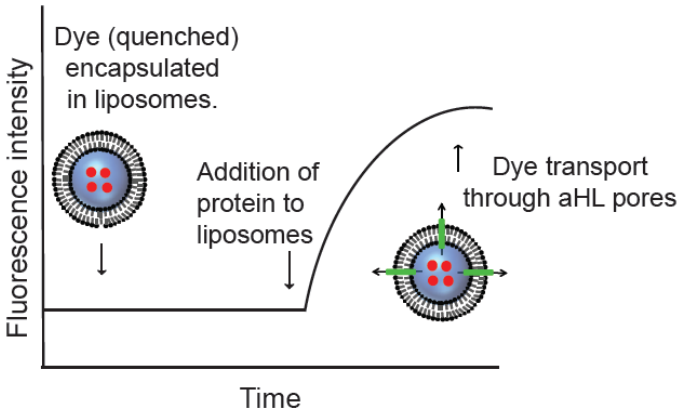


**Figure 3.5: Schematic to explain the principle behind dye leakage from liposomes in presence of pore forming protein.** *In the absence of protein, the dye encapsulated in the liposomes are quenched and almost non-fluorescent. On pore formation, the dye exits into the bulk solution outside the liposome where it gets diluted leading to a regain in fluorescence.*

A dye leakage assay was chosen as an initial assay to investigate any possible effects that F-amphiphiles might have on incorporation of αHL into liposome (LUV)

membranes. The dye chosen for the leakage assays was 5(6)-carboxyfluorescein. This fluorescent dye has two carboxyl groups and the double negative charge reduces the permeability of the dye across the lipid membrane and therefore the dye does not leak rapidly from liposomes. When encapsulated within liposomes at high concentration (0.2M), the dye is virtually non-fluorescent due to the formation of non-fluorescent dimers of 5(6) carboxyfluorescein [22]. When pores are formed in the liposomes due to insertion of the protein, the dye is released from the liposome, gets diluted and results in an increase in fluorescence (Figure 3.5). To cause dye leakage, the αHL monomer must both assemble and insert into the LUV bilayer, while the preformed αHL heptamer must undergo direct insertion from dilute detergent. At the end of the assay, the maximal fluorescence signal is measured after the liposomes are lysed with detergent. Both the αHL monomer and the pre-formed αHL heptamer were examined in the presence of the F-amphiphiles, each at three concentrations: (i) below the CMC, (ii) at around the CMC, and (iii) above the CMC. None of three F-amphiphiles caused any leakage from the liposomes in absence of protein. This is in accordance with previously published reports [8]. At concentrations above the CMC, $F_6FC$, $F_6OM$ and $C_6$-FTAC was found to completely prevent both the αHL monomer and the αHL heptamer from permeabilizing the liposomes as no dye leakage was observed (Figure 3.6). Lower concentrations of the F-amphiphiles slowed αHL insertion to varying extents when compared to control experiments in the absence of F-amphiphiles. In control experiments the F-amphiphiles were found to have no effect on the fluorescent properties of the dye.

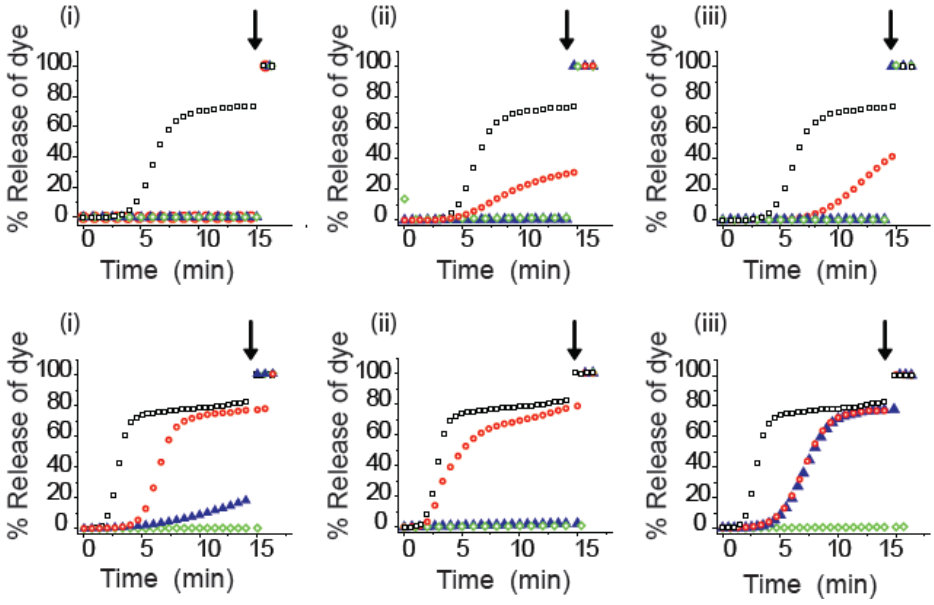


**Figure 3.6**: **Dye leakage assays to determine the effects of F-amphiphiles on LUV permeabilization by αHL.** *The release of self-quenched CF causes an increase in fluorescence emission at 520 nm, which is monitored in the assays. Upper panel: (i) insertion of αHL monomer in the presence of $F_6FC$; (ii) insertion of αHL monomer in the presence of $F_6OM$; (iii) insertion of αHL monomer in the presence of $F_6TAC$. Lower panel: (i) insertion of αHL heptamer in the presence of $F_6FC$; (ii) insertion of αHL heptamer in the presence of $F_6OM$; (iii) insertion of αHL heptamer in the presence of $F_6TAC$. The traces are color coded: insertion of αHL in the absence of an F-amphiphile (black open squares); insertion of αHL at below the CMC (red open circles); insertion of αHL at around the CMC (blue filled triangles); insertion of αHL at above the CMC (green open diamonds). The arrow in each trace indicates the addition of Triton X-100 to the cuvette to fully lyse the liposomes.*

Dye leakage experiments in liposomes described above are ensemble measurements and give little information about the effects (if any) of F-amphiphiles on the properties of single channels of α-hemolysin. To resolve this issue, single-channel current recording experiments were performed in presence of F-amphipiles. This method enables direct monitoring of channel properties such current rectification, gating etc.

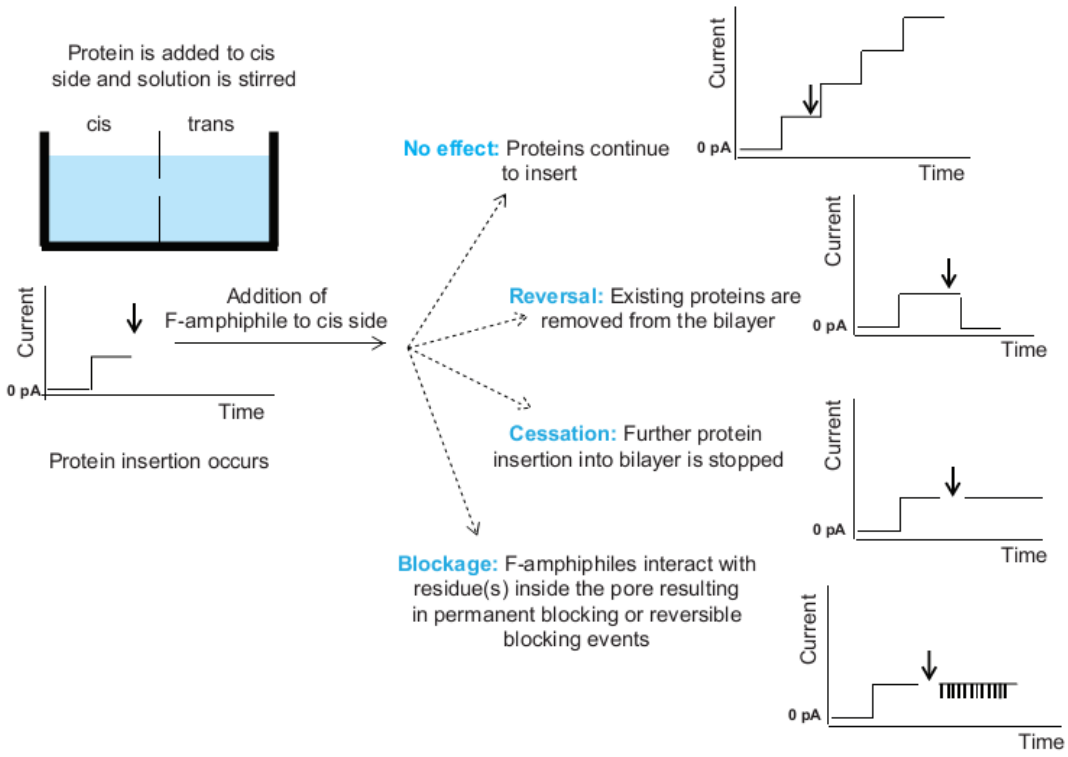


**Figure 3.7: Possible outcomes after addition of F-amphiphiles in the planar bilayer chamber:** *(i) the addition of F-amphiphiles has no effect on the insertion of proteins into the bilayer (ii) the addition of F-amphiphiles removes already inserted protein from the bilayer. This will result in a decrease in the measured current (iii) the addition of F-amphiphiles prevents new protein from going into the bilayer (iv) the addition of F-amphiphiles results in "blocking events" of the already inserted pore.*

### 3.2.3 Effect of F-amphiphile on wt-alpha hemolysin insertion in planar bilayers

This work employs the use of a chamber which contains two sides separated by a Teflon septum (contains an aperture approximately 100 μm in diameter). Each side of the chamber also contains areas that accommodate an Ag/AgCl electrode, which allows a potential to be applied to the solution. The two sides of the chamber are electrically isolated by forming a bilayer across the aperture. αHL proteins can be inserted into the

bilayer by addition into the solution in one of the chambers (usually the cis side), followed by stirring or pipetting the solution (details of the method can be found in Chapter 2).The addition of F-amphiphiles into the cis side on protein insertion could result in one or combinations of the following possibilities: (i) the addition of F-amphiphiles has no effect on the insertion of proteins into the bilayer (ii) the addition of F-amphiphiles removes already inserted protein from the bilayer. This will result in a decrease in the measured current (iii) the addition of F-amphiphiles prevents new protein from going into the bilayer (iv) the addition of F-amphiphiles results in "blocking events" of the already inserted pore. All these possibilities are summarized in figure 3.7.

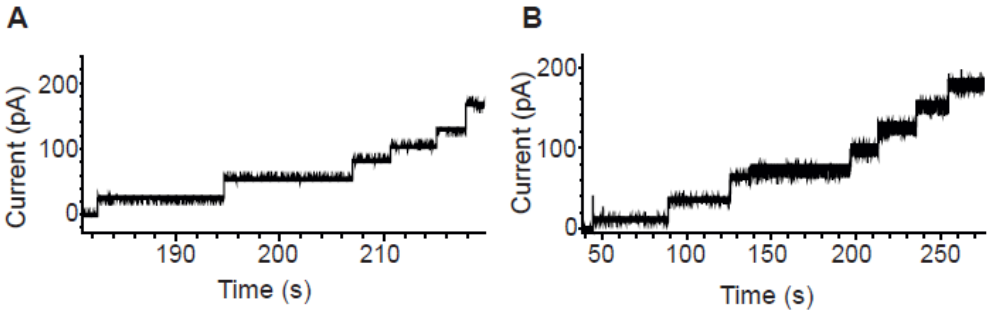


**Fig 3.8: Multi-channel insertions of alpha-hemolysin:** *(A) αHL heptamer (B) αHL monomer. The recording buffer was 300 mM NaCl, 2.7 mM KCl, 10 mM $Na_2HPO_4$, and 2 mM $KH_2PO_4$ (pH 7.4) and the applied potential was +100mV.*

In control experiments, in the absence of F-amphiphiles, multiple insertions of wt-αHL heptamers and monomers were observed when these proteins were added to the cis compartment (electrically grounded side) of the bilayer apparatus (Figure 3.8). In another control experiment, when F-amphiphiles were present in the trans compartment, (i.e the chamber opposite to the chamber in which protein was added) at final

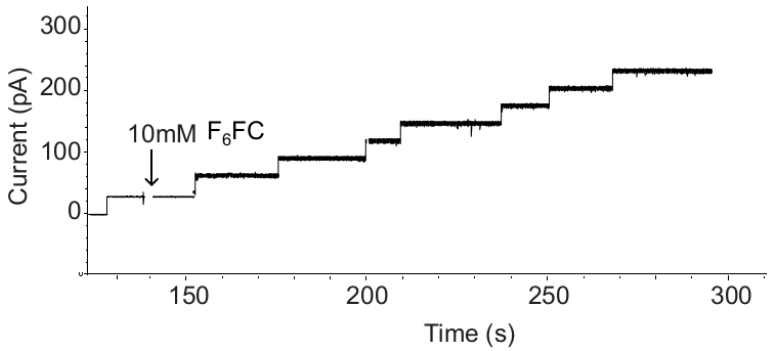


**Figure 3.9***: Effect of trans addition of F-amphiphiles on αHL pore formation in planar lipid bilayers. Multiple insertions of WT αHL heptamers (cis) can be seen when $F_6FC$ (10 mM) is added to the trans side. The recording buffer was 300 mM NaCl, 2.7 mM KCl, 10 mM $Na_2HPO_4$, and 2 mM $KH_2PO_4$ (pH 7.4)and the applied voltage is +100mV. The arrow indicates the point during the experiment when the F-amphiphile was added.*

concentrations above the CMC, it did not affect insertion of αHL into bilayers (Figure 3.9). By contrast, both $F_6FC$ and $C_6$-FTAC, when present at concentrations above the CMC in the cis compartment, caused complete arrest but not reversal of the insertion of both the αHL heptamer and monomer (Figure 3.10). The presence of F-amphiphiles at such high concentrations did not cause any blockade of the wild type α-hemolysin channel.

### 3.2.4 F-amphiphiles can control the number of proteins in the bilayer

In the previous section, I report that the addition of F-amphiphiles prevents more αHL protein from going into the bilayer. We wanted to assess the utility of this observation as a means to control very efficiently the number of proteins in the lipid bilayers. The principle being that the addition of F-amphiphiles after the desired number of channels have gone in, will prevent further channels from going in. As a proof of concept, I

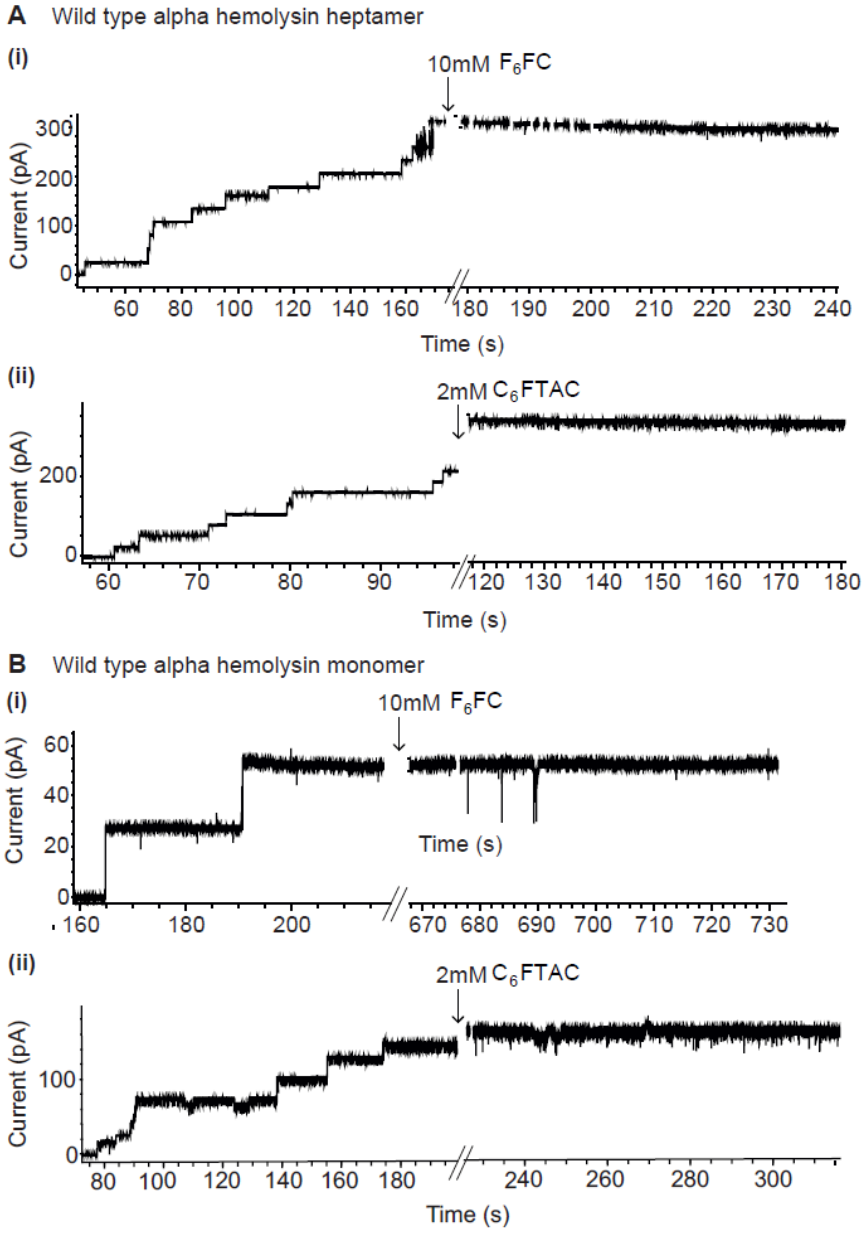


**Figure 3.10: Effects of F-amphiphiles on αHL pore formation in planar lipid bilayers.** *(A) Arrest of the insertion of αHL heptamers: (i) by the addition of $F_6FC$ (10 mM, cis). and (ii) by the addition of $C_6$-FTAC (2mM, cis). (B) Arrest of the insertion of αHL monomers: (i) by the addition of $F_6FC$ (10 mM, cis). and (ii) by the addition of $C_6$-FTAC (2mM, cis). All recordings were made in 300 mM NaCl, 2.7 mM KCl, 10 mM $Na_2HPO_4$, and 2 mM $KH_2PO_4$ (pH 7.4) at +100mV. The arrows indicate the point during the experiment when the F-amphiphiles was added.*

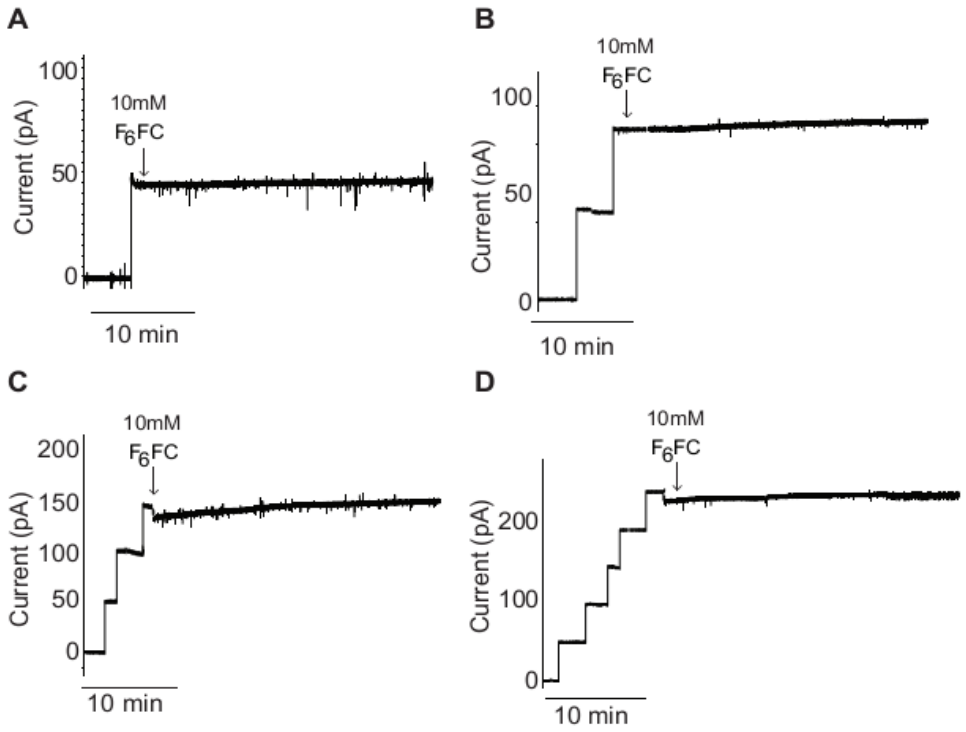


**Figure 3.11: F-amphiphiles provide a means to effectively control the exact number of proteins in the bilayer.** *The F-amphiphile $F_6FC$ (10mM, cis) is added after the desired number of channels have gone into the bilayer. (A) The addition of $F_6FC$ after a single channel has inserted (B) The addition of $F_6FC$ after two channels have inserted (C) The addition of $F_6FC$ after three channels have inserted (D) The addition of $F_6FC$ after five channels have inserted. In all cases, channel insertion into bilayer was monitored over a period of 30 minutes (experiment was stopped after 30 minutes). These recordings were made in 1M KCL, 10mM Tris, pH 7.0 at +50mV. The arrows indicate the point during the experiment when the F-amphiphiles was added.*

demonstrate that by using F-amphiphiles, I can get exactly one, two, three and five channels respectively in the bilayer (Figure 3.11). To be able to control the number of proteins in the bilayer is extremely important for single molecule measurements. Our laboratory examines the single-molecule chemistry of small molecules using single-channel current measurements which can reveal rare reaction pathways or illuminate

fast reaction steps embedded between slow steps. Thus, we envisage that F-amphiphiles might prove useful in single-molecule studies.

### 3.2.5 F-amphiphiles do not affect pores already inserted in the membrane

As described before, no reversal of channel insertion was observed on addition of the F-amphiphiles to the bilayer. However, to be of genuine utility in controlling insertion of protein into lipid bilayers, the addition of F-amphiphile should not affect the functional properties of pores and channels that have already inserted into bilayers. As a proof of concept, the detailed characterization of the pore properties in presence of F-amphiphiles was carried out with $F_6FC$. This choice was dictated by the fact that the $F_6FC$ amphiphile is commercially available.

In routinely used buffered salt solutions, the α-hemolysin pore exhibits no gating and remains open for extended periods of time at trans-membrane potentials of less than ±100mV. The presence of an unpaired negatively charged residue D128 at the *trans* entrance to the β-barrel provides a significant acceleration for cation flow through the channel [23]. This affects the symmetry in ion conduction and the αHL pore is known to be slightly anion selective with a higher conductance at positive voltages (rectification). This results in an asymmetric current-voltage (I-V) graph for αHL (Figure 3.12A). The unitary αHL channel conductance in 300 mM NaCl, 2.7 mM KCl,10 mM $Na_2HPO_4$, and 2 mM $KH_2PO_4$ pH 7.4 buffer was determined to be 276±20pS (+100mV) and 213±6pS (-100mV) in the absence of F-amphiphiles and 260±23pS (+100mV) and 205±10pS (-100mV) in the presence of $F_6FC$. The

rectification ratios (defined as $I_{+100mV}$ / $I_{-100mV}$) determined from the I-V relationship was 1.29 and 1.27 in the absence and presence of F-amphiphiles respectively. Both the values of channel conductance and rectification ratios agree well with previously published reports [23].

Cyclodextrins are adapter molecules which bind non-covalently to the αHL pore (Figure 3.12B). They cause a reduction in current flowing through the pore upon becoming lodged in the lumen of the pore. The interaction of β-cyclodextrin (βCD) with the α-hemolysin is very well characterized. Values of $\tau_{on}$ and $\tau_{off}$ for βCD binding were obtained from dwell-time histograms fitted to single exponentials. Kinetic constants were calculated by using $k_{off} = 1/\tau_{off}$, $k_{on} = 1/\tau_{on}$ [βCD], and $K_d = k_{off} / k_{on}$, where [βCD] is the concentration of βCD. Values for $k_{on}$ and $k_{off}$, and $K_d$ are quoted as the mean ± SD. The residence time for βCD in the wild-type αHL pore has been calculated to be several hundred microseconds [24-26]. We also examined the interaction of βCD (trans) with αHL pores in the presence of $F_6FC$ (cis) (Figure 3.12 C-F). The values of $k_{on}$ and $k_{off}$, and hence $K_d$, for βCD were comparable to previously reported values (Table 3.1). Both the I-V curves and the cyclodextrin binding results indicate that although $F_6FC$ prevents the insertion of proteins into lipid bilayers, it does not affect the functional properties of proteins that are already in them.

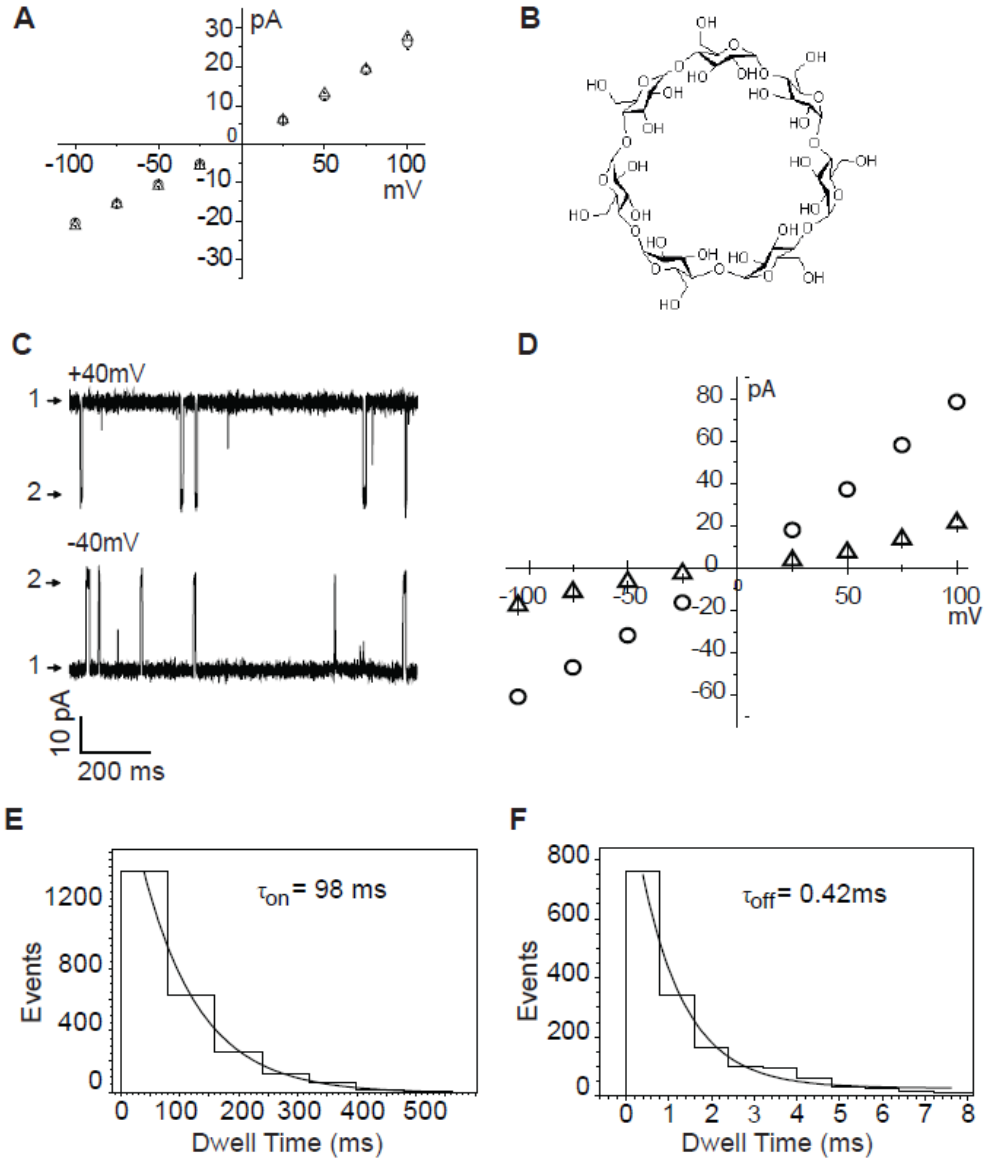


**Figure 3.12:** *Detailed characterization of wild type aHL in presence of $F_6FC$. (A) I−V curve of a single WT αHL heptamer in the absence (°) and presence (△) of $F_6FC$ (10 mM, cis). The recording buffer was 300 mM NaCl, 2.7 mM KCl, 10 mM $Na_2HPO_4$, and 2 mM $KH_2PO_4$ pH 7.4. Each point on the I-V curve is is the mean ± standard deviation from three separate single-channel recordings. (B) Structure of beta-cyclodextrin which is a seven sugar ringed molecule. (C) Representative single channel current traces from a WT-αHL heptamer at ±40 mV showing blockades by βCD (40 μM, trans) in the presence of $F_6FC$ (10 mM, cis). Levels 1 and 2 indicate the unoccupied and occupied αHL pore. (D) IV curve of αHL in the absence (open circles) and presence of bound βCD (open triangles). The recording buffer was 1 M NaCl, 10 mM $Na_2HPO_4$, pH 7.5.*

*Each point on the I-V curve is is the mean ± standard deviation from three separate single-channel recordings. (E, F) Representative dwell time histograms at +40 mV for the interaction of βCD (40 μM, trans) with WT-αHL in the presence of 10 mM $F_6FC$ (cis): $\tau_{on}$, inter-event interval; $\tau_{off}$, βCD dwell time. The results from the kinetic analysis are summarized below in Table 3.1.*

| | Voltage (mV) | $F_6FC^b$ | $g_{\alpha HL}$ (pS) | $g_{\alpha HL \cdot \beta CD}$ (pS) | $k_{on}$ ($M^{-1}s^{-1}$) | $k_{off}$ ($s^{-1}$) | $K_d$ (M) |
|---|---|---|---|---|---|---|---|
| 1[c] | +40 | - | 721±6 | 253±4 | $2.8\pm0.2\times10^5$ | $2.1\pm0.2\times10^3$ | $7.8\pm0.3\times10^{-3}$ |
| 2 | +40 | + | 721±4 | 232±4 | $2.5\pm0.4\times10^5$ | $2.4\pm0.3\times10^3$ | $9.6\pm0.4\times10^{-3}$ |
| 3[c] | -40 | - | 651±4 | 240±3 | $4.0\pm0.3\times10^5$ | $1.3\pm0.1\times10^3$ | $3.4\pm0.3\times10^{-3}$ |
| 4 | -40 | + | 650±3 | 257±3 | $3.1\pm0.1\times10^5$ | $1.7\pm0.1\times10^3$ | $5.4\pm0.5\times10^{-3}$ |

[a] *$g_{\alpha HL}$ and $g_{\alpha HL.\beta CD}$ are, respectively, the unitary conductance in the absence of βCD and the unitary conductance with βCD bound in 1 M NaCl, 10 mM $Na_2HPO_4$, pH 7.5. $k_{on}$, $k_{off}$, and $K_d$ are quoted as the mean ± SD from three experiments.* [b] *The concentration of $F_6FC$ was 10 mM in the cis compartment.* [c] *Values taken from a previous report [27].*

**Table 3.1:** *Conductance Values and Kinetic Constants for the Binding of βCD to the αHL Pore in the Presence of $F_6FC$*

### 3.2.6 Effect of F-amphiphile on insertion of other mutants of alpha-hemolysin in planar bilayers

The determination of the high resolution X-ray structure (1.9Å) of alpha hemolysin [28] has made it possible to engineer the *wild type* pore. Engineered α- hemolysin pores have been used for stochastic sensing [29, 30], in nanopore DNA sequencing [16, 31, 32], as nanoreactors for probing single molecule chemistry [33, 34], and in the construction of nanodevices [35]. After showing that F-amphiphiles could control the insertion of wild type α-hemolysin in the bilayer, experiments were done to assess the utility of F-amphiphiles in controlling the insertion of some mutants of αHL.

The E111N/K147N (NN) mutant (charged residues at the constriction have been removed) has been previously reported to show better base discrimination between bases of DNA [32]. Based on these studies, many triple mutants were made to improve base discrimination between DNA bases [16]. One such triple mutant, the E111N/K147N/M113N (NNN) homo-heptamer was used to study the effect (if any) of the F-amphiphile $F_6FC$ on its insertion into the bilayer.

Nanopores such as α-hemolysin have been used to study reactions at the single-molecule level as it can reveal information often masked in ensemble measurements (such as the presence of short lived reaction intermediates). Cysteine containing hetero-heptamers have proved useful in studying biologically relevant thiol chemistry at the single molecule level [36]. One such cysteine mutant of α-hemolysin which was studied for the inhibitory effects of $F_6FC$ was a hetero-heptamer of αHL: $(G137C)_1(WT)_6$.

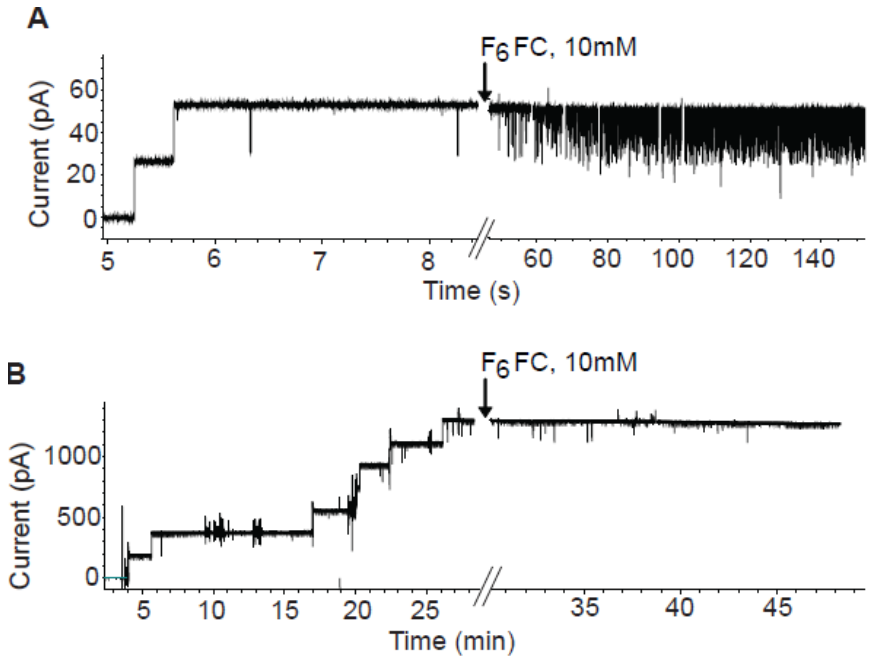


**Figure 3.13:** *Effects of F-amphiphiles on αHL mutant proteins in planar lipid bilayers. (A) Arrest of the insertion of αHL (NNN) homo-heptamers on addition of $F_6FC$ (arrow, 10 mM, cis). The addition of $F_6FC$ resulted in blocking events of the pore. The recording buffer was 300 mM NaCl, 2.7 mM KCl, 10 mM $Na_2HPO_4$, and 2 mM $KH_2PO_4$ pH 7.4 and the applied potential was +100 mV. (B) Arrest of the insertion of $(G137)_1(WT)_6$ cysteine hetero-heptamer at +100 mV, on addition of $F_6FC$ (arrow, 10mM, cis). The buffer used for the recording was2M KCL, 10mM MOPS chelexed at pH 7.0.*

Similar to the WT-αHL results reported above, $F_6FC$ also stopped the insertion of both the αHL mutants into bilayers (Figure 3.10). No blocking events were observed in the presence of $F_6FC$ with the cysteine hetero-heptamer (Figure 3.13B). Unfortunately, although $F_6FC$ stopped further insertion of the triple mutant of αHL (E111N/K147N/M113N) into bilayers, $F_6FC$ was found to cause blocking events (Figure 3.13A). These studies show that although $F_6FC$ can successfully stop the insertion of both the WT-αHL and its mutants, different mutants of αHL were found to

interact differently with $F_6FC$. These results imply that each mutant of αHL should be tested first to check for any effects of $F_6FC$.

### 3.2.7 Effect of $F_6FC$ on insertion of other proteins (MspA and Kcv) in bilayers

In order to assess if the observed inhibitory effects of $F_6FC$ on protein insertion was specific to αHL, we investigated the ability of $F_6FC$ to control the insertion of membrane proteins other than α-hemolysin. The two proteins chosen were (i) the octameric porin MspA, produced by Mycobacterium which is also largely a β-structure protein like α-hemolysin (Figure 3.14A), and (ii) the α-helical tetrameric membrane protein Kcv found in *Paramecium bursaria* Chlorella virus (Figure 3.14B).

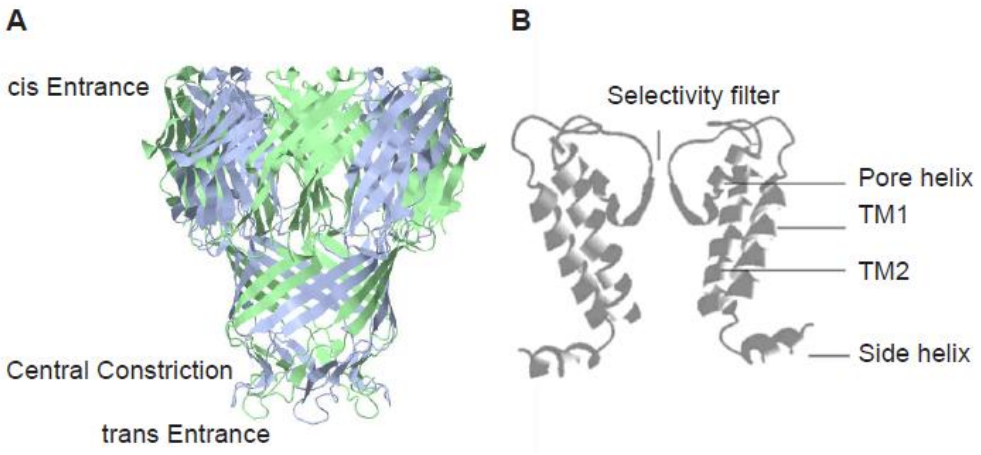


**Figure 3.14:** *Structure of MspA and Kcv. (A) Cartoon representation of the MspA porin (Generated by Emma Wallace). The structure consists of a thick rim at the top, a stem consisting of the wide β barrel, and the base at the bottom which contains a constriction site. (B) Putative structure of full length Kcv. For purposes of clarity, only two of the four subunits of the tetrameric channel is shown. The homology model was generated by sequence alignment of pore region of KirBac 1.1 and the full length Kcv and the crystallographic co-ordicnates of Kir bac 1.1. The image was taken from the book: "Viral Membrane Proteins: Structure, Function, And Drug Design" by Wolfgang B. Fischer.*

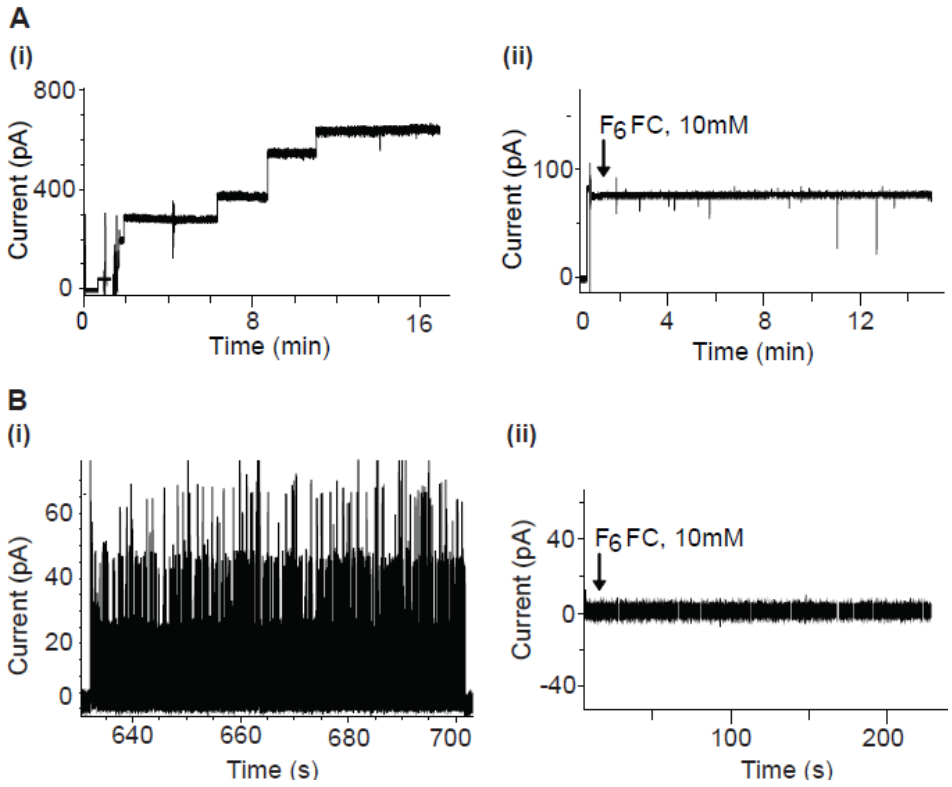


**Figure 3.15:** *Representative electrical recording showing the effect of F6FC on the insertion of MspA and Kcv into planar lipid bilayers. (A) (i) MspA (NNNRRK mutant) pore activity in the absence of F-amphiphile at +50 mV. (ii) Effect of the addition of $F_6FC$ (arrow, 10 mM, cis) after the insertion of an MspA pore. No further insertion events occur. The recording buffer for MspA was 1.0 M KCl, 10 mM Tris.HCl, pH 7.0. (B)(i) Condensed view of a trace showing WT-Kcv channel activity in the absence of F-amphiphile at +100 mV. Numerous individual openings are seen, with occasional coincident openings of two and three channels. (ii) WT-Kcv was added to the cis chamber just after $F_6FC$ addition (arrow, 10 mM, cis) at +100 mV. No openings are seen. The recording buffer for Kcv was 200 mM KCl, 10 mM HEPES, pH 7.0.)*

Similar to αHL, channel insertions of MspA also ceased on addition of $F_6FC$ (10mM, cis) (Figure 3.15A). In three separate attempts, we found that no Kcv channels inserted into a bilayer when $F_6FC$ was present at concentrations above the CMC, while channel

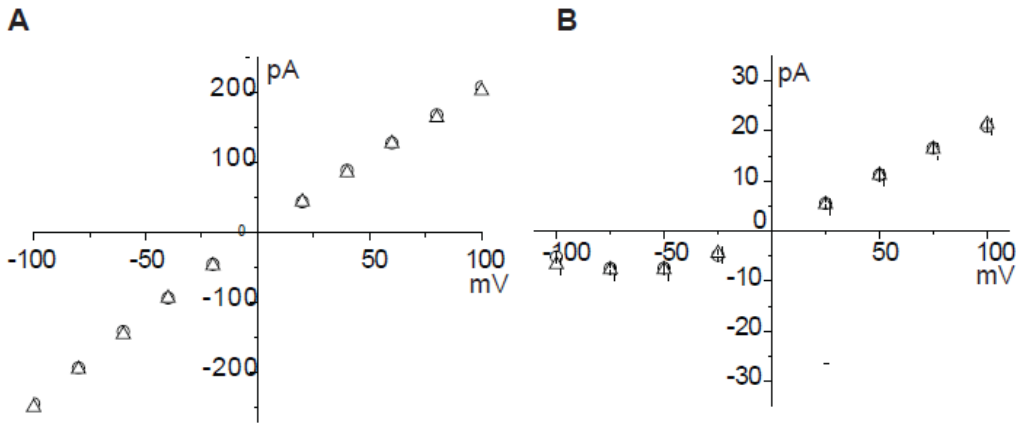


**Figure 3.16:** *Current-Voltage graphs of MspA and Kcv in presence of F6FC. (A) I−V curve of a single MspA pore in the absence (°) and presence (△) of $F_6$FC (10 mM, cis). The recording buffer for MspA consisted of 1.0 M KCl and 10 mM Tris-HCl (pH 7.0). Each data point on the I-V curve is the mean ± standard deviation from three separate single-channel recordings. (B) I−V curve of a single WT Kcv channel in the absence (° ) and presence (△) of $F_6$FC (10 mM, cis). The recording buffer consisted of 200 mM KCl and 10 mM HEPES (pH 7.0). Each data point on the I-V curve is the mean ± standard deviation from three separate single-channel recordings.*

insertion occurred in all three attempts in the absence of an F-amphiphile (Figure 3.15B). In neither case was insertion reversed, or blocking events seen which is similar to what was observed with WT α-hemolysin. To ascertain that it does not affect the properties of proteins already inserted in the bilayer, we measured the I-V curves of the two proteins MspA and Kcv in the absence and presence of F-amphiphiles (Figure 3.16). F-amphiphiles did not effect the I-V characteristics of the two proteins which is also similar to what was observed with the WT-αHL.

### 3.2.8 Possible mechanism(s) of action of F-amphiphiles

As mentioned earlier (section 3.2.4), these experiments show that F-amphiphiles provide a useful means of controlling the number of membrane proteins entering a lipid bilayer. Traditionally, in lipid bilayer experiments the number of channels in the bilayer is controlled using the method of perfusion (i.e the buffer in the cis chamber containing the uninserted protein is exchanged with fresh buffer without protein). However, perfusion often results in pressure gradients across the bilayer membranes resulting in disruption of the membranes. Using F-amphiphiles to control the number of channels in the bilayer involves just the addition of F-amphiphiles to the chamber, and thus is simpler and more convenient over methods such as perfusion which often result in the breaking of the bilayer.

This section discusses the most likely mechanism in which we think F-amphiphiles could be stopping the insertion of membrane proteins into bilayers. The fact that both major classes of membrane protein (β barrels and α-helix bundles) are similarly affected under the conditions of our experiments, a common mechanism for the arrest of insertion must be invoked.

A possible mechanism for the inhibitory effect of F-amphiphiles on the insertion of protein into bilayers could be the denaturation of un-inserted protein in the aqueous phase by F-amphiphiles. This possibility arises from the observations that have shown that channel insertion of αHL monomers into bilayers ceased in the presence of high concentrations of urea, but channels already in the membrane continued to conduct normally [37, 38].

Recent studies in our group have shown that the αHL heptamer is quite resistant to denaturation and is stable even at high 8.0M urea [39]. This was shown from SDS-PAGE experiments where they looked at the extent of dissociation of the αHL heptamer to monomer after incubation of the protein at various urea concentrations. SDS−PAGE with the αHL heptamer in presence of F-amphiphiles seems to indicate that when compared to the control, there is no increase in the amount of dissociation of αHL heptamer to monomers (Figure 3.17A). These results suggested that F-amphiphiles do not denature the αHL heptamer.

The integrity of the αHL monomer in the presence of or after treatment with the F-amphiphiles was confirmed by a hemolytic assay (Figure 3.17B). In liposome and planar bilayer experiments, the monomer was observed to not insert in bilayers in presence of F-amphiphiles (above CMC). However, under the same conditions, hemolytic assays show that aHL monomers can assemble on erythrocytes and lyse them. The ability of αHL monomers to act on rabbit erythrocytes under conditions under which they will not insert into lipid bilayers might be explained by the presence of strong receptors on the red cells that promote irreversible binding and assembly [40], in competition with sequestration by F-amphiphile aggregates (sequestration by F-amphiphile aggregates is discussed below). Thus, denaturation of un-inserted protein is unlikely to be the mechanism for the inhibitory effects of F-amphiphiles on protein insertion in the bilayer.

Single chain F-amphiphiles have previously been reported to form a variety of lamellar structures such as multi-lamellar vesicles and connected bilayers (Figure

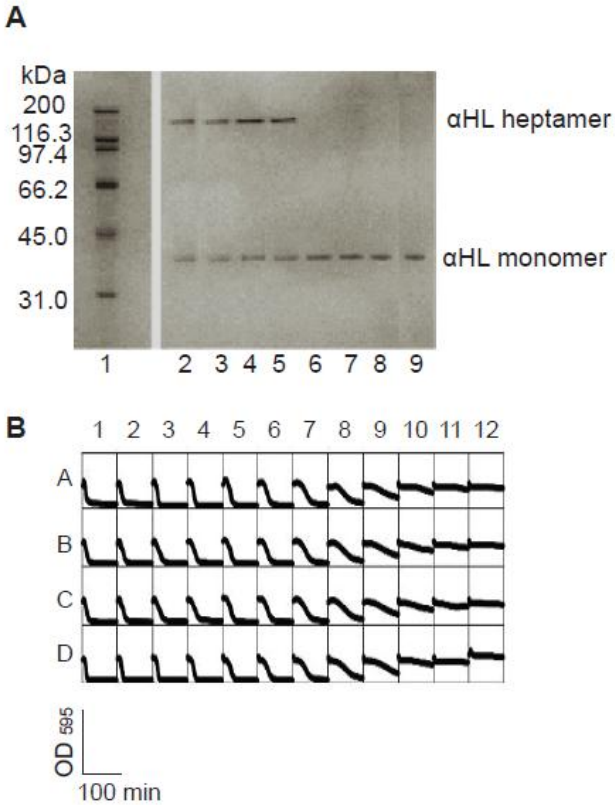


**Figure 3.17:** *(A) Stability of αHL pore in the presence of F-amphiphiles. (A) WT-αHL monomer and heptamer were incubated at room temperature for 15 min with F-amphiphiles at concentrations 5 times the reported CMCs. Monomer and heptamer samples (~1 μg) were then run on 12% Bis-Tris SDS polyacrylamide gels in XT-MOPS buffer at 200 V. Lanes 1: Protein marker. Lanes 2 and 6: WT-αHL heptamer and monomer, respectively, in absence of F-amphiphiles; lanes 3 and 7: WT-αHL heptamer and monomer, respectively, incubated with 10mM $F_6FC$; lanes 4 and 8: WT-αHL heptamer and monomer, respectively, incubated with 5mM $F_6OM$; lanes 5 and 9: WT-αHL heptamer and monomer, respectively, incubated with 2mM $C_6FTAC$. (B) Haemolytic activity of the αHL monomer in the presence of F-amphiphiles. The concentrations of $F_6FC$, $F_6OM$, and $F_6TAC$ in lanes B1−D1 (after the addition of red cells) were 10, 5, and 2 mM, respectively. αHL prepared by IVTT (5 μL) was added to lanes A1−D1. The protein and amphiphile were then subjected to 2-fold serial dilution in 10 mM MOPS and 150 mM NaCl (pH 7.4) over the 11 remaining wells (final volume of 50 μL per well), followed by the addition of washed 1% rRBCs (50 μL) to each well. The concentration of the F-amphiphile in well 1 is above the CMC in each case. In all wells, the protein had been subjected to an F-amphiphile above the CMC before dilution.*

3.18A) [41]. So, we speculate that a possible mechanism to explain the arrest of protein insertion into bilayers on addition of F-amphiphiles is due to the sequestration of proteins by F-amphiphile aggregates (Figure 3.18B). F-amphiphiles are immiscible with lipids, and the relative distribution of the protein in these two phases will be determined by mass action law. Under our experimental conditions with a low lipid concentration (micro-molar range), the αHL, MspA, and Kcv proteins are suggested to partition quickly onto or into the F-amphiphile aggregates, which are present at higher concentrations (milli-molar range), and remain unavailable for insertion into lipid bilayers.

Ladokhin and colleagues have carefully examined the effects of F-amphiphiles on the insertion into bilayers of diphtheria toxin T domain and annexin B12 [8, 9, 42]. In these cases, insertion was reversible and high concentrations of the F-amphiphile removed the proteins from bilayers. The proteins that we have tested bind tightly to bilayers and cannot be removed by F-amphiphiles, although insertion ceases in the presence of these agents, suggesting that the systems are under kinetic rather than thermodynamic control [13] in the cases that we have examined.

As, can be seen from the SDS PAGE gel of αHL monomers with F-amphiphiles (Figure 3.17A), αHL monomers do not oligomerize to form heptamers in the fluorinated aggregates. It is likely that the αHL monomer is sequestered by binding of the protein to the surface of the fluorinated aggregates. For the αHL heptamer and other pores, it is likely that the proteins are sequestered by insertion of the pore into the

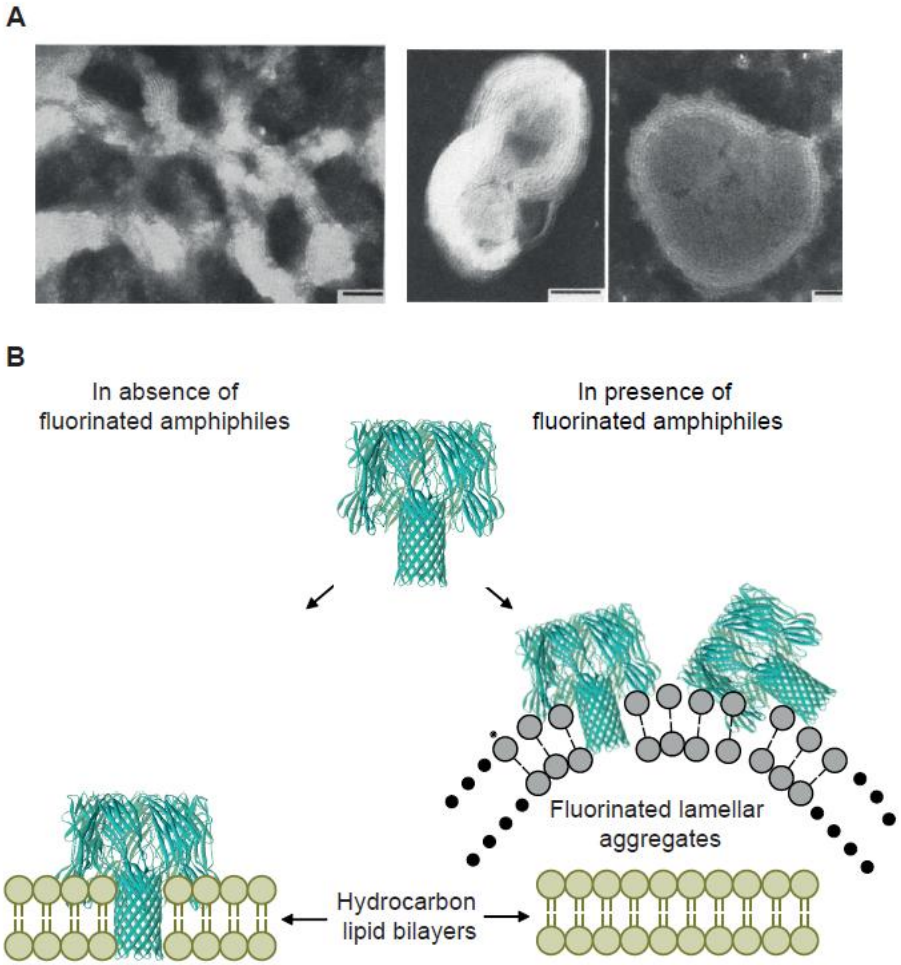


**Figure 3.18: Possible mode of action of F-amphiphiles:** *(A) Examples of bilayer like aggregates formed by the single tailed F-amphiphile* ($C_8F_{17}C_2H_4OP(O)_2^-OC_2H_4N^+(CH_3)_3$) *in aqueous solution as seen by transmission electron microscopy. (left) uniformly stacked bilayers formed by hand shaking at 25°C (3% w/v) (right) isolated multi-layered vesicles obtained in dilute solutions after gentle shaking at room temperature (0.5% w/v). (B) Proposed mechanism of action in which membrane proteins partition partially or fully into the aggregates formed by F-amphiphiles (grey) and are therefore unavailable for insertion into lipid bilayers (yellow).*

fluorinated aggregates. However, further experiments will be needed to confirm the nature in which these proteins are being sequestered by the aggregates.

## 3.3 Conclusions and future directions

The work described in this chapter has investigated some new aspects of F-amphiphiles in membrane biochemistry by examining the effects of two new F-amphiphiles: $F_6FC$ and $F_6OM$, as well as the previously reported $C_6$-FTAC, on the insertion of the αHL pore, the MspA pore, and the Kcv potassium channel into bilayers. In both planar lipid bilayers and liposome systems, we found an inhibitory effect of F-amphiphiles on protein insertion at all concentrations of the F-amphiphiles tested. However, the F-amphiphiles had no effect on the properties of proteins that had already inserted into bilayers. Since F-amphiphiles affected three different proteins similarly, we propose a common mechanism of action: sequestration of protein into lamellar aggregates formed by F-amphiphiles. The use of F-amphiphiles to control protein insertion in the bilayer is a novel use of F-amphiphiles and is advantageous over existing methods such as perfusion which often result in the breaking of the bilayer. This work holds promise for use in single-channel studies of membrane proteins in planar bilayers, where it is imperative to control the number of proteins in the bilayer.

It would be of relevance to both expand the utility of this approach and perform experiments to confirm our proposed mechanism of action for the cessation of protein insertion in presence of high concentrations of F-amphiphiles. Experiments performed at varying pH, temperature, and in the presence of bilayers formed from different lipids (eg: charged lipids) might provide an insight into the range of conditions for which this approach might be used.

## 3.4 Bibliography

[1] J. Popot, "Amphipols, Nanodiscs, and Fluorinated Surfactants: Three Nonconventional Approaches to Studying Membrane Proteins in Aqueous Solutions," *Annual Review of Biochemistry, Vol 79,* pp. 737-775, 2010 2010.

[2] P. Lonostro, "Phase-separation properties of fluorocarbons, hydrocarbons and their copolymers," *Advances in Colloid and Interface Science,* vol. 56, pp. 245-287, Mar 1995.

[3] F. Shepherd and A. Holzenburg, "The potential of fluorinated surfactants in membrane biochemistry.," *Anal Biochem,* vol. 224, pp. 21-7, Jan 1995.

[4] E. Chabaud, P. Barthelemy, N. Mora, J. L. Popot, and B. Pucci, "Stabilization of integral membrane proteins in aqueous solution using fluorinated surfactants," *Biochimie,* vol. 80, pp. 515-530, May-Jun 1998.

[5] F. Lebaupain, A. G. Salvay, B. Olivier, G. Durand, A. S. Fabiano, N. Michel, *et al.*, "Lactobionamide surfactants with hydrogenated, perfluorinated or hemifluorinated tails: Physical-chemical and biochemical characterization," *Langmuir,* vol. 22, pp. 8881-8890, Oct 2006.

[6] A. Maher, D. Gregory, B. Cecile, R. Simon, E. Christine, and P. Bernard, "A diglucosylated fluorinated surfactant to handle integral membrane proteins in aqueous solution.," *Journal of fluorine chemistry,* vol. 134, pp. 63-71, February 2012.

[7] J. Talbot, A. Dautant, A. Polidori, B. Pucci, T. Cohen-Bouhacina, A. Maali, *et al.*, "Hydrogenated and fluorinated surfactants derived from Tris(hydroxymethyl)-acrylamidomethane allow the purification of a highly active yeast F1-F0 ATP-synthase with an enhanced stability," *Journal of Bioenergetics and Biomembranes,* vol. 41, pp. 349-360, AUG 2009 2009.

[8] S. Palchevskyy, Y. Posokhov, B. Olivier, J. Popot, B. Pucci, and A. Ladokhin, "Chaperoning of insertion of membrane proteins into lipid bilayers by hemifluorinated surfactants: application to diphtheria toxin.," *Biochemistry,* vol. 45, pp. 2629-35, Feb 2006.

[9] M. Rodnin, Y. Posokhov, C. Contino-Pépin, J. Brettmann, A. Kyrychenko, S. Palchevskyy, *et al.*, "Interactions of fluorinated surfactants with diphtheria toxin T-domain: testing new media for studies of membrane proteins.," *Biophys J,* vol. 94, pp. 4348-57, Jun 2008.

[10] K. Park, C. Berrier, F. Lebaupain, B. Pucci, J. Popot, A. Ghazi, *et al.*, "Fluorinated and hemifluorinated surfactants as alternatives to detergents for membrane protein cell-free synthesis.," *Biochem J,* vol. 403, pp. 183-7, Apr 2007.

[11] C. Breyton, F. Gabel, M. Abla, Y. Pierre, F. Lebaupain, G. Durand, *et al.*, "Micellar and Biochemical Properties of (Hemi)Fluorinated Surfactants Are Controlled by the Size of the Polar Head," *Biophysical Journal,* vol. 97, pp. 1077-1086, Aug 2009.

[12] K. Park, E. Billon-Denis, T. Dahmane, F. Lebaupain, B. Pucci, C. Breyton, *et al.*, "In the cauldron of cell-free synthesis of membrane proteins: playing with new surfactants," *New Biotechnology*, vol. 28, pp. 255-261, APR 30 2011 2011.

[13] Y. O. Posokhov, M. V. Rodnin, S. K. Das, B. Pucci, and A. S. Ladokhin, "FCS study of the thermodynamics of membrane protein insertion into the lipid bilayer chaperoned by fluorinated surfactants," *Biophysical Journal*, vol. 95, pp. L54-L56, Oct 2008.

[14] A. A. Pavia, B. Pucci, J. G. Riess, and L. Zarif, "New perfluoroalkyl telomeric nonionic surfactants - synthesis, physicochemical and biological properties," *Makromolekulare Chemie-Macromolecular Chemistry and Physics*, vol. 193, pp. 2505-2517, Sep 1992.

[15] J. G. Riess, S. Pace, and L. Zarif, "Highly effective surfactants with low hemolytic-activity," *Advanced Materials*, vol. 3, pp. 249-251, May 1991.

[16] D. Stoddart, A. J. Heron, J. Klingelhoefer, E. Mikhailova, G. Maglia, and H. Bayley, "Nucleobase Recognition in ssDNA at the Central Constriction of the alpha-Hemolysin Pore," *Nano Letters*, vol. 10, pp. 3633-3637, Sep 2010.

[17] A. Graciaa, P. Creux, J. Lachaise, and R. S. Schechter, "Competitive adsorption of surfactants at air/water interfaces," *Journal of Colloid and Interface Science*, vol. 261, pp. 233-237, May 2003.

[18] S. Bhakdi and J. Tranumjensen, "Alpha-toxin of staphylococcus-aureus," *Microbiological Reviews*, vol. 55, pp. 733-751, Dec 1991.

[19] M. Montoya and E. Gouaux, "beta-barrel membrane protein folding and structure viewed through the lens of alpha-hemolysin," *Biochimica Et Biophysica Acta-Biomembranes,* vol. 1609, pp. 19-27, Jan 2003.

[20] H. Bayley, "Membrane-protein structure Piercing insights," *Nature,* vol. 459, pp. 651-652, Jun 2009.

[21] O. Braha, B. Walker, S. Cheley, J. J. Kasianowicz, L. Z. Song, J. E. Gouaux, *et al.*, "Designed protein pores as components for biosensors," *Chemistry & Biology,* vol. 4, pp. 497-505, Jul 1997.

[22] R. Chen and J. Knutson, "Mechanism of fluorescence concentration quenching of carboxyfluorescein in liposomes: energy transfer to nonfluorescent dimers.," *Anal Biochem,* vol. 172, pp. 61-77, Jul 1988.

[23] S. Y. Noskov, W. Im, and B. Roux, "Ion permeation through the alpha-hemolysin channel: Theoretical studies based on Brownian dynamics and Poisson-Nernst-Plank electrodiffusion theory," *Biophysical Journal,* vol. 87, pp. 2299-2309, Oct 2004.

[24] L. Q. Gu and H. Bayley, "Interaction of the noncovalent molecular adapter, beta-cyclodextrin, with the staphylococcal alpha-hemolysin pore," *Biophysical Journal,* vol. 79, pp. 1967-1975, Oct 2000.

[25] L. Q. Gu, S. Cheley, and H. Bayley, "Prolonged residence time of a noncovalent molecular adapter, beta-cyclodextrin, within the lumen of mutant alpha-hemolysin pores," *Journal of General Physiology,* vol. 118, pp. 481-493, Nov 2001.

[26] A. Banerjee, E. Mikhailova, S. Cheley, L. Q. Gu, M. Montoya, Y. Nagaoka, *et al.*, "Molecular bases of cyclodextrin adapter interactions with engineered protein nanopores," *Proceedings of the National Academy of Sciences of the United States of America*, vol. 107, pp. 8165-8170, May 2010.

[27] L.-Q. Gu and H. Bayley, "Interaction of the non-covalent molecular adapter, b-cyclodextrin, with the staphylococcal a-hemolysin pore," *Biophys.J.*, vol. 79, pp. 1967-1975, 2000.

[28] L. Z. Song, M. R. Hobaugh, C. Shustak, S. Cheley, H. Bayley, and J. E. Gouaux, "Structure of staphylococcal alpha-hemolysin, a heptameric transmembrane pore," *Science*, vol. 274, pp. 1859-1866, Dec 1996.

[29] Y. Astier, D. E. Kainov, H. Bayley, R. Tuma, and S. Howorka, "Stochastic detection of motor protein-RNA complexes by single-channel current recording," *Chemphyschem*, vol. 8, pp. 2189-2194, Oct 2007.

[30] X. F. Kang, S. Cheley, X. Y. Guan, and H. Bayley, "Stochastic detection of enantiomers," *Journal of the American Chemical Society*, vol. 128, pp. 10684-10685, Aug 2006.

[31] J. J. Kasianowicz, E. Brandin, D. Branton, and D. W. Deamer, "Characterization of individual polynucleotide molecules using a membrane channel," *Proceedings of the National Academy of Sciences of the United States of America*, vol. 93, pp. 13770-13773, Nov 1996.

[32] D. Stoddart, A. J. Heron, E. Mikhailova, G. Maglia, and H. Bayley, "Single-nucleotide discrimination in immobilized DNA oligonucleotides with a

biological nanopore," *Proceedings of the National Academy of Sciences of the United States of America*, vol. 106, pp. 7702-7707, May 2009.

[33] A. F. Hammerstein, S. H. Shin, and H. Bayley, "Single-Molecule Kinetics of Two-Step Divalent Cation Chelation," *Angewandte Chemie-International Edition*, vol. 49, pp. 5085-5090, 2010.

[34] S. R. Lu, W. W. Li, D. Rotem, E. Mikhailova, and H. Bayley, "A primary hydrogen-deuterium isotope effect observed at the single-molecule level," *Nature Chemistry*, vol. 2, pp. 921-928, Nov 2010.

[35] G. Maglia, A. J. Heron, W. L. Hwang, M. A. Holden, E. Mikhailova, Q. H. Li, *et al.*, "Droplet networks with incorporated protein diodes show collective properties," *Nature Nanotechnology*, vol. 4, pp. 437-440, Jul 2009.

[36] H. Bayley, T. Luchian, S.-H. Shin, and M. B. Steffensen, "Single-Molecule Covalent Chemistry in a Protein Nanoreactor.," in *Springer Series in Biophysics*, ed, 2008.

[37] M. Pastoriza-Gallego, G. Oukhaled, J. Mathe, B. Thiebot, J. M. Betton, L. Auvray, *et al.*, "Urea denaturation of alpha-hemolysin pore inserted in planar lipid bilayer detected by single nanopore recording: Loss of structural asymmetry," *Febs Letters*, vol. 581, pp. 3371-3376, Jul 2007.

[38] X. F. Xu and M. Colombini, "Self-catalyzed insertion of proteins into phospholipid membranes," *Journal of Biological Chemistry*, vol. 271, pp. 23675-23682, Sep 1996.

[39] D. Japrung, M. Henricus, Q. Li, G. Maglia, and H. Bayley, "Urea facilitates the translocation of single-stranded DNA and RNA through the alpha-hemolysin nanopore.," *Biophys J*, vol. 98, pp. 1856-63, May 2010.

[40] A. Valeva, N. Hellmann, I. Walev, D. Strand, M. Plate, F. Boukhallouk, *et al.*, "Evidence that clustered phosphocholine head groups serve as sites for binding and assembly of an oligomeric protein pore," *Journal of Biological Chemistry*, vol. 281, pp. 26014-26021, Sep 2006.

[41] M. P. Krafft, F. Giulieri, and J. G. Riess, "Can single-chain perfluoroalkylated amphiphiles alone form vesicles and other organized supramolecular systems," *Angewandte Chemie-International Edition in English*, vol. 32, pp. 741-743, May 1993.

[42] Y. Posokhov, M. Rodnin, S. Das, B. Pucci, and A. Ladokhin, "FCS study of the thermodynamics of membrane protein insertion into the lipid bilayer chaperoned by fluorinated surfactants.," *Biophys J*, vol. 95, pp. L54-6, Oct 2008.

# Chapter 4

## Bilayers formed by fluorinated amphiphiles.

### 4.1 Introduction

#### 4.1.1 Bilayers from hydrocarbon based lipids

A lipid bilayer consists of two opposed layers of amphipathic lipid molecules, with the hydrophilic head-groups facing outwards and in contact with water and the hydrophobic tails buried in the interior of the bilayer structure. Biological membranes contain hundreds of different lipid species that can be categorized into three main classes: glycerophospholipids, sphingolipids, and sterols; with glycerophospholipids being the most abundant. Examples of glycerophospholipids are phosphatidylcholine (PC), phosphatidylethanolamine (PE), phosphatidylserine (PS), and phosphatidylinositol (PI). Phosphatidylcholines are the most abundant phospholipid in animal and plants, often amounting to almost 50% of the total lipid [1].

In order to study the properties of the bilayer and proteins embedded in them, simpler and more easily manipulated system model membranes were developed. For over fifty years now, the most common model bilayers have been planar bilayers and liposomes [2]. Initial studies were performed with lipids derived from natural sources such as hen egg.

However, studies with lipids from natural sources suffered two drawbacks: firstly preparations of lipids derived from cell membranes invariably consisted of mixtures of compounds and thus the composition of bilayers formed from these preparations was not defined. Secondly, naturally occurring lipids always contained a degree of unsaturation, and so they are highly susceptible to oxidation [3].

To circumvent this problem, in 1971 Redwood et al. described the formation of stable bilayers with reproducible electrical properties from a synthetic lipid: DPhPC [3]. Since then, DPhPC has become one of the most commonly used lipids in electrophysiological measurements and there is extensive literature available on liposomes and planar bilayers formed from a variety of synthetic lipids. However, most bilayer studies have been limited to hydrocarbon amphiphiles.

### 4.1.2 Bilayers and vesicles formed from fluorinated amphiphiles

In 1982, Kunitake and co-workers first described the formation of bilayer membranes (vesicles in solution) from a new class of synthetic lipids: double chain fluoroalkyl amphiphiles [4]. Stable fluorinated vesicles have since been made from numerous single [5-7] and double and triple chain F-amphiphiles [8-11], hybrid fluorocarbon–hydrocarbon double chain amphiphiles [12-14] and as well as from combinations of semifluorinated amphiphiles with standard phospholipids [15, 16]. Most of the vesicles formed by F-amphiphiles were stable enough to withstand sterilization at 121°C and had long room-temperature shelf-life [17]. Vesicles formed from fluorinated amphiphiles, contain an internal fluorinated core within their bilayer membrane which

imparts interesting properties. The release of entrapped 5(6)-carboxyfluorescein from F-vesicles whether in buffer or serum was considerably slower than from liposomes made from hydrocarbon analogs [18-20]. Incorporation of F-alkyl segments into liposomes made of DMPC or DPPC protected the lipids from hydrolysis by pancreatic phospholipase $A_2$ [21]. Fluorinated vesicles showed improved resistance to detergents such as bile salts (sodium taurocholate) relative to conventional liposomes (including cholesterol-containing ones) [22]. These properties have made fluorinated vesicles promising candidates as drug carriers.

Barthélémy et al. studied the structure of stable black newton films formed from highly fluorinated non-ionic single tail fluorinated amphiphiles by using X-ray reflectivity [23]. The newton films were formed by immersing a metal frame in a solution containing an amphiphile and then drawing up the frame to form the film with the fluorinated tails facing the air and the hydrophilic heads facing inwards to form the central core. The thickness of the hydrophilic layer was found to depend on the hydration of the polar head-group. The same study also suggests that the introduction of an alkyl terminal segment on the fluorocarbon tail destabilized the packing of fluorocarbon chains and prohibited the formation of a bilayer.

Another study reported structural data on multi-layered fluorinated phospholipid vesicles formed from a variety of fluoroalkylated glycerophosphocholines (PCs) [24]. Due to the bulky volume of an F-alkyl chain, adjacent alkyl chains were spaced further apart in fluoroalkylated PCs than in analogous hydrocarbon PCs. The study also reports that in fluorinated monolayers formed by PCs at the air-water interface with a terminal

$CF_3$ group, dipole potentials ranged from -680 mV for PCs with both chains fluoroalkylated to -180 mV for PCs with one chain fluoroalkylated. This is in stark contrast to dipole potentials measured in egg PC monolayers (+415 mV) at the air-water interface. The electric field arising from the negative fluorine dipoles was found to extend to the bilayer head-group region and affect the binding of negatively charged ions such as tetraphenylboron.

In 2008, Saito et al. looked at the bilayer properties of partially fluorinated phospholipid 1,2-di(F8CCH8)PC (FPC) and the non-fluorinated counterpart 1,2-di(H8CCH8)PC (HPC) by using molecular dynamics [25]. The fluorinated bilayer showed a higher free energy barrier (by 1.2 kcal /mol) to water than the non-fluorinated bilayer. As mentioned earlier, fluorocarbon chains adopt the all-trans conformations due to higher trans-gauche energy barrier [26]. This results in a dense packing of fluorocarbon chains in the bilayer which leads to the restricted translational and rotational motions of water molecules in the membrane. The paper proposes that the entropy loss of water molecules could be responsible for the increase of the free energy of water in the core of a fluorinated bilayer.

Existing reports on fluorocarbon bilayers, which have compared properties such as permeability and stability with standard phosphatidylcholine (PC) bilayers, have focussed on fluorinated vesicles as promising drug carriers. However, this chapter addresses the utility of fluorinated bilayers as a new platform for studies of membrane protein. It should be noted that such an approach has not been reported before.

### 4.1.3 Overview of chapter

As discussed in section 4.1.2, there is a strong tendency for even short single chain F-alkyl amphiphiles to aggregate to form multi-lamellar structures in aqueous solution [6]. We thought it would be interesting to study the ability of F-amphiphiles to form stable free standing bilayers. Although, vesicular membranes have been formed from F-amphiphiles, there exists no report till date which has described the electrical properties of a fluorinated bilayer and studied the behaviour of proteins in such bilayers. In this chapter, I report for the first time the successful formation of a free-standing fluorinated bilayer.

The F-amphiphile $F_6FC$ was chosen for this study as: (i) its close analogue $F_8FC$ has been reported to spontaneously form very stable bilayer vesicles [6] and (ii) $F_6FC$ has been previously shown by me in chapter three to show interesting properties in studies of membrane proteins. We showed that $F_6FC$ when present at high concentrations (above CMC, 10mM), can stop protein insertion into a DPhPC bilayer. We speculate that it is due to sequestration of protein into aggregates of $F_6FC$. So, we thought it would be interesting to study protein insertion and behaviour in fluorinated bilayers.

Two types of fluorinated bilayers were studied: (i) symmetric $F_6FC$ bilayers where both leaflets of the bilayer were composed of $F_6FC$ and (ii) asymmetric DPhPC-$F_6FC$ bilayers one leaflet of which was composed exclusively of the single chain F-amphiphile $F_6FC$ and the other of the double chain hydrocarbon lipid DPhPC (Figure

4.1). Electrical properties (specific capacitance, I-V curves, and break-down voltage) of these bilayers were characterized and compared with conventional DPhPC lipid bilayers. I then go onto show that proteins can be inserted in fluorinated bilayers and study the behaviour of two proteins (full length WTαHL and the truncated barrel mutant (TBMΔ8NN) in them.

Planar bilayers although extensively used for single-channel studies, are not conducive for studying asymmetric lipid bilayers. Planar asymmetric bilayers are formed across an aperture by bringing together monolayers of different lipid compositions. However, when this bilayer breaks, it results in the loss of asymmetry as the lipids on either side of the aperture can now mix. Such experiments must be restarted, making the use of planar bilayers to study asymmetric bilayers tedious. For this reason, experiments with the fluorinated bilayer were carried out using droplet interface bilayers.

## 4.2 Results and discussion

### 4.2.1 Formation of bilayer

A lipid bilayer membrane impermeable to ions separating two aqueous solutions acts as a capacitor when an electric field is applied. The aqueous solutions are the plates of the capacitor and the lipid membrane is the dielectric. If electrodes are placed in the solutions separated by the membrane, it is possible to measure the membrane capacitance. The formation of a bilayer at the interface of two monolayer-coated aqueous droplets is monitored by measuring the bilayer capacitance (details can be

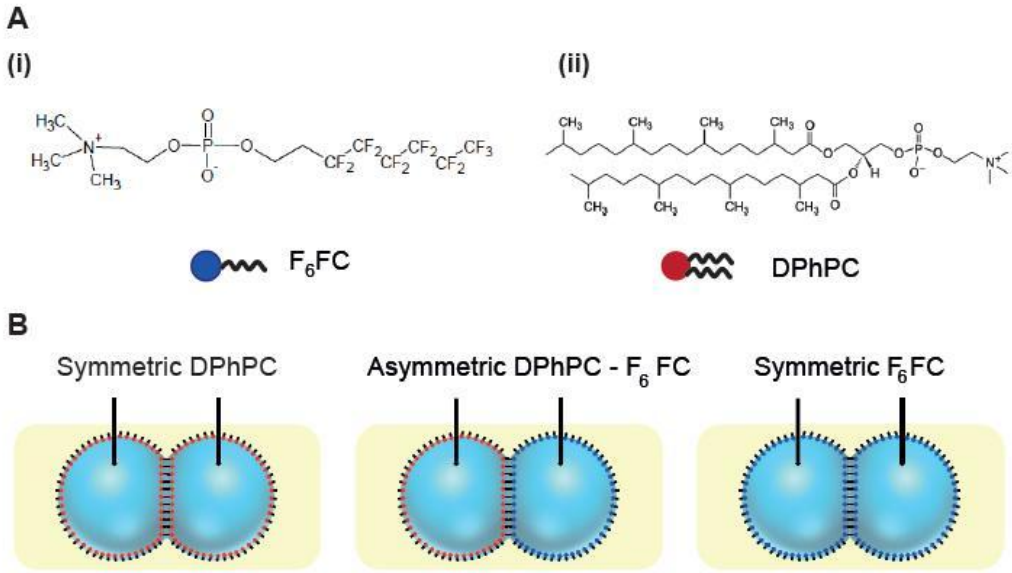


**Figure 4.1: Types of bilayers studied:** *(A) Structures of amphiphiles used in this study. (i) A short single- tailed fluorinated amphiphile $F_6FC$ (ii) A long double-tailed hydrocarbon based lipid molecule DPhPC. (B) Types of bilayers that can be formed by the above two amphiphiles (i) Symmetric DPhPC bilayers where both leaflets of the bilayer are made up of DPhPC (ii) Asymmetric DPhPC-$F_6FC$ bilayers were one leaflet of the bilayer is made from $F_6FC$ and the other leaflet from DPhPC and (iii) Symmetric $F_6FC$ bilayers where both leaflets of the bilayer are made from $F_6FC$.*

found in chapter 2). On bringing together well-equilibrated droplets of DPhPC and $F_6FC$ we observe successful formation of asymmetric DPhPC-$F_6FC$ and symmetric $F_6FC$ bilayers (Figure 4.2). Although fluorocarbons are known to be both hydrophobic and lipophobic, the fluorinated amphiphile $F_6FC$ successfully forms a monolayer at the oil-water interphase. This is possible because the magnitude of the lipophobic effect is a third of the hydrophobic effect [27]. The time required for formation of both the symmetric $F_6FC$ and the asymmetric DPhPC-$F_6FC$ bilayers was found to be comparable to the time required by symmetric DPhPC bilayers. In all three cases (symmetric

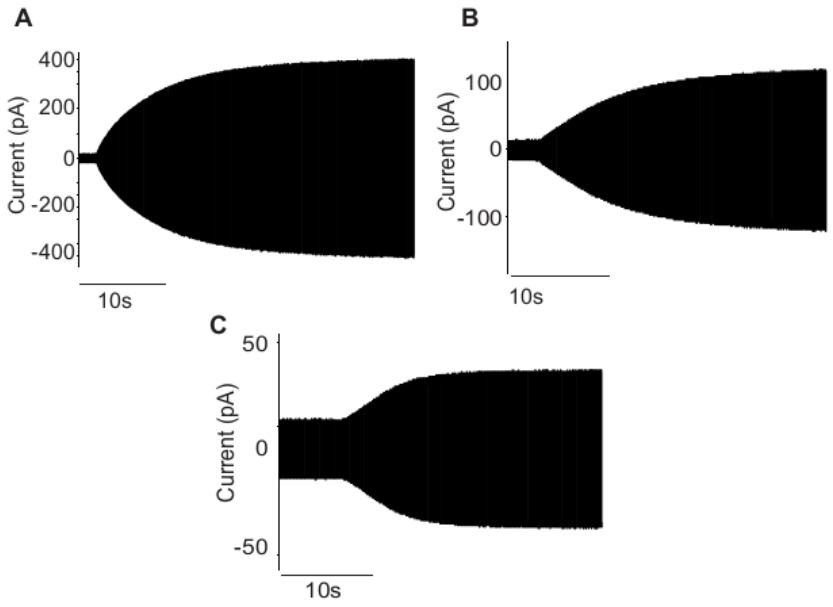


**Figure 4.2: Comparison of bilayer formation.** *Panel (A) bilayer formation is observed by monitoring the increase in bilayer capacitance. (i) Symmetric DPhPC bilayers (ii) Asymmetric DPhPC-F6FC bilayers (iii) Symmetric F6FC bilayers. The bilayers were formed in 1M KCl, 10mM Tris, pH 7.*

DPhPC, asymmetric DPhPC-$F_6$FC, and symmetric $F_6$FC) bilayers took between 20 and 40 seconds to form (Figure 4.2). An observation that can be made from the above figure is the difference in the values of the stabilized (final) capacitance (Figure 4.2). Final capacitances for symmetric DPhPC, asymmetric DPhPC-$F_6$FC, and symmetric $F_6$FC were determined to be 400 ± 100 pF, 110 ± 40 pF, and 40 ± 20 pF respectively (n=5).

For symmetric $F_6$FC bilayers, the low value of steady-state capacitance arises due to a very small contact area between the droplets. From photographs, the contact area for symmetric $F_6$FC bilayers (0.000086 ± 0.00003 $cm^2$) was calculated to be an

order of magnitude smaller when compared to the symmetric DPhPC (0.00063 ± 0.00009 $cm^2$) and the asymmetric DPhPC – $F_6FC$ (0.00035 ± 0.00007$cm^2$). For symmetric $F_6FC$ bilayers, the interface never flattens out, resulting in a very small bilayer area. A possible reason could be the steric hindrance arising from the large size of the terminal $–CF_3$ group on the $F_6FC$ chain.

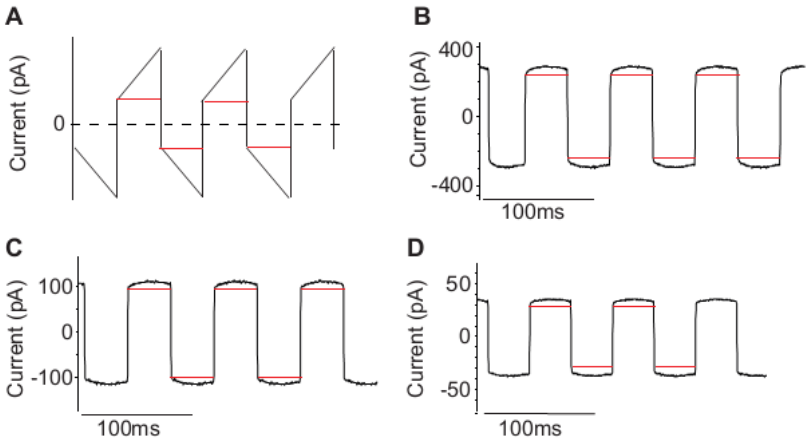


**Figure 4.3: Expanded square wave current traces of final (stabilized) bilayer capacitance.** *(A) Since the lipid bilayer behaves as a capacitor, the application of triangular potential results in a square wave current (in red). In bilayers with a current leakage, the square wave gets modified by an ohmic component (B) symmetric DPhPC bilayers (B) asymmetric DPhPC – $F_6FC$ bilayers (C) symmetric $F_6FC$ bilayers. In all three bilayers, the ohmic deviation from the idealized square wave output (in red) is minimal suggesting that the current leakage through these bilayers is minimal.*

From the expanded view of the bilayer capacitances, it can be seen that two fluorinated monolayers can be brought together to form a non-leaky bilayer. The capacitive current in a leaky bilayer is modified by an ohmic component (Figure 4.3A).

However in the case of both fluorinated bilayers, the ohmic deviation from the idealized square wave output was minimal suggesting that the fluorinated bilayers formed were non-leaky (Figure 4.3 C,D). This observation was encouraging because it allowed me to explore further the possibility of using fluorinated bilayers as a platform for studying membrane proteins.

### 4.2.2 Characterization of the electrical properties of the bilayers

#### 4.2.2.1 Specific capacitance of the bilayer

A lipid bilayer membrane can be thought of as a parallel plate capacitor [28], whose capacitance is given by:

$$C = k\varepsilon_0 A / d$$

where C is the capacitance, k = relative permittivity of the dielectric material, $\varepsilon_0$ is the permittivity of free space ( = 8.854 X $10^{-12}$ F $m^{-1}$), A is the area of the plates, and d is the separation between the plates. In a droplet interface lipid bilayer, k and d refer to the dielectric constant and thickness of the hydrophobic core of the membrane respectively and A refers to the contact area between the two droplets (Figure 4.4 A, B). The area was determined from a photograph of two droplets which are in contact to form a bilayer. The contact length ($l_c$) at the interface of the two droplets was determined with the help of a calibrated graticule. The graticule was calibrated using a silver wire (Sigma Aldrich, product no. 348759) of known thickness (1.5 mm in this case). The thickness of the wire corresponded to 22 divisions on the graticule. This

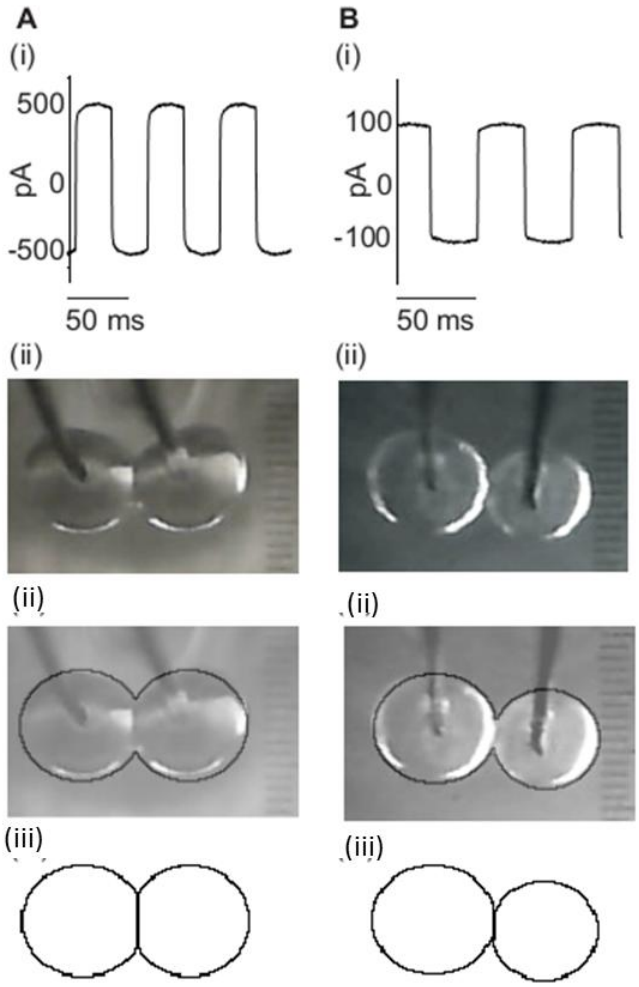


**Figure 4.4: Specific capacitance measurements**. *(A) Representative specific capacitance data for symmetric DPhPC. (i) Capacitance trace showing that the total capacitance was 500 pF (ii) image of two DPhPC droplets in contact (iii) the above image fitted to a circle for purposes of contact length determination (iv) the final result of the fitting. In this case the contact length was determined to be 315 µm and the specific capacitance was determined to be 0.65 µF.cm$^{-2}$. (B) Representative specific capacitance data for asymmetric DPhPC-$F_6$FC. (i) Capacitance trace showing that the total capacitance was 110 pF (ii) image of a DPhPC droplet in contact with a $F_6$FC droplet (iii) the above image fitted to a circle for purposes of contact length determination (iv) the final result of the fitting. In this case the contact length was determined to be 155 µm and the specific capacitance was determined to be 0.38 µF.cm$^{-2}$.*

meant that each division of the graticule corresponds to 0.068 mm. The contact area was calculated from the contact length using the equation: $A = \pi(l_c/2)^2$.

The capacitance per unit bilayer area or the specific capacitance ($C_m$) is determined by the relative permittivity of the dielectric material (k) and thickness of the hydrophobic layer of the membrane that determines the "effective d ". The specific capacitance values of symmetric DPhPC bilayers and asymmetric DPhPC-$F_6$FC bilayers were estimated to be 0.68±0.16 μF/cm$^2$ (n=5) and 0.38±0.12 μF/cm$^2$ (n=5) respectively and are within the range of specific capacitance values (0.3 μF/cm$^2$ to 1 μF/cm$^2$) reported for lipid bilayers [29]. The error in the specific capacitance measurements for symmetric $F_6$FC bilayers was large (0.2 μF/cm$^2$ – 0.6 μF/cm$^2$). This is because (i) the contact area is very small and the bilayer interface is not flat thus resulting in large uncertainities in the area measurements (ii) the total capacitance is only slightly larger (~2X) than the background capacitance.

The specific capacitance of DPhPC bilayers in planar and droplet systems is very well characterized and the value determined in this work corroborates well [30]. On the other hand, capacitance values for fluorinated bilayers have not been reported before. We try to estimate an expected value for the capacitance to see if it agrees with the experimental value.

Based on the formula for a parallel plate capacitor, we have:

$$\frac{C_{asym}}{C_{sym}} = \left( \frac{k_{asym} / d_{asym}}{k_{sym} / d_{sym}} \right) \qquad (1)$$

The thickness of a bilayer is approximately twice the length of the amphiphile(s) constituting the bilayer [28]. The maximum length of a hydrophobic chain ($L_c$) is the length of the molecule in the all-trans configuration. Using formulas reported previously [31]; the chain length of $F_6FC$ and DPhPC was calculated to be 13Å and 20Å respectively. Thus, the expected bilayer thickness for symmetric DPhPC and asymmetric DPhPC- $F_6FC$ bilayer is 40Å and 33Å respectively.

Due to the low polarizability of fluorine, fluorocarbons have been reported to have low-dielectric constants (~1.6) [32,33]. DPhPC bilayers have been reported to have a dielectric constant of 2.2 [30]. For purposes of calculation, the dielectric constant of the asymmetric bilayer is taken to be 1.9 (the mean of the two individual dielectric constants). By plugging in values of the bilayer thickness(s), dielectric constants and DPhPC specific capacitance into equation 1, we get:

$$C_{asym} = C_{sym}\left(\frac{k_{asym}}{k_{sym}}\right)\left(\frac{d_{sym}}{d_{asym}}\right) = 0.68\left(\frac{1.9}{2.2}\right)\left(\frac{40}{33}\right) = 0.71 \quad \mu F/cm^2 \qquad (2)$$

Thus, the ideal parallel plate capacitor equation predicts a value larger than the experimentally determined value. The parallel plate capacitor equation is only valid for capacitors filled with a homogenous dielectric. In the case of an asymmetric DPhPC-$F_6FC$ bilayer, the dielectric constant changes from 1.9 to 2.2 when going from the $F_6FC$ leaflet to the DPhPC leaflet. In such capacitors, the dielectric is not the mean of the individual values, but varies according to the equation: $\alpha + \beta.x$ where $\alpha$ is a dimensionless constant, x is the distance from one plate, and $\beta$ is constant with units of

length$^{-1}$. Thus, the capacitance of a non-homogenous capacitor like asymmetric DPhPC-$F_6$FC bilayer can be better explained by the equation:

$$C_m = \left(\frac{C}{A}\right) = \left(\frac{\beta\varepsilon_0}{\ln(1+\beta.d/\alpha)}\right) \quad (3)$$

#### 4.2.2.2 Break-down voltage of bilayers

Another important property of the lipid bilayer is the breakdown voltage ($V_{br}$), which is an indicator of the stability of the bilayer (higher values for breakdown voltage indicate greater stability of the bilayers). It is widely believed that the electric breakdown of a lipid bilayer proceeds mainly through formation of hydrophilic pores in the lipid matrix [34]. Molecules in a lipid bilayer rearrange themselves to form aqueous pores on application of an external electric field [35, 36]. The membrane usually reseals after the end of the exposure to the electric field provided it does not exceed a critical strength and duration. However, if the duration or strength of the electric field is too high the membrane does not reseal after the electric field is switched off and eventually breaks.

The breakdown voltage ($V_{br}$) is defined as the voltage when the bilayer ruptures and a sudden increase of current across the bilayer is observed. The breakdown voltage was determined using a voltage ramp as suggested by Kramar et al. [36]. According to this protocol, each lipid bilayer is exposed to the voltage ramp only once, unlike determination of the breakdown voltage by repeatedly applying a rectangular voltage pulse where the bilayer is exposed to a voltage pulse many times, which affects the stability and consequently the breakdown voltage of the lipid bilayer.

Breakdown voltage was determined to be 320 ± 40mV (n = 3), 190 ± 35mV (n = 2), and 90 ± 30 mV (n = 2)for symmetric DPhPC, asymmetric DPhPC-$F_6$FC, and symmetric $F_6$FC bilayers respectively (Figure 4.5) and lie within the reported range (200 mV–1 V) of trans-membrane potentials that result in bilayer breakdown for hydrocarbon based bilayers [37, 38]. Thus, we find the stabilities of the three bilayers studied to decrease in the order: Symmetric DPhPC > Asymmetric DPhPC – $F_6$FC > Symmetric $F_6$FC.

A number of theoretical models have been put forward to explain what happens when a lipid bilayer breakdown. The most widely accepted theory of lipid bilayer breakdown is the transient aqueous pore formation model [39]. Hydrophobic pores are spontaneously formed in the bilayer owing to fluctuations or thermal motion of lipid molecules. When the size of these hydrophobic pores exceeds a critical size, a reorientation of the lipids becomes energetically favourable. This reorientation of the lipids converts the hydrophobic pores into hydrophilic ones with the head groups forming the pore walls. These hydrophilic pores grow in size until the bilayer ruptures. Although, this lipid rearrangement is energetically favourable, there is still a price to pay for reorganizing the lipids at the pore edge.

The work done to form a cylindrical hydrophilic pore of radius r is given by:

$$\Delta W(r) = 2\pi r\gamma - \Gamma\pi r^2$$

where $\gamma$ is the edge tension and $\Gamma$ the surface tension of the membrane.

The edge tension (also called line tension) is the energy penalty per unit length of the pore circumference and is the driving force for pore closure or resealing. The edge tension emerges from the physicochemical properties and the amphiphilic nature of lipid molecules. The surface tension of the membrane favours pore opening as the formation of a pore reduces the surface area of the membrane. The above expression implies that spontaneous pore formation is inhibited by an energy barrier. Thus, under physiological conditions, spontaneous thermal fluctuations might create pores, but the probability of surmounting the barrier is small.

Previous reports have shown that the presence of single-chain amphiphiles such as $C_{12}E_8$ or lyso-PC reduce the breakdown voltage of the bilayer [34, 40]. Both $C_{12}E_8$ and lyso-PC are conically shaped amphiphiles. The increase in susceptibility of bilayers containing $C_{12}E_8$ and lyso-PC to electroporation is because these conical shaped amphiphiles can fit into the high curvature of the monolayer at the edge of the pore. This decreases the line tension at the edge of the pore (i.e it decreases the driving force for the closure of the pore) and thus acts to lower the energy barrier that needs to be surmounted for the formation of the pore.

The above explanation could also be the most likely reason for the lower breakdown voltages observed with fluorinated bilayers made from the short chain single-tailed $F_6FC$ amphiphile. The short chain ($C_8$) single-tailed amphiphile probably increases the spontaneous curvature of the fluorinated membranes, thereby decreasing the linear tension at the edge of a pore. Thus, the energy barrier needed to be overcome for pore formation is reduced in the case of these fluorinated bilayers and making them

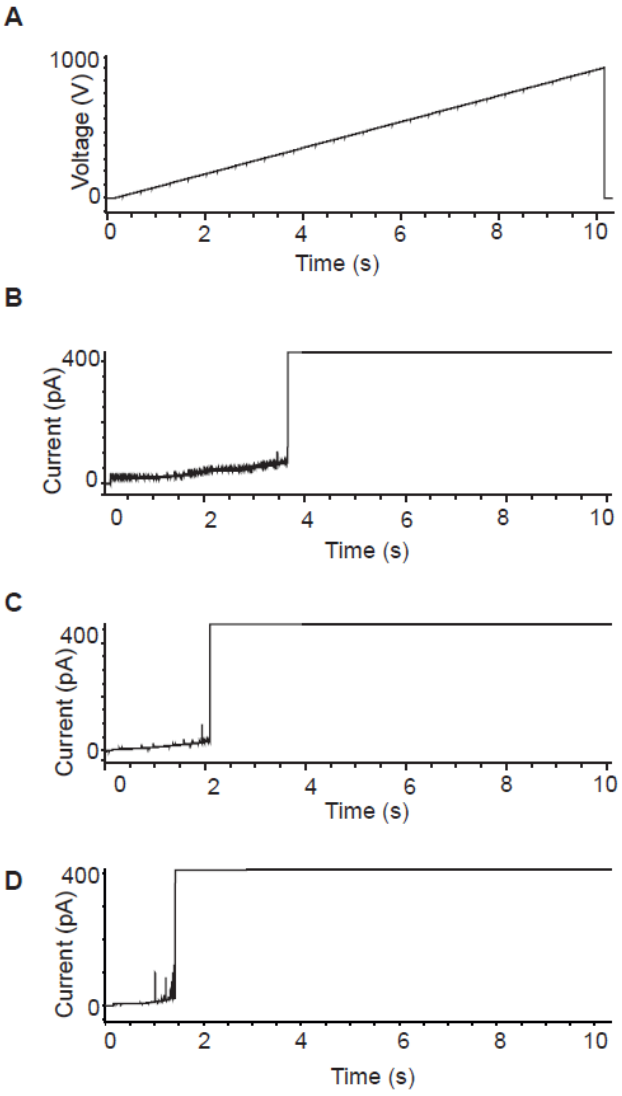


**Figure 4.5: Representative traces of breakdown voltage.** *(A) Linear rising voltage ramp (ramp speed: 100mV/s) that was used for determination of breakdown voltage. (B) Typical trace (n=3) showing symmetric DPhPC bilayers breaking at 340mV. (C) Typical trace showing asymmetric DPhPC-F6FC bilayers breaking at 193mV (n=2). (D) Typical trace showing symmetric F6FC bilayers breaking at 126mV. The buffer was 1M KCL, 10mM Tris, pH 7.0.*

more susceptible to electroporation.

#### 4.2.2.3 Current-voltage characteristics of the bilayer

In this section we investigate the electrical properties of symmetric DPhPC bilayers, asymmetric DPhPC-$F_6$FC bilayers, and symmetric $F_6$FC bilayers by measuring the current across the membranes at different applied voltages. The following observations can be made from the I-V plots of the three bilayers (Figure 4.6): (a) for all three bilayers, the current increases non-linearly with the voltage (b) The magnitude of the current flowing through the bilayer in the absence of protein increases the order: symmetric DPhPC < asymmetric DPhPC-$F_6$FC < symmetric $F_6$FC (c) for both the symmetric DPhPC and $F_6$FC bilayers, the I-V curve is symmetric at both positive and negative potentials, while it is distinctly asymmetric at positive and negative potentials for the asymmetric DPhPC – $F_6$FC bilayers. A possible explanation for the above observations is discussed below.

A perfectly sealed lipid bilayer acts as an insulator. This is because, in the absence of aqueous pores or channels, the transfer of a monovalent ion through a lipid membrane encounters a free energy barrier of $\Delta G_B$=62RT, where R is the gas constant and T is the Kelvin temperature [41]. However on application of high voltages, lipid bilayers transiently lose their barrier due to spontaneous formation of pores, which lowers the value of the above barrier by a factor of 3 – 4 [34]. These short-lived spontaneous hydrophilic pores determine the membrane conductivity and information on pore size and number can be drawn from the dependence of membrane conductivity on

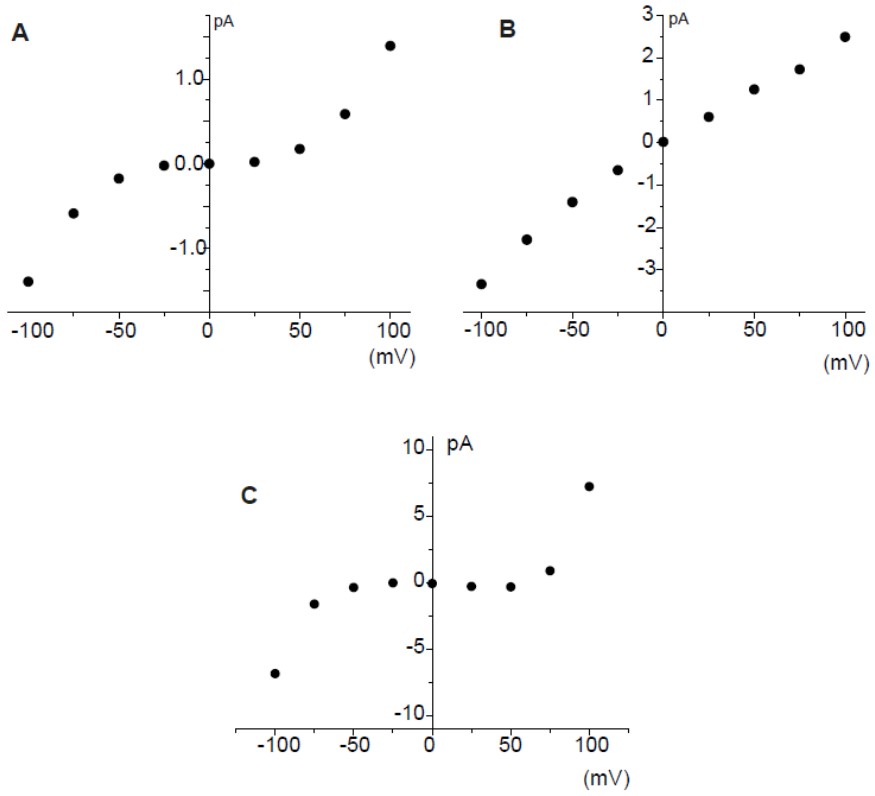


**Figure 4.6: I-V curves of bilayers in absence of protein:** *(A) symmetric DPhPC (B) asymmetric DPhPC – $F_6$FC bilayer (C) Symmetric $F_6$FC bilayers. In the case of the symmetric DPhPC and symmetric $F_6$FC bilayers, the current is symmetric with respect to the applied voltage but becomes strongly non-linear at higher applied biases. For the asymmetric DPhPC-$F_6$FC bilayer the non-linearity is reduced and the I-V curve is now distinctly asymmetric at positive and negative potentials. The graphs shown here are representative measurements (n=3) obtained in 1M KCL, 10mM Tris, pH 7.0.*

membrane voltage. Previous reports have shown that the rate of pore formation in a bilayer is exponentially dependent on $V^2$ [34,41] . The voltage applied causes a gradual increase in the size of the hydrophilic pores, resulting in more current flowing through the bilayer. Consequently, the conductivity of the membrane is a non-linear function of voltage.

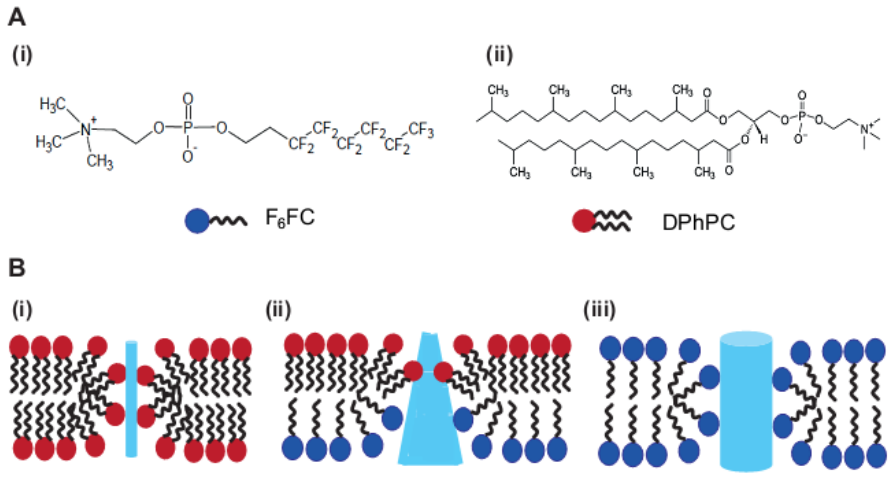


**Figure 4.7: Schematic showing types of hydrophilic pores formed during electroporation.** *(A) Structures of amphiphiles used in this study. (i) A short single-tailed fluorinated amphiphile $F_6FC$ (ii) A long double-tailed hydrocarbon based lipid molecule DPhPC. (B) Types of hydrophilic pores formed: (i) Symmetric DPhPC (ii) asymmetric DPhPC-$F_6FC$ and (iii) Symmetric $F_6FC$ bilayers. For symmetric DPhPC and symmetric $F_6FC$ bilayers, it is likely that cylindrical pores (symmetrical on both sides) are formed, whereas conical shaped pores (asymmetrical on both sides) are formed in the asymmetric bilayers. Larger pores formed in fluorinated bilayers could account for the larger magnitude of current passing through the fluorinated bilayers on application of a potential.*

The asymmetry in the I-V curve for asymmetric DPhPC-$F_6FC$ bilayers is indicative of asymmetric pore formation. For symmetric DPhPC and symmetric $F_6FC$ bilayers, it is likely that cylindrical pores (symmetrical on both sides) are formed, whereas conical shaped pores (asymmetrical on both sides) are formed in the asymmetric bilayers (Figure 4.7). This could be a possible explanation for the asymmetry in the I-V curve. The larger magnitude of current passing through the fluorinated bilayers is probably reflective of larger pores formed in fluorinated bilayers. However, the noteworthy point

is that the I-V graph of the DPhPC-$F_6$FC bilayer shows an asymmetry which is a good evidence for the asymmetry of the bilayer.

Before moving onto the behaviour of proteins in fluorinated bilayers, I summarize the results of the electrical characterization of the two bilayers discussed thus far in table 4.1 below:

| | **Symmetric DPhPC** | **Asymmetric DPhPC – $F_6$FC** | **Symmetric $F_6$FC** |
|---|---|---|---|
| Final value of total capacitance | 400 ± 100 pF | 110±40 pF | 40 ± 20 pF |
| I-V curves | Symmetric but non-linear at higher potentials | Decreased non-linearity but asymmetric | Symmetric but non-linear at higher potentials |
| Specific capacitance [a] | 0.68±0.16 μF/cm$^2$ | 0.40±0.12 μF/cm$^2$ | Not determined [b] |
| Breakdown voltage | 320±40mV | 190±55mV | 90 ± 30 mV |

**Table 4.1: Summary of the electrical characterization of symmetric DPhPC, asymmetric DPhPC-$F_6$FC, and symmetric $F_6$FC bilayers.** *The values are written as mean±s.d and are determined from two to three different attempts. [a] For the specific capacitance measurements, the biggest source of error is the area determination from the photograph of the droplets. [b] The specific capacitance for symmetric $F_6$FC bilayers could not be determined with accuracy and was found to vary between 0.2 μF/cm$^2$ and 0.6 μF/cm$^2$. The uncertainty in the measurement of specific capacitance for symmetric $F_6$FC bilayers is large as (i) the contact area is very small and (ii) marginal increase of capacitance over the background capacitance (Figure 4.2).*

### 4.2.3 Behaviour of proteins in fluorinated bilayers

To the best of my knowledge, there exists no study on whether membrane proteins are capable of inserting into fluorinated bilayers and their behaviour in such bilayers. In this

section, I assess the ease of protein insertion in fluorinated bilayers and provide, for the first time, single channel current behaviour of two proteins in these fluorinated bilayers and compare their behaviour in symmetric DPhPC bilayers. The two proteins studied were the full-length α-hemolysin pore and the truncated beta barrel mutant TBMΔ8NN.

This study is interesting for two reasons. In chapter three, we showed that protein insertion is effectively stopped in presence of high concentration of fluorinated amphiphiles. It was interesting to see if based on these results I could form asymmetric bilayers of DPhPC and $F_6FC$, such that protein insertion occurred only from the DPhPC side but not from the fluorinated side. Also, the two leaflets of the asymmetric DPhPC-$F_6FC$ bilayers are likely to have different bending rigidities which may influence the channel activity in different ways. Channel activity has been previously been shown to be modulated by bilayer structure [42]. Protein behaviour in the bilayers have been compared according to (a) ease of insertion (b) channel activity of the pore once inserted (c) open pore noise level.

#### 4.2.3.1 Full length wild type alpha-hemolysin

##### 4.2.3.1.1 Protein insertion in symmetric DPhPC bilayers

In a routinely used buffer solution, such as 1M KCl, 10mM Tris, pH 7.0, symmetric DPhPC bilayers were found to be stable and almost no current passed through the bilayer in the absence of protein. However, the addition of αHL heptamer protein led to a rapid increase of membrane current and is attributed to the formation of stable

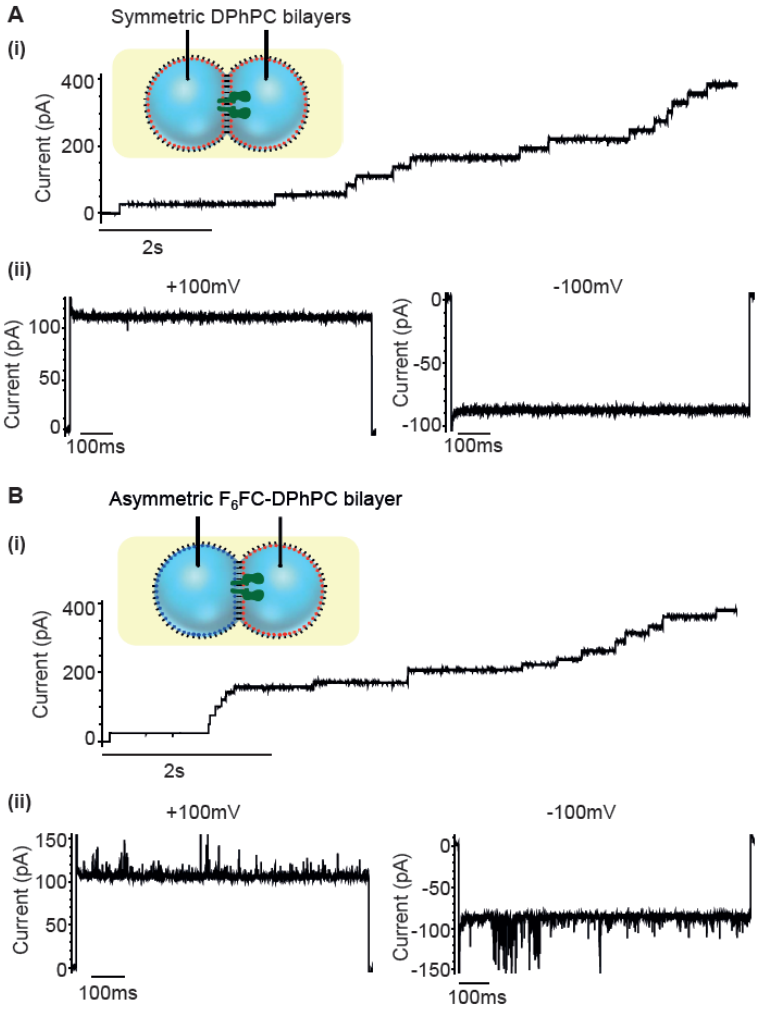


**Figure 4.8: Electrical recordings of full-length αHL in symmetric and asymmetric bilayers.** *(A) Symmetric DPhPC bilayer: (i) Multiple insertions of the full length α-hemolysin pore at +25mV. The step sizes are homogenous measuring 27.2±1.0 pA (ii) Representative single channel trace of the full length pore at ± 100mV showing no channel gating or closure. (B) Asymmetric $F_6$FC-DPhPC bilayer: (i) Multichannel insertions of the full length α-hemolysin pore from the DPhPC side in an asymmetric DPhPC – $F_6$FC bilayer at +25mV. The step sizes are homogenous measuring 26.3±1.6 pA (ii) Representative single channel trace of the full length pore at ± 100mV showing no channel gating or closure. The buffer was 1M KCL, 10mM Tris, PH 7.0.*

heptameric pores in the bilayer (Figure 4.8A(i)). These current traces show that the step sizes corresponding to each heptamer insertion was homogenous and its amplitude was determined to be 27.2±1.1 pA at +25mV. In accordance with previous studies, the full length α-hemolysin pore exhibited no gating and remained open for extended periods of time at trans-membrane potentials of less than +100mV (Figure 4.8A(ii)).

The presence of an unpaired negatively charged residue D128 at the entrance to the channel provides a significant acceleration for cation flow through the channel [42]. This affects the symmetry in ion conduction and results in an asymmetric current-voltage (I-V) graph (Figure 4.9A). The rectification ratio (defined as $I_{+100mV}/ I_{-100mV}$) determined from the I-V relationship was 1.26. Both the values of channel conductance and the rectification ratio agree well with previously published reports [43]. The behaviour of the full length α-hemolysin in symmetric DPhPC bilayers is very well characterized and thus can be a good "standard" against which I can compare the behaviour of protein in the fluorinated bilayers.

#### 4.2.3.1.2 Protein insertion in asymmetric DPhPC-$F_6$FC bilayers

The protein insertion in asymmetric bilayers was studied under three conditions (i) protein insertion from the DPhPC side, (ii) protein insertion from the fluorinated side at low concentrations of $F_6$FC (1mM) and, (iii) protein insertion from the fluorinated side at high concentrations of $F_6$FC (10mM). When a droplet with a fluorinated $F_6$FC monolayer coating is brought into contact with a DPhPC coated α-hemolysin-containing droplet, a rapid increase in current was observed. In these set of experiments,

the full length protein is inserting from DPhPC side such that the lower part of the beta-barrel is embedded in the fluorinated $F_6FC$ leaflet of the bilayer.

The rate of αHL heptamer insertion into asymmetric bilayers from the DPhPC side is similar to the incorporation rate in symmetric DPhPC bilayers (Figure 4.8B (i)). The step sizes corresponding to each insertion was determined to be 26.3±1.6 pA at +25mV and was comparable to that observed in symmetric DPhPC bilayers.

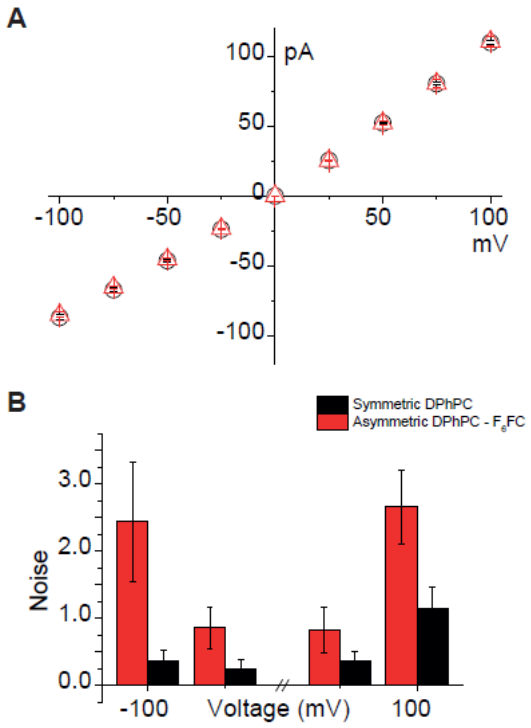


**Figure 4.9: Comparison of αHL behaviour in symmetric and asymmetric bilayers.** *(A) I-V curve of the full length αHL in symmetric DPhPC bilayers (black circles) and when it inserts from the DPhPC side in the asymmetric bilayers (red triangles). Each data point on the I-V curve is plotted as the mean±s.d from atleast three different experiments (B) The noise of the open channel in asymmetric bilayers is much more than the noise of the open channel in symmetric bilayers. Shown here is the noise of the open channel in the two bilayers at ±75mV and ±100mV. The buffer was 1M KCL, 10mM Tris, pH 7.0.*

Also, interestingly, no channel gating or closure was observed at applied potentials of ≤ +100mV despite the lower half of the barrel being in a fluorinated monolayer, (Figure 4.8B (ii)). The rectification property of the α-hemolysin pore remained unchanged as evidenced by the current-voltage plot (Figure 4.9A) and the rectification ratio (defined as I+100mV / I-100mV) was determined to be 1.29. Although the overall behaviour of the full length protein is comparable in both symmetric and asymmetric bilayers, the noise in the open pore current signal was significantly increased (upto a factor of 5 depending on the voltage) in the case of asymmetric bilayers (Figure 4.9B).

In the next set of experiments to examine protein insertion in asymmetric bilayers, the protein was present in the $F_6FC$ droplet. The concentration of $F_6FC$ in the fluorinated droplet is 1mM. As discussed in chapter three, at this concentration, it does not stop protein from inserting in the bilayer. The most striking difference between protein inserting from the DPhPC side and from the fluorinated side is the rate of protein insertion. Insertion of αHL heptamer from the DPhPC side is extremely efficient and single channel insertion events require very little protein inside the droplets (~1 - 10 pg). In DPhPC bilayers, high concentrations of the protein (~1 -10 ng) results in a rapid increase in current corresponding to multiple insertions. In comparison, protein insertion from the fluorinated side was not very efficient. Mostly single channel insertions of the heptamer were seen at relatively high concentrations of protein (~ 20 ng) while no channel insertion of the protein was observed at low concentrations of the protein (~1 – 10 pg). However, once the protein managed to insert, the activity of the channel is comparable to what is seen in symmetric DPhPC

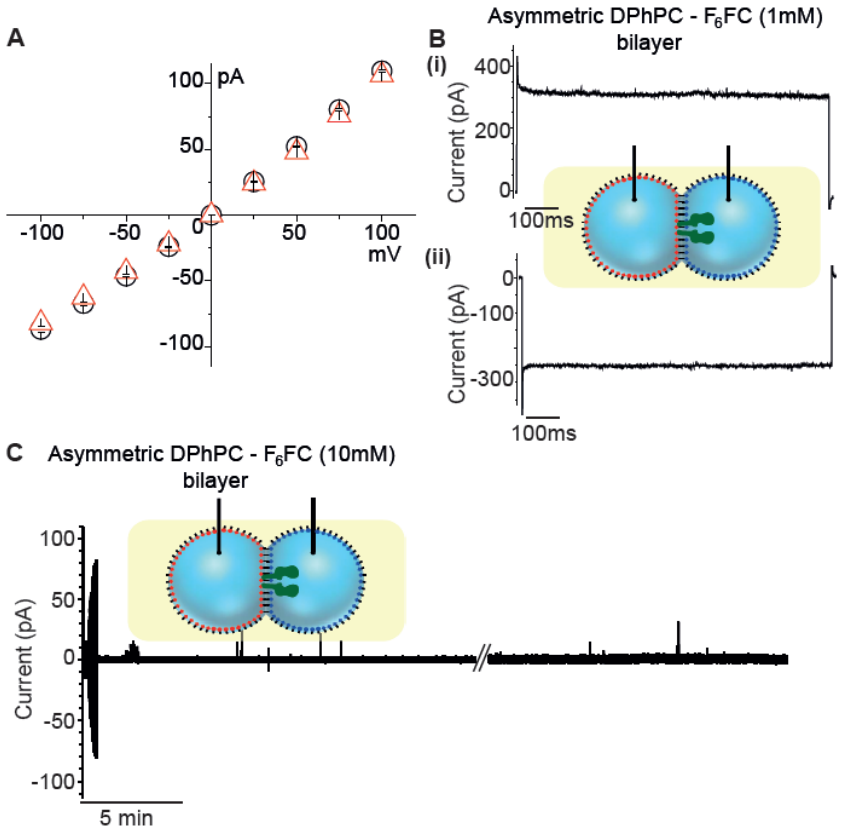


**Figure 4.10: Behaviour of the full length αHL heptamer protein in asymmetric DPhPC – $F_6$FC bilayers when presented from the fluorinated side.** *(A)The I-V curves of the protein in symmetric DPhPC bilayers (black circles) and in the asymmetric bilayer (red triangles). Each data point on the I-V curve is plotted as the mean±s.d from atleast three different experiments (B) Shown here is a multi-channel (3) record of full length α-hemolysin in an asymmetric DPhPC-F6FC bilayer after insertion from the F-side (1mM). No gating or closure of the channel was seen at ±100mV. (C) No insertion of protein was seen from the fluorinated side when the concentration of $F_6$FC inside the droplet was increased to 10mM. The traces before and after the break in the recording were acquired at 25mV and 50mV respectively. The buffer used in all cases is 1M KCL, 10mM Tris, pH 7.0.*

bilayers as observed from the I-V curves (Figure 4.10A). The rectification ratio (defined as I+100mV / I-100mV) was determined from the I-V curves to be 1.29. In this case too, no

gating or channel closure was observed. (Figure 4.10B). When the concentration of F6FC inside the droplet was increased to 10mM, no channel insertion was seen, which is in accordance with results obtained in chapter three (Figure 4.10C).

#### 4.2.3.2 Truncated barrel mutant (TBMΔ8NN) of alpha-hemolysin

Truncated beta barrel mutants of α-hemolysin were made by David Stoddart (a former student of the Bayley group) in an attempt to improve DNA base recognition [46] (a brief description of the protein and how it was made is provided in chapter 2). Molecular dynamic simulations (carried out by J. Klingelhoefer) estimated that the TBMΔ8NN was shorter than the full length protein by 18.5Å (Figure 4.11 A). Stoddart found that TBMΔ8NN although unable to lyse rabbit cell membranes, could form short-lived pores in planar lipid bilayers made from DPhPC (Figure 4.11B). Pore insertion was observed only at higher positive potentials (ie +200 mV); in DPhPC bilayers and no significant pore activity was seen at lower or negative potentials. Qualitatively, the life-time of the pores could be increased from seconds to minutes by doping the DPhPC bilayer with a short chain lipid (11 carbons) such as DLPC (1, 2-dilauroyl-sn-glycero-3-phosphocholine) (Figure 4.11B). In his thesis, he proposed that the presence of shorter chain lipids in the bilayer aids in bilayer thinning or leaflet curvature which allows for protein insertion or opening (Figure 4.11C) [46]. These results seemed to suggest that the presence of a short chain lipid in the DPhPC bilayer improved the open times of the TBMΔ8NN pores.

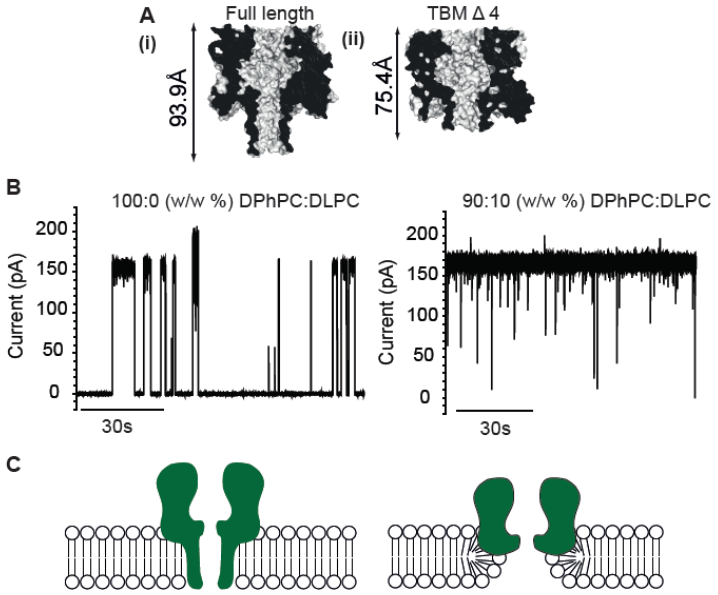


**Figure 4.11**: **Introduction to TBMΔ8NN pores** (A) *Molecular dynamics simulations (performed by J. Klingelhoefer) comparing the length of the mutated TBMΔ8NN protein with the full length alpha-hemolysin pore. The TBMΔ8NN protein is shorter than the full length protein by 18.5Å. (B) Current-voltage (I-V) characteristics of the TBM Δ4 protein pore. (left) TBM Δ4 proteins typically formed short-lived open pores (applied potential of +200 mV) in bilayers made from DPhPC. (right) The open times of the pore was improved on supplementing the DPhPC bilayers with 10% (w/w) DLPC which has shorter fatty acid tails, compared to DPhPC. (C) The full length αHL pore (upper - green) forms an entirely proteinaceous channel, however TBM pores (lower - green) may form part lipid, part protein conducting channels.(This figure has been adapted from David Stoddart's D.Phil thesis [44])*

The F-amphiphile $F_6FC$ has a very short chain (C8). Thus, the asymmetric DPhPC – $F_6FC$ bilayers presented an attractive system (as well as a hitherto unexplored) platform to study the behaviour of the TBMΔ8NN protein. First, we wanted to check if TBMΔ8NN could insert in fluorinated bilayers given their short transmembrane segment and second, once inserted, if they could form stable pores.

#### 4.2.3.2.1 TBMΔ8NN in symmetric DPhPC droplet bilayers

The behaviour of the TBMΔ8NN pores were previously characterized in planar DPhPC bilayers by Stoddart [46]. However, the fluorinated bilayers and the properties of proteins in them are being studied in droplet bilayers. To enable a direct comparison of TBMΔ8NN behaviour in symmetric DPhPC and asymmetric DPhPC-$F_6$FC bilayers, I characterized the behaviour of TBMΔ8NN pores in DPhPC droplet bilayers. The behaviour of TBMΔ8NN in DPhPC droplet bilayers was agrees well with results obtained in planar DPhPC bilayers. At the protein concentrations tested (0.01 ng), very little or no channel activity was observed on the application of low positive potentials or negative potentials (eg: 2 channel events over the course of 1 minute at +25mV) (Figure 4.12A). At the same protein concentration, relatively more channel activity was observed at high applied potentials (≥ +150mV) (eg: 6 channel events over the course of 30 seconds at +150mV. Like observed in planar bilayers, the pores formed by TBMΔ8NN in droplet bilayers were also short-lived (hundreds of milliseconds) (Figure 4.12B).

#### 4.2.3.2.2 TBMΔ8 in asymmetric DPhPC – $F_6$FC droplet bilayers

It has been proposed that TBMΔ8NN forms half protein-half lipid channels in the bilayer [46] (Figure 4.11C). This would have interesting consequences in the asymmetric DPhPC-$F_6$FC bilayers. In the first set of experiments, TBMΔ8NN was present in the DPhPC droplet. In this situation, TBMΔ8NN inserts from the DPhPC side with the lower half of the toroidal lipid pore being formed by the single short chain

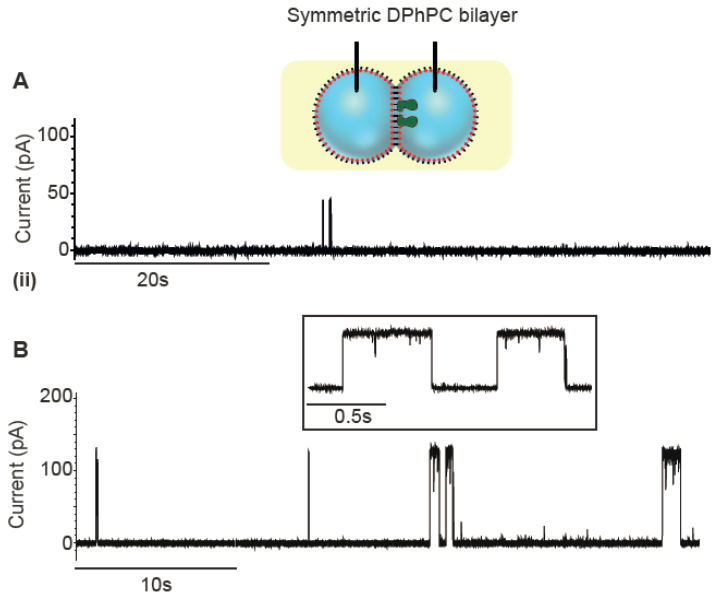


**Figure 4.12: Behaviour of TBMΔ8NN in symmetric DPhPC bilayers.** *(A) The application of a low positive potential (+25mV) does not result in significant channel activity. In this particular recording, only 2 channel events were seen over a course of 1 minute. (B) Channel activity observed on application of a high applied potential (+150mV). The inset shows an expanded trace of a channel event showing that TBMΔ8NN forms short-lived pores (few seconds at 150mV) in symmetric DPhPC bilayers. The buffer was 1M KCL, 10mM Tris, pH 7.0.*

$F_6$FC amphiphile. Under these circumstances, protein insertion into the bilayer is extremely favourable as protein insertion occurs at even very low protein concentrations (0.0004 ng). Also, in this case TBMΔ8NN activity was observed at low applied potentials (25mV) and also at negative applied potentials. Unlike short-lived pores formed in DPhPC bilayers (few milliseconds), TBMΔ8NN formed stable pores with open times on the order of seconds (1886.72 ± 1091.41 milliseconds at +25mV) in the asymmetric bilayer at low applied potentials and negative potentials (Figure 4.13).

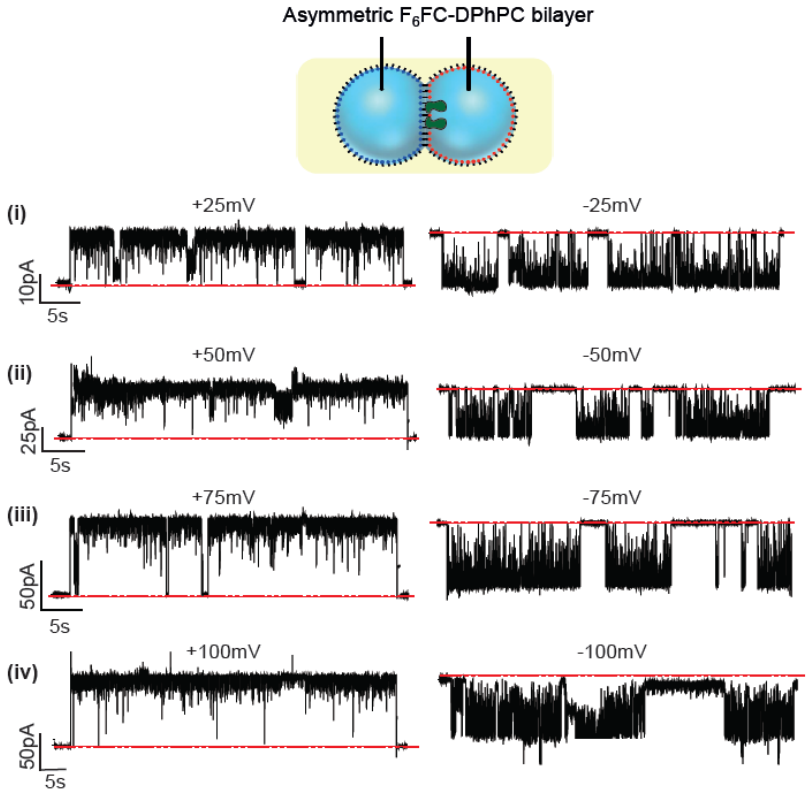


**Figure 4.13: Single channel activity of TBMΔ8NN in asymmetric $F_6$FC-DPhPC bilayers** *after insertion from the DPhPC side at (i) ±25mV (ii) ±50mV (iii) ±75mV and (iv) ±100mV. The red line indicates the zero level current. The buffer used was 1M KCL, 10mM Tris, pH 7.0.*

As can be seen, the open pore level was now very noisy. In the next of experiments, TBMΔ8NN is present in the $F_6$FC droplet (1mM). In this situation, TBMΔ8NN inserts from the fluorinated side with the lower half of the "channel" being formed by DPhPC. As was the case with the full length αHL protein, the insertion of TBMΔ8NN protein from the fluorinated side was not very efficient as protein insertion was observed only at high concentrations of the protein (0.02ng).

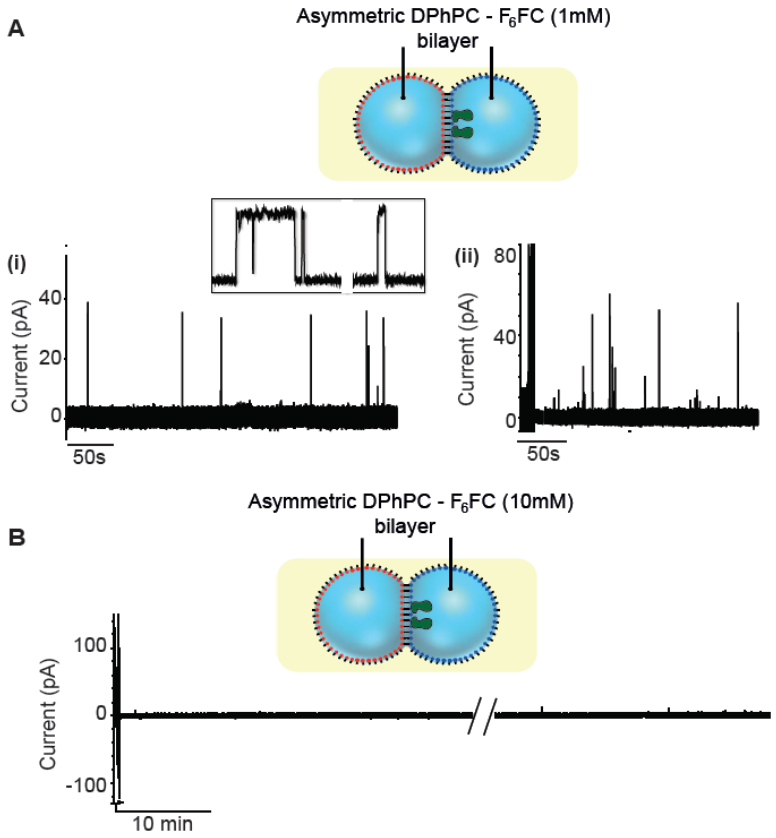


**Figure 4.14: Behaviour of TBMΔ8NN in asymmetric bilayers** *(A) after insertion from F6FC side at 25mV (i) and 50mV (ii). The inset shows an expanded trace to show that the channels are transient short-lived pores on the order of a few milliseconds. (C) No insertion of channel was observed when the concentration of $F_6$FC was increased to 10mM. The traces before and after the break in the recording were taken at 25mV and 50mV respectively. The buffer used was 1M KCL, 10mM Tris, pH 7.0.*

Nonetheless, once insertion occurred, the nature of the protein activity was qualitatively similar to that observed in DPhPC (i.e. short lived pores with open times on the order of a few milliseconds) (Figure 4.13B). As mentioned earlier, the short chain single-tailed $F_6$FC amphiphile is conical shaped. Because of this, it tends to increase the curvature of

the membrane and prefers to be located around the edges of pores in the membrane. For this reason, when the lower half of the "channel" was formed by $F_6FC$, the pores formed had longer open times on the order of seconds as the fluorinated $F_6FC$ monolayer is more amenable to bending and can support stable pores of TBMΔ8NN. When the concentration of $F_6FC$ inside the droplet was increased to 10mM, no insertion of TBMΔ8NN was observed from the fluorinated side, which again correlates well with previously observations (Figure 4.14B).

### 4.3 Note on DIB formation using fluorinated amphiphiles

The most commonly used amphiphile for the formation of droplet interface bilayers has been the double chained lipid molecule DPhPC. In this section, using surface tension measurements, I compare the monolayer formation of DPhPC and F6FC (Figure 4.15). The following three observations are immediately apparent from the figure: (i) the final value of surface tension is much lower in the case of $F_6FC$ (13 mN/m) than DPhPC (35 mN/m). This is in accordance with previous reports which report that F-amphiphiles are very efficient at reducing the surface or interfacial tension [45]. (ii) The second observation is that starting value of surface tension in the two cases is very different (~ 52 mN/m for DPhPC and ~ 16 mN/m for $F_6FC$). This suggests that the single-tailed $F_6FC$ is more surface active than DPhPC which is why it has a greater tendency to migrate to the interface. During drop shape surface tension experiments, the readings are taken after the drop has been formed at the end of the capillary (for details, see section 2.2.3). The initial interfacial tension of newly formed water droplet in

.

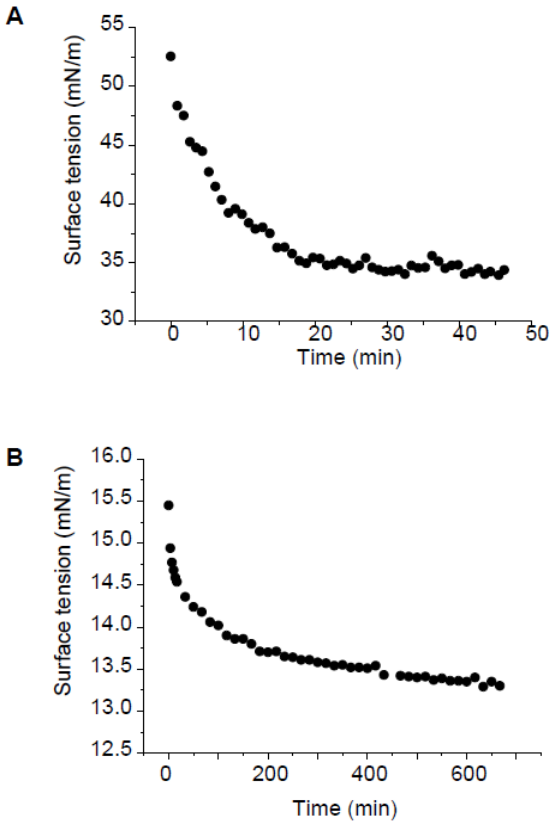


**Figure 4.15: Comparing monolayer formation by DPhPC and F6FC at the oil-water interface.** *The time required to form a monolayer by $F_6FC$ was visualized by measuring the surface tension of the droplet over time. (A) 1mM DPhPC in water (B) 10 mM $F_6FC$ in water. The oil used was hexadecane.*

hexadecane is the same in both cases (i.e 53 mN/m). However, since $F_6FC$ is more surface active, it begins migrating to the water-hexadecane interface at the same time as the drop starts forming. Thus, by the time the readings are taken, the tension has dropped from 53 mN/m to 16 mN/m. (iii) The third observation that can be made from

Figure 4.15, is that despite being more surface active, it is $F_6FC$ which takes a really long time to form a well packed monolayer at the interface. DPhPC when present either in the aqueous or oil phase spontaneously and rapidly (~ 30 minutes) forms a self-assembled lipid monolayer (Figure 4.15A). In comparison, it was found that an aqueous droplet containing the single tailed fluorinated amphiphile $F_6FC$ takes many hours (7-10hrs) to acquire a fluorinated monolayer coating at the droplet interface with hexadecane (Figure 4.15B). Long monolayer formation times (upto days) at the air-water interface has been previously reported for F-amphiphiles [46, 47] and they have been attributed to the slow dissociation kinetics (on the order of seconds) of the monomer amphiphile from the complex lamellar aggregates formed in aqueous solution by F-amphiphiles. Another likely reason for $F_6FC$ to take really long to form monolayers could be that although it migrates to the surface quickly, it takes longer for it to re-order and arrange itself into a densely packed monolayer.

## 4.4 Conclusions

The work in this chapter presents a new platform to study membrane proteins. Traditionally, bilayers have been made from double tailed amphiphilic lipid molecules. It is known that a minimum of C9 hydrocarbon chain length is needed for phosphatidylcholine (PC) molecules to form bilayers [48, 49]. In contrast, even short single chain F-amphiphiles can form lamellar phases and vesicles [31]. This is because the F-alkyl chain has a larger cross-sectional area compared to hydrocarbons, which imparts the amphiphiles with truncated cone geometry which favours the lamellar

phase. I show that it is possible to form free standing bilayers with the short single chain F-amphiphile $F_6FC$. Both symmetric $F_6FC$ bilayers and asymmetric DPhPC – $F_6FC$ bilayers could be successfully formed. Conical-shaped amphiphiles such as the short-tailed $F_6FC$ prefer curved edges. A consequence of this is that fluorinated bilayers of $F_6FC$ have low breakdown voltages. Symmetric $F_6FC$ bilayers have a breakdown voltage of less than +100mV and therefore both electrical characterization and studies of protein behaviour were carried out only in the asymmetric DPhPC – $F_6FC$ bilayers.

The electrical properties of the asymmetric bilayer such as specific capacitance, breakdown voltage and current – voltage relationships were determined and compared with symmetric DPhPC bilayers. The specific capacitance and current–voltage curves of asymmetric bilayers are noteworthy. Asymmetric bilayers have a lower specific capacitance than the symmetric DPhPC. This result was counter-intuitive given that $F_6FC$ has a shorter chain length. Strong evidence for the asymmetry of the DPhPC-$F_6FC$ bilayers came from the I-V measurements. In the absence of protein, the I-V curves for a symmetric DPhPC bilayer were symmetric. In contrast, the I-V curve for the asymmetric bilayer was found to be asymmetric. Studies of protein insertion and behaviour in fluorinated bilayers proved equally interesting. For both the proteins studied, we observed that the insertion of proteins from the fluorinated side in asymmetric bilayers was not as efficient as insertion from the DPhPC side as evidenced by dilution experiments. However, once inserted the full length protein activity is similar irrespective of the side it inserted from as was seen from the I-V curves. However, the channels were significantly noisier when the β-barrel of αHL was present

in the $F_6FC$ monolayer. Studies with the truncated barrel mutant TBMΔ8NN provided more evidence for the asymmetry of the DPhPC – $F_6FC$ bilayers. TBMΔ8NN which does not have the required length to span a lipid bilayer has been proposed to form half protein-half lipid channels (Figure 4.11C). Thus, TBMΔ8NN channel activity should be dependent on the nature of the amphiphile forming the lower leaflet of the bilayer. When the lower leaflet of the channel was formed by the conical-shaped $F_6FC$ amphiphile, stable channels were formed; when the monolayer was formed by long chain DPhPC, TBMΔ8NN formed short lived transient pores. When asymmetric bilayers are formed with higher concentrations of $F_6FC$ (10mM), no protein insertion (both full length αHL and TBMΔ8NN) was seen. This is in accordance with results reported in Chapter 3 and can be explained by the sequestration of protein by the residual $F_6FC$ in the droplet after monolayer formation.

## 4.5 Bibliography

[1] K. Ekroos, C.S. Ejsing, U. Bahr, M. Karas, K. Simons, and A. Shevchenko, "Charting molecular composition of phosphatidylcholines by fatty acid scanning and ion trap MS3 fragmentation," *Journal of Lipid Research*, vol. 44, pp. 2181-2192, Nov 2003.

[2] F. J. Morera, G. Vargas, C. Gonzalez, E. Rosenmann, and R. Latorre, "Ion-Channel Reconstitution," in *Methods in Membrane Lipids*. vol. 400, ed, 2007.

[3] W. R. Redwood, F. R. Pfeiffer, J. A. Weisbach, and T. E. Thompson, "Physical properties of bilayer membranes formed from a synthetic saturated phospholipid in decane," *Biochimica Et Biophysica Acta*, vol. 233, pp. 1-&, 1971.

[4] T. Kunitake, Y. Okahata, and S. Yasunami, "Formation and enhanced stability of fluoroalkyl bilayer-membranes,"*Journal of the American Chemical Society*, vol. 104, pp. 5547-5549, 1982.

[5] M. P. Krafft, F. Giulieri, and J. G. Riess, "Supramolecular assemblies from single-chain perfluoroalkylated phosphorylated amphiphiles," *Colloids and Surfaces a-Physicochemical and Engineering Aspects*, vol. 84, pp. 113-119, Apr 1994.

[6] M. P. Krafft, F. Giulieri, and J. G. Riess, "Can single-chain perfluoroalkylated amphiphiles alone form vesicles and other organized supramolecular systems,"

*Angewandte Chemie-International Edition in English*, vol. 32, pp. 741-743, May 1993.

[7] A. Pasc-Banu, M. Blanzat, M. Belloni, E. Perez, C. Mingotaud, I. Rico-Lattes, *et al.*, "Spontaneous vesicles of single-chain sugar-based fluorocarbon surfactants," *Journal of Fluorine Chemistry*, vol. 126, pp. 33-38, Jan 2005.

[8] T. Kunitake and N. Higashi, "Bilayer-membranes of triple-chain, fluorocarbon amphiphiles," *Journal of the American Chemical Society*, vol. 107, pp. 692-696, 1985.

[9] C. Santaella and P. Vierling, "Molecular order and mobility within liposomal membrane made from highly fluorinated phospholipids," *Chemistry and Physics of Lipids*, vol. 77, pp. 173-177, Aug 1995.

[10] C. Santaella, P. Vierling, and J. G. Riess, "Highly stable liposomes derived from perfluoroalkylated glycerophosphocholines," *Angewandte Chemie-International Edition in English*, vol. 30, pp. 567-568, May 1991.

[11] C. Santaella, P. Vierling, J. G. Riess, T. Gulikkrzywicki, A. Gulik, and B. Monasse, "Polymorphic phase-behavior of perfluoroalkylated phosphatidylcholines," *Biochimica Et Biophysica Acta-Biomembranes*, vol. 1190, pp. 25-39, Feb 1994.

[12] F. Guillod, J. Greiner, and J. G. Riess, "Vesicles made of glycophospholipids with homogeneous (two fluorocarbon or two hydrocarbon) or heterogeneous (one fluorocarbon and one hydrocarbon) hydrophobic double chains, " *Biochimica Et Biophysica Acta-Biomembranes*, vol. 1282, pp. 283-292, Jul 1996.

[13] L. Zarif, T. Gulikkrzywicki, J. G. Riess, B. Pucci, C. Guedj, and A. A. Pavia, "Alkyl and perfluoroalkyl glycolipid-based supramolecular assemblies," *Colloids and Surfaces a-Physicochemical and Engineering Aspects*, vol. 84, pp. 107-112, Apr 1994.

[14] C. Guedj, B. Pucci, L. Zarif, C. Coulomb, J. G. Riess, and A. A. Pavia, "Vesicles and other supramolecular systems from biocompatible synthetic glycolipids with hydrocarbon and/or fluorocarbon chains," *Chemistry and Physics of Lipids*, vol. 72, pp. 153-173, Aug 1994.

[15] J. Sabin, G. Prieto, J. Estelrich, F. Sarmiento, and M. Costas, "Insertion of semifluorinated diblocks on DMPC and DPPC liposomes. Influence on the gel and liquid states of the bilayer," *Journal of Colloid and Interface Science*, vol. 348, pp. 388-392, Aug 2010.

[16] M. Schmutz, B. Michels, P. Marie, and M. P. Krafft, "Fluorinated vesicles made from combinations of phospholipids and semifluorinated alkanes. Direct experimental evidence of the location of the semifluorinated alkane within the bilayer," *Langmuir*, vol. 19, pp. 4889-4894, Jun 2003.

[17] J. G. Riess, "Introducing a new element - Fluorine - Into the liposomal membrane," *Journal of Liposome Research*, vol. 5, pp. 413-430, 1995.

[18] F. Frezard, C. Santaella, P. Vierling, and J. G. Riess, "Fluorinated phospholipid-based vesicles as potential-drug carriers - encapsulation/sustaining of drugs and stability in human serum," *Artificial Cells Blood Substitutes and Immobilization Biotechnology*, vol. 22, pp. 1403-1408, 1994.

[19] F. Frezard, C. Santaella, P. Vierling, and J. G. Riess, "Permeability and stability in buffer and in human serum of fluorinated phospholipid-based liposomes," *Biochimica Et Biophysica Acta-Biomembranes*, vol. 1192, pp. 61-70, Jun 1994.

[20] V. Ravily, C. Santaella, and P. Vierling, "Membrane permeability and stability in buffer and in human serum of fluorinated di-O-alkylglycerophosphocholine-based liposomes," *Biochimica Et Biophysica Acta-Biomembranes*, vol. 1285, pp.79-90, Nov 1996.

[21] N. Privitera, R. Naon, and J. G. Riess, "Hydrolysis of dmpc or dppc by pancreatic phospholipase a(2) is slowed down when (perfluoroalkyl) alkanes are incorporated into the liposomal membrane," *Biochimica Et Biophysica Acta-Lipids and Lipid Metabolism*, vol. 1254, pp. 1-6, Jan 1995.

[22] C. Gadras, C. Santaella, and P. Vierling, "Improved stability of highly fluorinated phospholipid-based vesicles in the presence of bile salts," *Journal of Controlled Release*, vol. 57, pp. 29-34, Jan 1999.

[23] P. Barthelemy, N. Cuvillier, Y. Chaudier, J. J. Benattar, and B. Pucci, "Stability of Newton black films of highly fluorinated non-ionic surfactants," *Journal of Fluorine Chemistry*, vol. 105, pp. 95-102, Aug 2000.

[24] T. McIntosh, S. Simon, P. Vierling, C. Santaella, and V. Ravily, "Structure and interactive properties of highly fluorinated phospholipid bilayers," *Biophysical Journal*, vol. 71, pp. 1853-1868, OCT 1996 1996.

[25] H. Saito, W. Shinoda, and M. Mikami, "Enhanced hydrophobicity of fluorinated lipid bilayer: A molecular dynamics study," *Journal of Physical Chemistry B*, vol. 112, pp. 11305-11309, SEP 11 2008 2008.

[26] M. P. Krafft, "Fluorocarbons and fluorinated amphiphiles in drug delivery and biomedical research," *Advanced Drug Delivery Reviews*, vol. 47, pp. 209-228, Apr 2001.

[27] M. P. Krafft and M. Goldmann, "Monolayers made from fluorinated amphiphiles," *Current Opinion in Colloid & Interface Science*, vol. 8, pp. 243-250, Aug 2003.

[28] S. H. White, "Study of lipid bilayer membrane stability using precise measurements of specific capacitance," *Biophysical Journal*, vol. 10, pp. 1127-&, 1970.

[29] R. S. Ries, H. Choi, R. Blunck, F. Bezanilla, and J. R. Heath, "Black lipid membranes: visualizing the structure, dynamics, and substrate dependence of membranes," *Journal of Physical Chemistry B*, vol. 108, pp. 16040-16049, Oct 2004.

[30] L.C.M. Gross, A. J. Heron, S.C. Baca, and M.I. Wallace, "Determining Membrane Capacitance by Dyamic Control of Droplet Interface Bilayer Area," *Langmuir*, vol. 27, pp. 14335-14342, Dec 2011.

[31] F. Giulieri and M.-P. Krafft, "Can the formation of vesicles from single-chain perfluoroalkylated amphiphiles be predicted?," *Colloids and Surfaces A: Physicochemical and Engineering Aspects*, vol. 84, pp. 121-127, 1994.

[32] P. Lonostro, "Phase-separation properties of fluorocarbons, hydrocarbons and their copolymers," *Advances in Colloid and Interface Science*, vol. 56, pp. 245-287, Mar 1995.

[33] T. Hiyama, *Organofluorine compounds:Chemistry and Applications*: Springer, 2000.

[34] R. W. Glaser, S. L. Leikin, L. V. Chernomordik, V. F. Pastushenko, and A. I. Sokirko, "Reversible electrical breakdown of lipid bilayers - formation and evolution of pores," *Biochimica Et Biophysica Acta*, vol. 940, pp. 275-287, May 1988.

[35] P. Kramar, D. Miklavcic, and A. M. Lebar, "A System for the Determination of Planar Lipid Bilayer Breakdown Voltage and Its Applications," *Ieee Transactions on Nanobioscience*, vol. 8, pp. 132-138, Jun 2009.

[36] P. Kramar, D. Miklavcic, and A. M. Lebar, "Determination of the lipid bilayer breakdown voltage by means of linear rising signal," *Bioelectrochemistry*, vol. 70, pp. 23-27, Jan 2007.

[37] C. Chen, S. W. Smye, M. P. Robinson, and J. A. Evans, "Membrane electroporation theories: a review," *Medical & Biological Engineering & Computing*, vol. 44, pp. 5-14, Mar 2006.

[38] S. H. White, "Electrical breakdown of bimolecular lipid-membranes as an electromechanical instability," *Biophysical Journal*, vol. 14, pp. 155-158, 1974.

[39] J. C. Weaver and Y. A. Chizmadzhev, "Theory of electroporation: A review," *Bioelectrochemistry and Bioenergetics*, vol. 41, pp. 135-160, Dec 1996.

[40] G. C. Troiano, L. Tung, V. Sharma, and K. J. Stebe, "The reduction in electroporation voltages by the addition of a surfactant to planar lipid bilayers," *Biophysical Journal*, vol. 75, pp. 880-888, Aug 1998.

[41] S. Kakorin and E. Neumann, "Ionic conductivity of electroporated lipid bilayer membranes," Bioelectrochemistry, vol. 56, pp. 163-166, May 2002.

[42] T. S. Tillman and M. Cascio, "Effects of membrane lipids on ion channel structure and function," *Cell Biochemistry and Biophysics*, vol. 38, pp. 161-190, 2003.

[43] S. Y. Noskov, W. Im, and B. Roux, "Ion permeation through the alpha-hemolysin channel: Theoretical studies based on Brownian dynamics and Poisson-Nernst-Plank electrodiffusion theory," *Biophysical Journal*, vol. 87, pp. 2299-2309, Oct 2004.

[44] D. Stoddart, "Progress Towards Ultra-rapid DNA Sequencing with Protein Nanopores," PhD, Chemistry Research Laboratory, University of oxford, Oxford, 2011.

[45] K. Erik, *Fluorinated surfactants and repellents*: CRC press, 2001.

[46] K. Kubo, Y. Moroi, K. Nomura, Y. Abe, and T. Takahashi, "Study on molecular aggregates of N-(1,1-dihydroperfluoroalkyl)-N,N,N-trimethylammonium chloride," *Langmuir*, vol. 18, pp. 8770-8776, NOV 12 2002 2002.

[47] E. Rogalska, R. Bilewicz, T. Brigaud, C. El Moujahid, G. Foulard, C. Portella, *et al*., "Formation and properties of Langmuir and Gibbs monolayers: a comparative study using hydrogenated and partially fluorinated amphiphilic derivatives of mannitol," *Chemistry and Physics of Lipids*, vol. 105, pp. 71-91, MAR 2000 2000.

[48] V. V. Kumar, "Complementary molecular shapes and additivity of the packing parameter of lipids," *Proceedings of the National Academy of Sciences of the United States of America*, vol. 88, pp. 444-448, Jan 1991.

[49] J. H. Kleinschmidt and L. K. Tamm, "Structural transitions in short-chain lipid assemblies studied by P-31-NMR spectroscopy," *Biophysical Journal*, vol. 83, pp. 994-1003, Aug 2002.

# Chapter 5

# Droplet interface bilayers as a platform for screening of membrane protein libraries

## 5.1 Introduction

The work in this chapter, explores another aspect of using droplet interface bilayers. We investigated whether DIBs can be used for screening libraries of membrane proteins. The study presented here is exploratory and, to the best of my knowledge, is the first investigation of such a possibility.

### 5.1.1 Membrane proteins

Integral membrane proteins span the lipid membrane and act as gateways to cells. They enable controlled flow for many ions, nutrients, waste products, hormones, drugs and large molecules such as proteins and DNA across the membrane. Membrane proteins are key regulators of cellular function and are also responsible for much of the communication between cells and their environment.

Membrane proteins are interesting because of their wide range of applications. Membrane proteins such as ion channels and G-Protein Coupled Receptors (GPCRs) have become prime drug targets and more than 50% of all drug targets are membrane proteins [1]. Once a target is validated, drug candidates are found by screening a large

library of compounds. For both target discovery and drug screening, platforms such as high-throughput screening (HTS) are becoming increasingly popular [2].

Another area of membrane protein studies, which has generated a lot of interest, is the application of engineered membrane proteins to biotechnology and nanotechnology. A lot of work in this area has been done by the Bayley group using the α-hemolysin (αHL) protein. The αHL heptamer has been engineered to make nanodevices [3], to act as a detector in stochastic sensing [4-10], in ultra-rapid DNA sequencing [11-14], and to serve as a nanoreactor for the observation of single molecule chemistry [15-19].

However, studies with engineered pores have been slow because each mutant needs to be generated and screened individually for its activity. In order to hasten the screening process, I explore the feasibility of using droplet interface bilayers as platforms for screening libraries of membrane protein for its activity. To put the present investigation in perspective, in the next few sections, I discuss some commonly used methods to screen drug libraries and some existing methods to screen membrane protein activity.

### 5.1.2 Screening methods for drug libraries

Ion channels are well-established therapeutic targets for diseases. As a result, there is a high demand for high-throughput screening (HTS) for drugs which act as ion-channel modulators. Existing methods used for screening potential blockers include automated patch clamping [20, 21], binding assays [22, 23], fluorescence-based assays using

membrane potential dyes [24-27], ion-flux assay [28, 29], methods based on microfluidics [30], and droplet interface bilayers [31].

Automated patch clamp, which is based on the planar patch clamp technique, has revolutionized the process of ion channel drug discovery as it exponentially increases the throughput of conventional patch clamp [20].

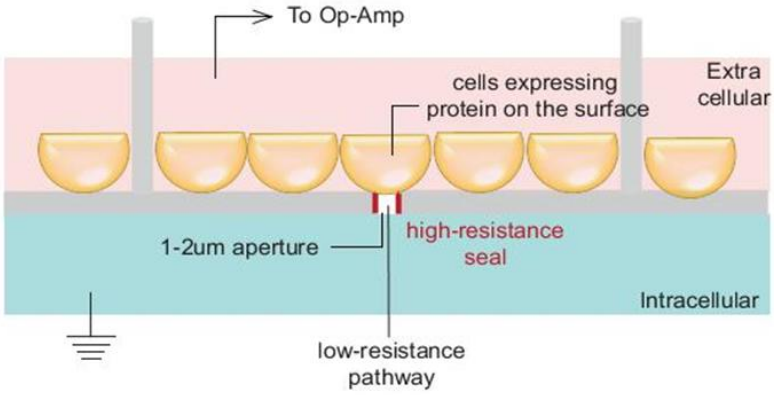


**Figure 5.1: An example of a commercially available automated patch clamp** *(Patchplate from Ionworsks Inc.). Cells expressing the protein of interest on the surface are pulled into the aperture by application of a negative pressure to achieve a 50-500 MΩ seal. Electrical access is achieved via a perforating agent. The figure has been adapted from Dunlop et al. [20].*

In this method, cell cultures are suspended on a planar partition into which micro-meter apertures emulating pipette openings are etched and they are connected to amplifiers (Figure 5.1). The application of negative pressure pulls the cells onto the holes to form giga-seals and to rupture the membranes to obtain whole-cell configuration and perform voltage-protocols in the absence and presence of drugs while recording the ionic currents. In the last few years, several automated patch-clamp instruments have been developed and are now commercially available [20]. The automated patch-clamp

system reduces user intervention and also increases the reproducibility of data obtained. However, two major disadvantages of automated patch clamp systems are the cost of the instrument and that they are only suitable for recording from cell lines with stable and high expression of the ion channels of interest.

Binding assays involve the binding of a radioactive tracer ($^{3}H$ or $^{125}I$) to the site of interest on the membrane protein [22, 23]. The presence of an unlabelled drug molecule which binds to the same site on the channel, results in competitive binding with the radiolabelled ligand. The activity of the unlabelled drug can be quantified ($IC_{50}$) by its ability to compete with the labelled ligand. The advantage of the method is that binding assay can be miniaturized into high-throughput microplate formats at moderate costs. However, although binding assays are relatively straightforward, they are not functional assays and give little information on the modulatory effect of the drug on the channel. Furthermore, the scope of the binding assay is limited by the availability of radiolabeled ligands.

Fluorescence-based assays using membrane potential dyes are based on the principle that the activation of ion channel(s) will lead to an ion flux across the membrane which will result in a change in membrane potential (Figure 5.2) [25, 26]. Voltage-sensing dyes measure changes in the membrane potential either by redistribution of the dye or by FRET between a dye pair such as the voltage-insensitive coumarin dye anchored in the membrane and the negatively charged oxonol derivative that can distribute itself across the membrane. Ion-specific fluorescent probes, such as calcium and thallium indicator dyes, are available for measuring ion channel activity.

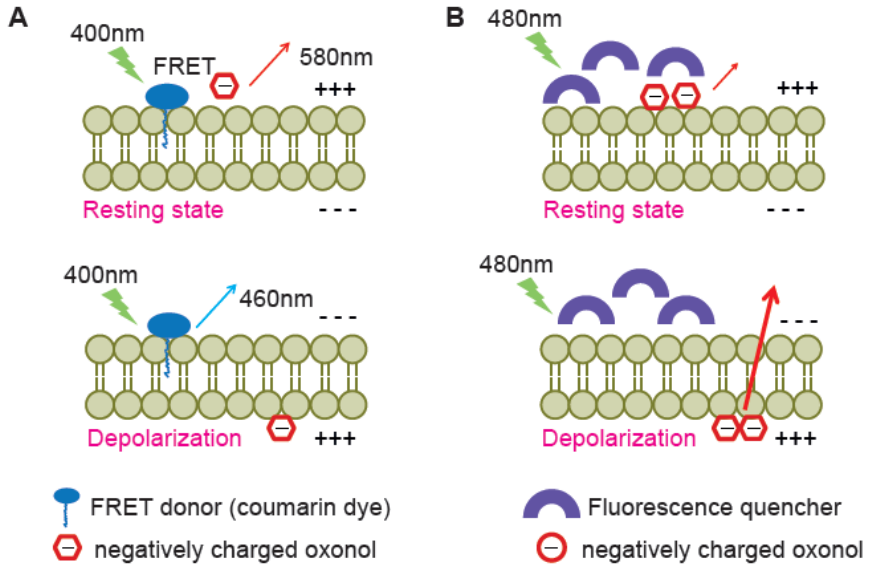


**Figure 5.2: Schematic illustration of the principle behind fluorescence-based assays using membrane potential dyes.** *(A.) FRET-based voltage sensing. The phospholipid-linked FRET donor (cumarin) is inserted into extracellular layer of cell membrane. The FRET acceptor (oxonol) is negatively charged and its distribution between the cell membrane is dependent on membrane potential. (B.) A commercial membrane potential dye kit. The voltage sensors (oxonol) are added together with fluorescence quenchers to cells. The distribution of voltage sensors is related to the membrane potential. At the normal resting membrane potential, the voltage sensors are associated with extracellular layer of cell membrane and the fluorescence is diminished due to presence of quenchers in the buffer. Upon depolarization, oxonol moves into the inner layer of the membrane leading to an increase in fluorescence signal.*

Traditionally, ion-flux assays have used radiolabelled ions [28, 29]. The openings of the ion channels are chemically initiated in the presence of fixed amounts of an appropriate radiotracer ($^{22}$Na for sodium channels and $^{86}$Rb for potassium channels, $^{45}$Ca for calcium channels, and $^{36}$Cl for chloride channels) and a potential ion channel modulator compound. Following flux activation, cells are separated from their medium and lysed.

The radiolabeled ions in both the lysate and supernatant are measured by scintigraphy. Inhibition or activation of the channel by the channel modulator compound will affect the concentration of radiolabeled ions, thereby changing the ratio of intracellular radiotracers (lysate) to extracellular radiotracers (supernatant). Radiotracer flux assays are easy to perform and are amenable to miniaturization and automation. The principal drawback of radiotracers lies in the potential toxicity and health hazard associated with radioactivity. This problem has been solved with the development of the cold/non-radioactive $Rb^+$ flux assay where $Rb^+$ is quantified by atomic absorption spectroscopy [28, 29].

Previous work in our lab has shown the potential of droplet interface bilayers to be used for screening blockers of ion – channels [31]. This method uses a chip with many wells, each of which contains an Ag/AgCl electrode that can be connected to the amplifier (Figure 5.3). The chip is filled with hexadecane containing lipids and then each well is loaded with the ion channel blocker (in buffer solution) that needs to be screened. A lipid monolayer is formed at the oil-water interface for each well. A droplet containing the protein is suspended from a moveable Ag/AgCl electrode (ground) in the oil-lipid mix. With the help of a micromanipulator, this droplet is sequentially connected to each well for recording and then disconnected by pulling on the droplet's electrode.

### 5.1.3 Screening methods for membrane protein libraries

The above mentioned methods of automated patch clamping and droplet interface

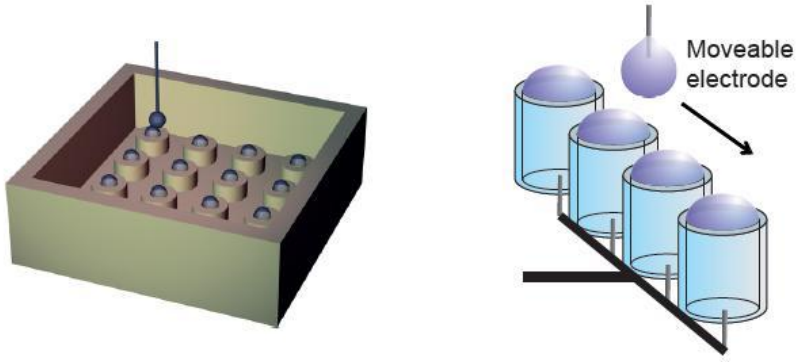


**Figure 5.3: Ion-channel screening chip using droplet interface bilayers.** *(Left) A simplified schematic of the chip. The chip is filled with a hexadecane – DPhPC oil mix and then each well is loaded with a potential ion channel blocker. A droplet containing the protein is suspended from the moveable Ag/AgCl electrode (grounded) in the oil-lipid mix. With the help of micromanipulators, this droplet is then sequentially connected to each well for recording, disconnected by pulling on the droplet's electrode, and then used to record from a second droplet. (Right) Detail schematic showing the wiring of the wells. The figure has been reproduced with permission from Syeda et al. [31].*

bilayers used for screening drug libraries, have been modified to enable high-throughput screening of membrane protein activity. Kreier et al. have recently reported the use of automated patch clamping as a method to greatly increase the efficiency of the characterization of reconstituted proteins [32]. The difference lies in using proteoliposomes in place of whole cells. Purified proteins in detergent (OmpF in this case) were reconstituted into giant unilamellar vesicles (GUV's) which were prepared by electroformation. The detergent was removed with bio-beads prior to bilayer formation. For formation of the bilayer, the proteoliposome solution was pipetted onto the patch clamp chip. The GUVs were positioned onto the apertures in the chip by application of a small negative pressure. The GUV's burst on touching the glass surface

of the chip and form planar bilayers. Once the seal is obtained, the buffer solution was perfused to remove the remaining vesicles in order to prevent further insertion of protein into the bilayer. This method resulted in stable pores of OmpF over long periods, which allowed for a thorough characterization of the protein. A limitation of the method is that it requires purified protein which is very often the bottle neck in membrane protein studies. Nonetheless, the planar patch method is compatible with automation and can in principle be a high-throughput method to screen libraries of membrane proteins.

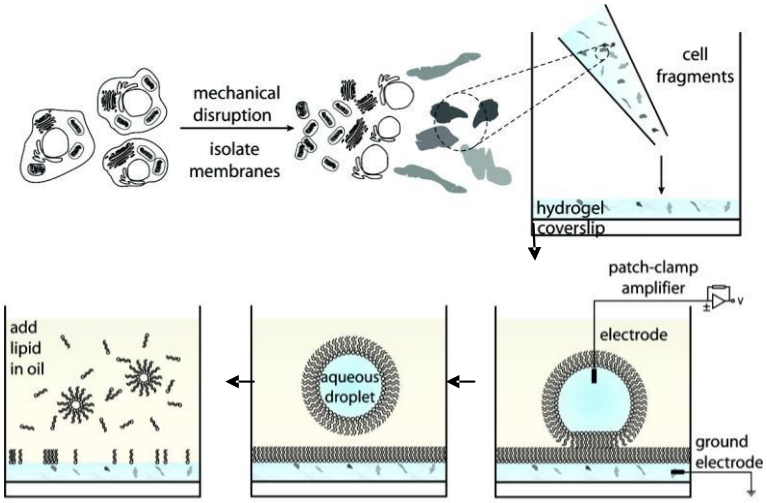


**Figure 5.4: Reconstitution method for incorporating eukaryotic ion channels into droplet bilayers.** *Cells are mechanically disrupted and membranes isolated. The cell membrane fragments are deposited onto an agarose-coated coverslip. A lipid in oil solution is added and a lipid monolayer forms at the interface. An aqueous droplet with a monolayer is added into the oil. Both monolayers come together to form a lipid bilayer; reconstitution of ion channels occurs during this process. An electrode is introduced into the droplet to measure ion flux. The figure has been reproduced with permission from Leptihn et al. [33].*

The second method which has promise in rapid screening of membrane protein libraries was reported by Leptihn et al. in 2011 [33]. Using droplet interface bilayers, they demonstrate a detergent-free method for the in vitro reconstitution of eukaryotic ion channels (Figure 5.4). The technique involves reconstitution of cell membrane fragments from recombinant overexpressing cells into droplet hydrogel bilayers. To obtain the cell membrane fragments, overexpressing cells were ruptured either by freeze – thaw cycles, sonication or by bursting the cell in hypo-osmotic buffers. The membrane fragments were collected by centrifugation and washed in appropriate buffer before being incorporated in droplet bilayers. To form the bilayer after depositing the membrane fragments on the agarose layer, hexadecane (containing DPhPC) is added. This results in a self–assembled lipid monolayer at the agarose–oil interface. An aqueous buffer droplet is then introduced in the oil phase containing the lipids. The droplet also acquires a monolayer coating of lipids. A bilayer forms when both monolayers are brought into contact. Upon bilayer formation, ion channels were found to immediately insert into the bilayer.

### 5.1.4 Proposed screening method

Engineering of membrane proteins such as the wild-type α-hemolysin gives rise to useful applications of the pore [6, 8, 13]. Engineering of pores involve mutating one or more amino acids of the pore to generate the desired property. However, it is tedious to make mutations and purify each of them before characterizing their behaviour in the bilayer. Screening of protein libraries (diverse collection of proteins or various mutants

of a single protein) offers a powerful method to recognize new binding interactions and identify binding partners. Our proposed screening method aims to provide a means of evaluating the effect of amino acid mutations at key residues, by screening for altered function.

We propose a cell-based screening assay (Figure 5.5). The first step in the screening of a library is the generation of the library. In keeping with the interesting applications of αHL, potential libraries that could be screened include αHL mutants with altered binding to cyclodextrin or mutants with improved rectification compared to the 7R mutant of αHL [3]. The library can be generated using existing protocols [34, 35]. The library which is made up of various plasmids (each of which harbours a mutation of interest) is transformed into bacteria (E.coli) using standard protocols such as electroporation or heat shock transformation.

Following transformation, it is common practice to plate and incubate the cells at 37°C overnight till colonies appear. In order to make our screening method truly high-throughput, it is imperative to by-pass the 'plating' step. As per our protocol, we intend to dilute the transformed E.coli culture and then generate droplets which encapsulate single cells. The culture density that would be required to achieve this will be determined by the size of the droplet. For a given density of bacterial culture, a droplet with a smaller volume (pL) has a higher probability to encapsulate a single cell, compared to a droplet with a larger volume (nL). However, since the functional read-out of the screening process involves electrical recordings, the size of the droplet needs to be quite large (approx. 200nl). This is the minimum size of a droplet into which an

electrode can be inserted for electrical recordings. The encapsulation of single cells in a nanolitre sized droplet was achieved by using low-density cell cultures.

Single cells encapsulated in droplets are then allowed to grow on-chip till the desired optical density is obtained. In a microfluidic device, growth of bacterial cells is monitored by imaging the cells at regular intervals using a microscope (epi-fluorescence, confocal reflection microscopy) [36, 37].

Single cell studies require that virtually all drops contain at most one cell , so that the majority of drops contain no cell at all. This is expected because the encapsulation process follows Poisson statistics [38, 39]. Following the growth of bacteria within droplets, the droplets expressing the protein need to be selected from a large background of empty droplets which contain no cell. This can be achieved by cloning a reporter gene such as GFP into the plasmids, so that cell-containing droplets can be detected using fluorescence.

Droplets of interest need to be sorted from the rest of the pool, and then lysed so that the protein can be released into the extracellular medium, followed by its incorporation into the bilayer and electrophysiological characterization. All these steps are summarized in figure 5.5.

### 5.1.5 Overview of chapter

In this chapter, I have conducted experiments which lay the groundwork for using droplet interface bilayers in protein screening. The screening of libraries in its entirety is quite detailed and would involve the development of microfluidics and imaging

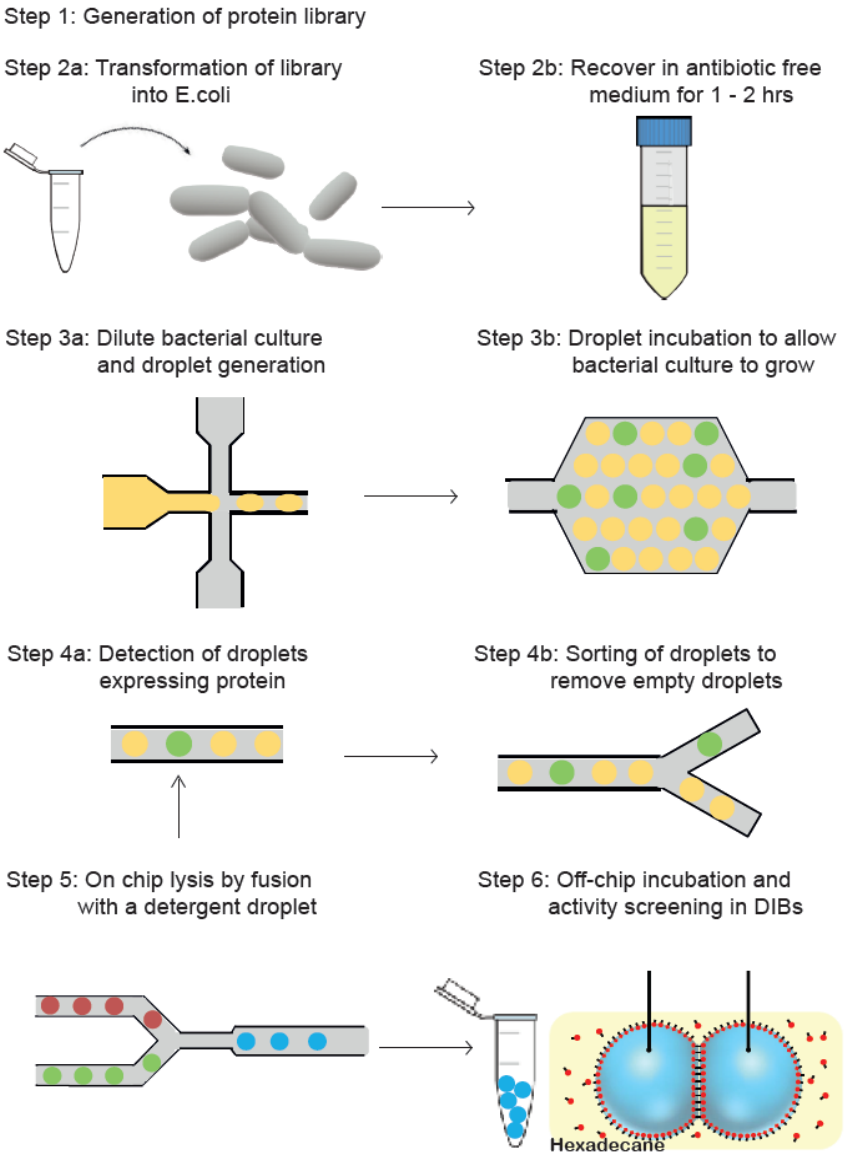


**Figure 5.5: Schematic illustration of proposed screening method:** *The protein library is transformed into E.coli and then the cells are allowed to recover in antibiotic free medium. The cell suspension is subsequently diluted in antibiotic containing medium and droplets are generated such that each droplet contains a single cell. Following on-chip growth of bacteria within the droplets, we select for droplets which are expressing protein from a large pool of empty droplets. Those droplets are sorted from the rest of the pool and lysed by fusing with a detergent droplet. Then the droplets can be collected for screening in droplet interface bilayers.*

systems. Therefore, I have chosen to focus only on those fundamental aspects of the proposed screening method that are sufficient to establish the feasibility of the method and to act as the proof of concept.

First, I demonstrated that successful bacterial growth can be obtained in droplets under conditions that are used for DIBs. This is the most fundamental step in the proposed cell-based screening assay. In the next step, I explored various lysis options in order to release the protein from the bacteria. I finally established that detergent lysis was the most feasible. Since lysing with detergent could interfere with bilayer experiments, I also investigated the stability of the bilayer in presence of both bacteria and lysis reagents.

Then I conducted dilution experiments with the bacterial culture to estimate roughly, the dilution that would be needed to encapsulate a single cell in a 200nL droplet under our conditions. This is an important step because much of the success of the screening process depends on the successful encapsulation of a single cell in the droplets. Finally, in order to enable selection of expressing droplets against a large pool of empty droplets with no cells, I successfully cloned the reporter gene EGFP along with the wild-type α-hemolysin gene into the pETDuet1 vector. This plasmid can be used as the starting point to generate the library of alpha hemolysin mutants.

## 5.2. Results and discussion

### 5.2.1 Factors affecting growth of bacteria in droplets

Recent research in microfluidics has focussed on encapsulating bacteria either in aqueous droplets or in agarose microparticles [39-44]. Most of the previous attempts have used single cells encapsulated in droplets to screen for enzymatic activities [45, 46], susceptibility to antibiotics etc. [47, 48]. To be able to use DIBSs in a single-cell based screening assay for membrane proteins, it is imperative to study the growth of bacteria in droplets and to study the effect(s) of commonly used DIB conditions on bacterial growth.

#### 5.2.1.1 Bacterial growth in a droplet compared to growth in a larger volume

This section compares the growth rate of a bacterial culture under two conditions (i) when grown in a small volume such as droplet (5µL) under an oil phase like hexadecane and (ii) when grown in a larger volume such as a starter culture (5ml) in a falcon tube. In proof of concept experiments, the bacterial growth in droplets was monitored by optical density measurements using a nanodrop spectrophotometer. The growth curve was plotted from readings of optical densities taken on a nanodrop spectrophotometer at regular intervals.

I find that bacteria can grow upto moderately high optical densities when grown inside a 5ul droplet. Bacterial cultures grown in a droplet under hexadecane for ~10hrs attain an optical density of $OD_{600}$ equal to 0.42±0.05 (path length = 1mm on the

nanodrop spectrophotometer). In comparison, bacterial cultures in large volumes (5ml) attain optical densities $OD_{600}$ equal to 0.64±0.01 over the same time period (Figure 5.6). Due to the smaller volume of the droplet, the E.coli was found to reach saturating densities at a lower optical density.

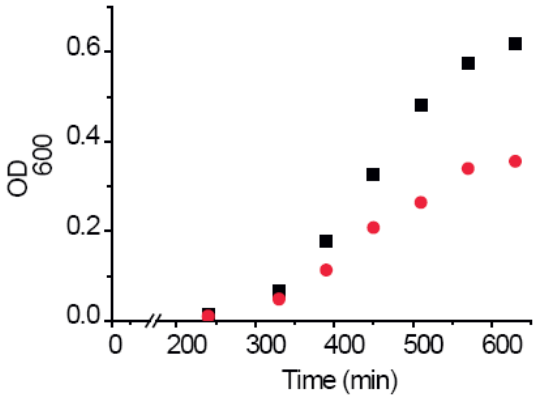


**Fig 5.6: Representative trace comparing the growth curve of bacterial culture in 5ul droplet (red circles) under hexadecane oil and 5ml starter culture (black squares).** *The growth medium was Luria Broth media with ampicillin antibiotic (100ug/mL). Both cultures were grown at 37°C with 200rpm shaking in the shaker incubator. (n=3).*

### 5.2.1.2 Effect of oil in which droplet is submerged on the bacterial growth

The compatibility of bacterial growth with commonly used oils in bilayer experiments namely hexadecane, squalene and silicone oil AR20 was tested. All the three oils mentioned above were found to support bacterial growth in droplets although to varying degrees (Figure 5.7). Bacterial droplets under squalene showed poor growth in comparison to droplets grown under hexadecane and silicone oil AR20. After about ten hours of growth, bacterial droplets under squalene had optical densities $O.D_{600}$ equal to 0.19±0.02 (n=3), whereas bacterial droplets under oils such as hexadecane and silicone

oil AR20 were found to exhibit better growth reaching $OD_{600}$ equal to 0.41±0.03 (n=3) and 0.33±0.04 (n=3) respectively. The differences in growth densities under the different oils are probably indicative of the oxygen solubilities and oxygen diffusion co-efficients of the respective oils.

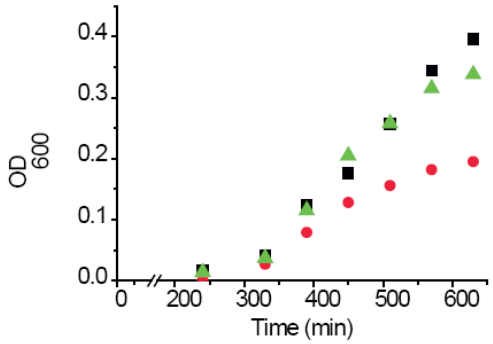


**Fig 5.7: Representative trace comparing the growth curve of bacterial culture in 5ul droplet under three different oils** *(i) hexadecane oil (black squares) (ii) silicone oil AR20 (green triangles) and (iii) squalene oil (red circles). The growth medium was Luria Broth media with ampicillin antibiotic (100ug/ml). The cultures were grown at 37°C with 200rpm shaking in the shaker incubator. (n=3).*

### 5.2.1.3 Bacterial growth in droplets in presence of lipids

Droplet interface bilayers can be formed by both lipid-in and lipid-out methods [49, 50]. The lipid-in method involves having liposomes inside the droplets which then diffuse to form monolayers at the interface of the droplet and oil. The lipid-out method involves having lipids in the oil phase which can diffuse to form a monolayer at the interface of the droplet and oil. We wanted to check the compatibility of bacterial growth in droplets in the presence of lipids. Both lipid-in and lipid-out methods were tested at two different lipid concentrations of 0.2mg.mL$^{-1}$ and 1mg.mL$^{-1}$. As can be seen

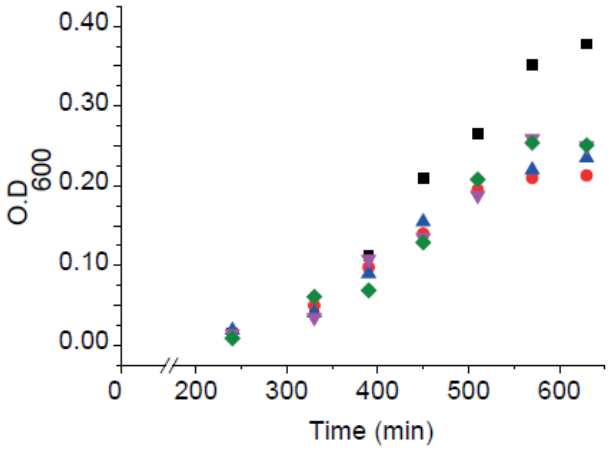


**Figure 5.8: Representative trace comparing the growth curve of bacterial culture (5µL) in the absence and presence of lipids** *(i) control with only hexadecane oil (black squares) (ii) presence of DPhPC liposomes inside the droplet along with the bacterial culture (a) 0.2mg/mL (pink triangles) and (b) 1mg/mL (green diamonds) (ii) presence of DPhPC lipid outside in the oil phase (a) 0.2mg/mL (red circles) and (b) 1mg/mL (blue triangles). The growth medium was Luria Broth media with ampicillin antibiotic (100µg/mL). Cultures were grown at 37°C with 200rpm shaking in the shaker incubator. (n=3).*

from figure 5.8, the presence of lipids in the system (irrespective of lipid-in or lipid-out and at both concentrations of lipid tested) lowered the final cell density of the bacterial cultures by almost 30% when compared to the final cell densities achieved in bacterial droplets in the absence of lipids. The reduced growth of bacteria in droplets in presence of lipids can be explained by decreased oxygen transfer into the droplets because of the formation of lipid monolayers at the oil/droplet interfaces. This observation corroborates earlier reports that have indicated reduced oxygen diffusion across a lipid monolayer [51, 52].

### 5.2.2 Stability of droplet bilayers in presence of bacteria

The proposed single-cell screening method involves on-chip growth of bacteria (expressing protein) within droplets made from Luria Broth (LB) medium. Hence, droplet bilayer formation and its stability were studied using droplets made of Luria Broth (LB) media. The work in this section tries to ascertain if there exists an upper limit to the bacterial density growing inside the droplets, beyond which stable bilayers cannot be formed. Three densities of bacterial culture were tested: (i) low densities ($OD_{600}$ = 0.5) (ii) moderate ($OD_{600}$ = 1.4) (iii) high ($OD_{600}$ = 3.0).

In control experiments, bringing together two monolayer-coated droplets of LB media (without bacteria) successfully formed a bilayer at the interface of the two droplets (Figure 5.9A). The bilayer that formed was not leaky and was found to be stable (for 10 minutes or more) on application of a potential of +50mV. The presence of ampicillin (100 µg/mL) in the LB-droplets did not destabilize the bilayer unlike other antibiotics such as amphotericin-B and nystatin which have been shown to cause marked mechanical instability to the membrane [53] .At low densities of bacterial culture ($OD_{600}$ ~ 0.5), droplets which had been incubated in the oil-lipid phase for 15-20 minutes formed bilayers efficiently and the bilayers were found to be stable even on application of a potential of +50mV. However, we find that it gets increasingly difficult to form bilayers when the culture density inside the droplet increases. This problem can be mitigated by allowing the droplets to incubate for a longer time (30 minutes to 1 hour) in the oil-lipid mix before bringing them together.

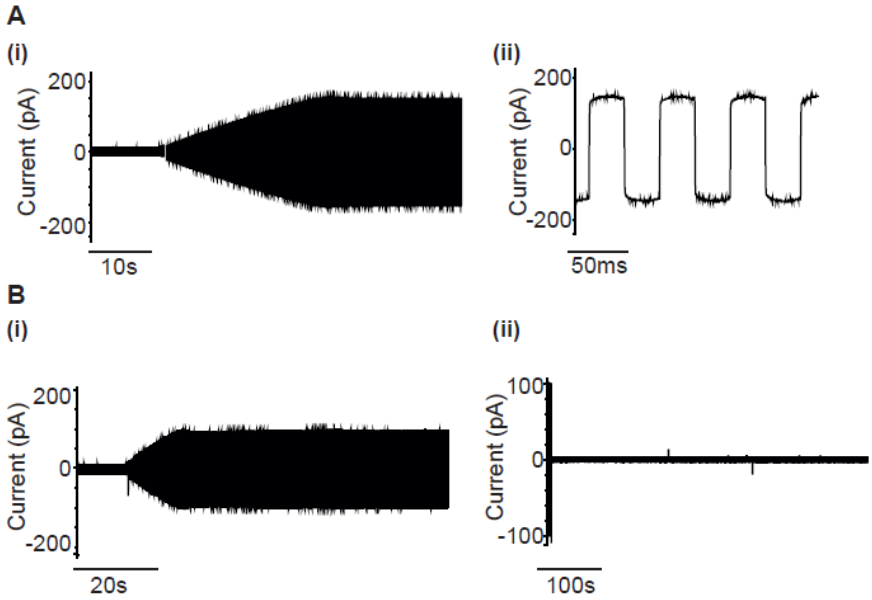


**Figure 5.9:** *(A) Successful bilayer formation between two LB droplets. (i) Condensed view of bilayer formation (ii) Expanded trace of bilayer capacitance showing that the bilayers are not leaky. (B) (i) Stable bilayer formation was achieved when one the droplets contained a cell culture ($OD_{600}$ = 0.143). (ii) The bilayers were found to be stable at 50mV for 10 minutes or more. The droplets were submerged under hexadecane containing DPhPC (5mg/mL). (n=3)*

By allowing longer incubation times, stable bilayers were obtained with both moderate (OD600 = 1.4) and relatively high density cultures (OD600 = 3.05) (Figure 5.9B). The reason behind the dependence of ease of bilayer formation and its stability on the bacterial density inside the droplet could be due to interactions between the bacteria and the lipid monolayer at high optical densities. Previous reports on marine bacteria have shown that bacteria have a tendency to accumulate near lipids films at an air/water interface [54]. This interaction between the bacteria and the lipid monolayer could be the reason for the longer incubation times needed for monolayer formation in presence of bacteria.

### 5.2.3 Bacterial lysis in droplets

In order to be able to assess the activity of the protein, it is essential that the bacteria be lysed so that the protein can be released into the extracellular medium and they can subsequently insert in bilayers. Traditional methods for bacterial lysis include (i) homogenization: where a cell suspension is sheared by forcing them through a narrow space like in a french press (ii) sonication: where high frequency sound waves generate mechanical shear stress by oscillating cavitation bubbles that break apart cells (iii) freeze-thaw cycles: In which repeated cycles of freezing and thawing disrupts the cell membrane as a result of ice crystal formation and (iv) lysis reagents: mostly contain a cocktail of mild detergents which dissolve the E.coli membrane leading to its lysis. With the exception of freeze-thaw, the other techniques are amenable to implementation in a microfluidic format [55-57].

Other methods used for on-chip lysis in microfluidic set-ups include thermal cycling [58], SDS detergent lysis [59], irreversible electroporation [60] and lysis by UV light [61]. However, lysis by heat could lead to denaturation of protein, and lysis by electroporation requires an external voltage source to apply high potentials. So, we decided to look at the suitability of detergent lysis and UV lysis for our system.

Although, SDS has been previously shown to successfully lyse cells [59], it is known to cause bilayer instability [62]. For this reason, we chose to explore other detergents. The choice of lysis reagent was Popculture reagent from Novagen. The reason for the choice of this specific detergent is explained below.

PopCulture reagent is a buffered mixture of concentrated detergents formulated to extract proteins from E.coli cells directly into their culture medium. PopCulture perforates the E. coli cell wall without denaturing soluble protein and protects protein from the pH extremes produced in high density culture media. Also according to the data sheet supplied by the manufacturer, popculture detergent formulation is mild enough to be suitable for further downstream applications without any purification. This aspect we found particularly useful for our purposes.

The popculture reagent is sold as a 10X concentrate and is used to lyse cell cultures at a final concentration of 1X. As detergents cause bilayer instability, we tested the ability of popculture to lyse the cells at different dilutions of the lysis reagent. The aim was to find the lowest dilution of lysis reagent which could cause lysis and yet be compatible with bilayer measurements. The popculture reagent at the appropriate dilution (0.5µl) was manually injected (by pipette) into a bacterial droplet (5µl) and incubated for 20 minutes. In the final screening process, the addition of detergent to the droplet can be performed on the microfluidic chip by droplet fusion. The extent of cell lysis on addition of popculture was determined by optical density measurements at 600nm.

Lysis was carried out on a moderately dense culture ($OD_{600}$ = 0.15). The recommended final concentration of lysis reagent (1X) resulted in 76±5% lysis (n=3). As expected, lower dilutions of the lysis reagent are less effective at causing lysis, with 0.1X and 0.01X dilutions of the popculture concentrate causing 26±4% (n=3) and 10±4% (n=3) cell lysis respectively (Figure 5.10).

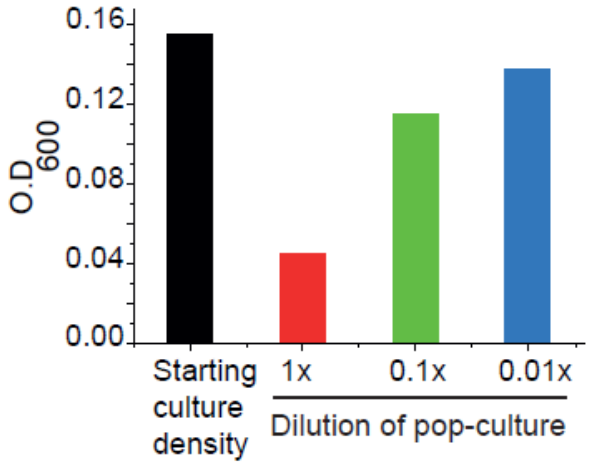


**Figure 5.10:** *Representative graph showing the extent of bacterial cell lysis achieved using popculture lysis reagent. To a 5µl droplet(s) containing bacterial culture ($O.D_{600}$ = 0.155), 0.5µL of popculture reagent at appropriate concentration was added to achieve final concentrations of 1X, 0.1X and 0.01X in the droplet. The extent of cell lysis was measured after 20 minutes incubation at RT by monitoring optical density at 600nm on a nanodrop spectrophotometer (path length = 1mm). Efficient lysis of cell culture was obtained with the recommended dilution of popculture concentrate (1X) (red column). However, even lower dilutions of popculture concentrate proved effective in lysing the cell albeit to a lower extent (green and blue column).*

To determine the amount of protein that is released on lysis into the extracellular medium, we performed a hemolytic assay. Hemolytic assays performed with rabbit erythrocytes are very sensitive and require as little as 1nM of α-hemolysin monomer to show detectable activity [63]. Results from the hemolytic assay show that sufficient protein is released into the extracellular medium even with 30% cell lysis (Figure 5.10). As BL21 (DE3) contains a chromosomal copy of T7 RNA polymerase and the T7 promoter is leaky, it was not necessary to induce protein synthesis by the addition of isopropyl β-D-thiogalactoside (IPTG). However, in the absence of induction no hemolytic activity was observed in the case of 15% cell lysis (Figure 5.11).

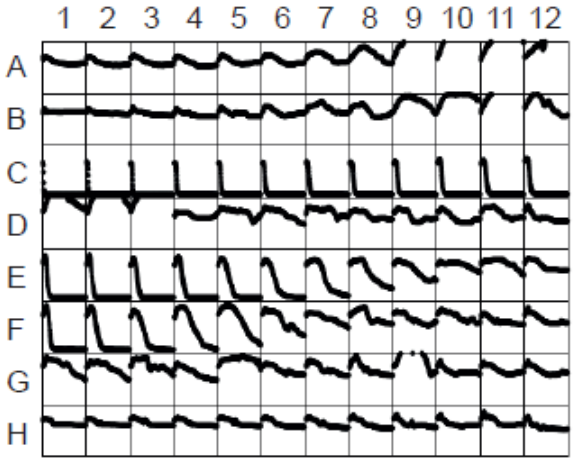


**Figure 5.11:** *Hemolytic assay performed to check if detergent lysis of cells was releasing enough protein into the extracellular medium. Lane A, H: MBSA buffer control. Lane B: 5ul of popculture lysis reagent (1X). Lane C: SDS-PAGE purified αHL monomer (5μL). Lane D: Non-lysed bacterial cells (5μL). Lane E: bacterial culture lysed with 1X popculture reagent (5). Lane F: bacterial culture lysed with 0.1X popculture reagent (5μL). Lane G: bacterial culture lysed with 0.01X popculture reagent (5μL). The cells and lysis reagent were then subjected to 2-fold serial dilution in 10 mM MOPS and 150 mM NaCl (pH 7.4) over the 11 remaining wells (final volume of 50 μL per well), followed by the addition of washed 1% rRBCs (50 μL) to each well.*

Next, I looked into the feasibility of using UV light for lysing the cells. Previous work has shown that BL21 (DE3) cells could be lysed (upto 60%) if they were transformed with a plasmid containing the lysis gene cassette under a UV inducible promoter [61]. In their control experiments without the lysis gene cassette, BL21 (DE3) cells could still be lysed (upto 45%) with UV light. They suggested that E. coli BL21 (DE3) contained a derivative of phage Lambda integrated in its genomic DNA, and showed a small but significant extent of cell lysis when exposed to UV. We wanted to exploit the natural susceptibility of BL21 (DE3) cells to UV light and investigate if efficient lysis of cells could be obtained under our experimental conditions where the droplet is submerged

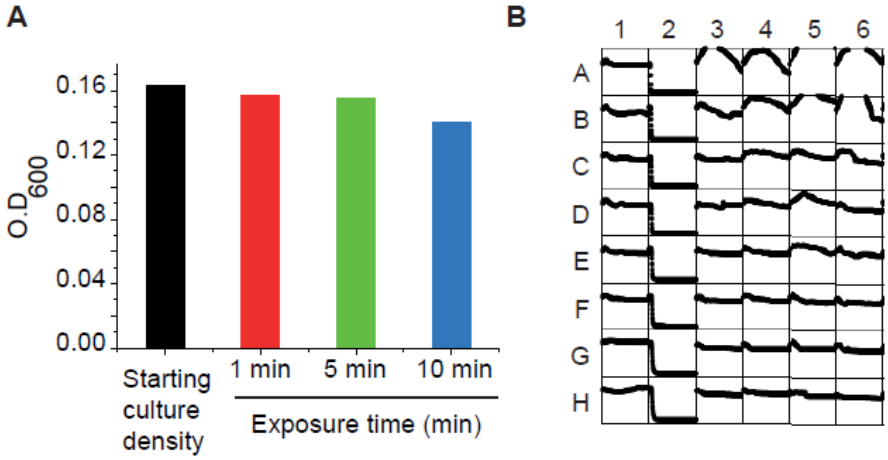


**Figure 5.12:** *Representative data showing bacterial cell lysis in droplets after exposure to UV light. (A) Droplets containing bacterial culture ($O.D_{600}$ = 0.16) submerged under hexadecane were exposed to UV light (254nm) for varying durations. The extent of cell lysis was measured post the UV exposure by monitoring optical density at 600nm on a nanodrop spectrophotometer (path length = 1mm). Almost no lysis was obtained after exposure to UV light for 1 and 5 minutes (red column and green column respectively). Increasing the duration of UV exposure to 10 minutes, results in approximately 25% cell lysis. (B) Hemolytic assay was performed to check if UV lysis of cells was releasing enough protein into the extracellular medium. Lane 1: MBSA buffer control. Lane 2: SDS-PAGE purified αHL monomer (5ul). Lane 3: Non-lysed bacterial cells (5ul). Lane 4, 5, and 6: bacterial culture (5ul) exposed to UV light (254nm) for 1 minute, 5 minutes and 10 minutes respectively. The cells were then subjected to 2-fold serial dilution in 10 mM MOPS and 150 mM NaCl (pH 7.4) over the seven remaining wells (final volume of 50 µL per well), followed by the addition of washed 1% rRBCs (50 µL) to each well.*

under a layer of oil. We tested three commonly used oils for bilayer experiments for UV lysis efficiency experiments.

As with detergent lysis, UV lysis efficiency was tested with a bacterial culture of moderate density ($O.D_{600}$ = 0.17). Unlike hexadecane, which is a saturated hydrocarbon, silicone oil AR20 and squalene contain aromatic rings and unsaturated bonds respectively, and absorb strongly in the UV region. Expectedly, poor lysis efficiencies of cells (under 10%) were observed for experiments carried out under

silicone oil (AR20) and squalene, For a bacterial droplet under hexadecane, we observed 25±10% (n=3) lysis for exposure times of 10 minutes or more. Lower exposure times (5 minutes or less) resulted in no significant cell lysis (Figure 5.12A). No protein activity was detected in hemolytic assays for cells lysed by UV light (Figure 5.12B). Thus, the option of UV lysis was not pursued further as this was found to be a nonviable option.

### 5.2.4 Droplet interface bilayer formation and its stability in presence of lysis reagent

Given that popculture lysis reagent was successful in lysing cells and releasing protein into the extracellular medium, experiments with droplet bilayers were carried out to assess if popculture reagent was compatible with stable bilayer formation.

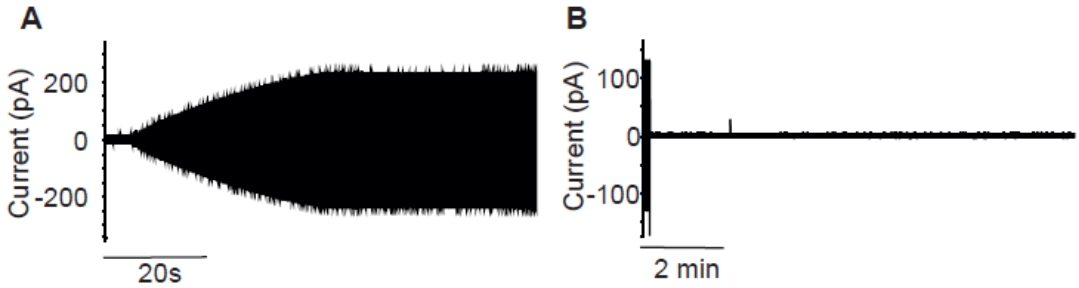


**Figure 5.13:** *Droplet bilayer stability in presence of lysis reagent. (A) Condensed trace showing bilayer formation in presence of 0.1 X popculture lysis reagents within the LB droplets. (B) Despite the presence of detergent, the bilayers obtained were stable at +50mV for 10 minutes or more. The droplets were allowed to incubate for 15 minutes before being brought into contact. The droplets were formed under hexadecane containing DPhPC lipids (5mg/ml).*

The popculture reagent (1X) although very efficient in lysing the cells (76%) was found to be incompatible with droplet bilayer measurements, as droplets containing 1X popculture reagent kept slipping off the electrode within seconds of being suspended. Stable and non-leaky bilayers could be achieved with higher dilutions of popculture (i.e. LB-droplets containing popculture at a final dilution of 0.1X. Thus, there exists a concentration of the lysis reagent (0.1X) that is compatible with bilayer experiments and as discussed in section 5.2.2, is still high enough to cause lysis (30%) of the cells (Figure 5.13).

### 5.2.5 Single-cell encapsulation in droplets

As mentioned previously, the culture density that would be required to encapsulate a single cell in a droplet will depend on the size of the droplet which in turn is limited by the size that will successfully allow the insertion of electrodes. Droplet interface bilayers have been successfully formed with 200nL droplets. So, I tried to gauge the cell density that would be required to achieve a single cell in a 200nL droplet. Experiments were carried out with cells transformed with EGFP, so that occupied droplets (containing cells) could be selected from a large pool of empty droplets (contains no cells) by using fluorescence.

My initial attempts were carried out using fluorescence microscopy. The idea was to image many droplets on a glass slide and count how many droplets were fluorescent implying that they contained cells. However, this approach did not turn out to be feasible as 200nl droplets were too large to be imaged using the microscope. Even

at the lowest resolution of the microscope (40X), only four 200nL droplets could be imaged at a time. Thus, screening of hundreds of droplets to determine droplet occupancy by fluorescence microscopy took over several hours and proved inefficient. To screen droplets quicker, I used 96-well microplates which contained a 200nL droplet in each well. The plates were then read using the spectramax M5 microplate reader. Each plate took less than 30 seconds to read, and at the end of the run, the number of empty droplets (no signal) and fluorescent droplets were counted to estimate the droplet occupancy.

Following transformation of cells with fluorescent protein plasmid(s), the cell suspension was allowed to recover in antibiotic free medium for two hours. Then, the transformed cells were diluted to varying extents (10X to $10^6$X) in antibiotic containing medium and hundreds of 200nL droplets were made in 96-well plates for each dilution. Initial experiments were performed with BL21 (DE3) cells transformed with EGFP DNA (Figure 5.14). The microplates were read using the spectramax M5 microplate reader by exciting at 490 nm and recording the emission at 520 nm. On excitation at 490nm, empty droplets which contained no cells, gave a low fluorescence signal (background). Droplets which contained cells transformed with EGFP gave rise to a very strong fluorescence emission at 520nm. At the end of the run, both the number of empty and occupied droplets was counted to determine droplet occupancy.

As would be expected, a low dilution of the transformed cells (10X) resulted in all the 200nL droplets (96/96) containing cells (Figure 5.14A). When the 10X dilution was diluted two orders of magnitude ($10^3$X), out of the 96 droplets screened, the

majority of droplets (94%) were still found to contain cells. However, there was a small percentage (6%) of droplets that contained no cells (Figure 5.14B). On diluting to $10^5$X, a large percentage of droplets were found to be empty. For this reason, at the $10^5$X dilution, I had to read more than one 96 well plate (four 96 well plates = 384 droplets) in order to estimate the percentage occupancy of droplets. At such high dilutions, majority of the droplets (370/384, i.e. 96%) were empty droplets with a handful of droplets (14/384, i.e. 4%) being occupied (Figure 5.14C). It is likely that under such high dilutions, the 14 droplets were initially encasing a single cell.

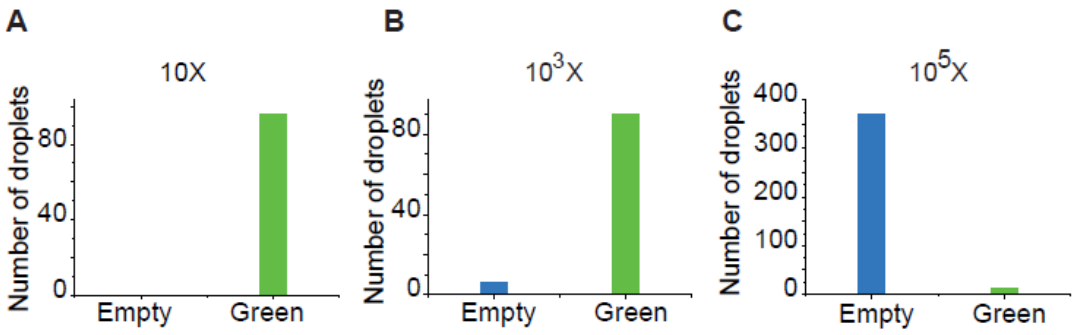


**Figure 5.14: Occupancy of 200nL droplets at different dilutions of the transformed culture (i.e different cell densities).** *E.coli BL21 (DE3) was transformed with EGFP-pET9d. (A) The lowest dilutions tested (10X) resulted in 100% occupancy of the droplets. Diluting the cell culture ($10^3$X) resulted in about 6% of the droplets being empty (B), while the number of emoty droplets increased to 96% on further dilution of the cell culture ($10^5$X) (C). These experiments were conducted using a 96-well microplate where a minimum of 96 droplets were read for each dilution. At the lowest dilution tested ($10^5$X), four plates (384 droplets) had to be read due to the high percentage of empty droplets. All the plates were read using the spectramax M5 (bio-rad) by exciting at 490nm and recording the emission signal at 520nm.*

However, a library contains more than one plasmid. As a proof of principle we wanted to check how the single cell dilutions were affected when E.coli was transformed with more than one plasmid. The two plasmids that were co-transformed into the E.coli cells

were: EGFP-pET9d and m-Cherry-pETm11. In the following discussion, cells transformed with EGFP are referred to as green bacteria and cells transformed with m-Cherry are referred to as red bacteria.

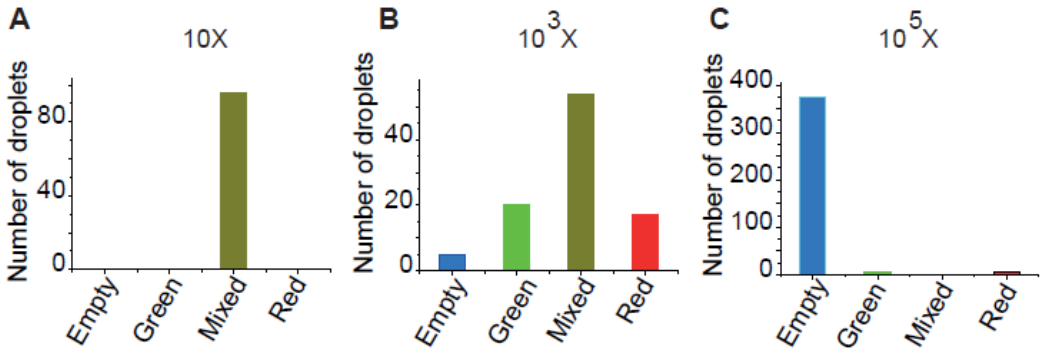


**Figure 5.15: Occupancy of 200nL droplets at different dilutions of the co-transformed culture (i.e different cell densities).** *E.coli BL21 (DE3) was co-transformed with EGFP-pET9d and mCherry-pETm11. (A) The lowest dilutions tested (10X) resulted in 100% occupancy of the droplets. None of the occupied droplets contained exclusively green or red bacteria Diluting the cell culture (103X) resulted in about 6% of the droplets being empty, while majority of the occupied droplets contained a mix of both green and red bacteria (56%) with the remaining droplets being exclusively red or green. The number of empty droplets increased to 96% on further dilution of the cell culture (105X). The occupied droplets contained exclusively green (6/384, i.e.2%) or red bacteria (4/384, i.e. 1%). These experiments were conducted using a 96-well microplate where a minimum of 96 droplets were read for each dilution. At the lowest dilution tested (105X), four plates (384 droplets) had to be read due to the high percentage of empty droplets. All the plates were read using the spectramax M5 (bio-rad) by exciting at 490nm and recording the emission signal at 520nm (EGFP) and by exciting at 580nm and recording emission at 640nm (mCherry).*

The results obtained on co-transformation of two plasmids were similar to what was obtained when the E.coli was transformed with EGFP alone (Figure 5.15). At low dilutions (10X), no empty droplets were seen. However, it was interesting that none of the occupied droplets contained exclusively green or red bacteria (i.e. all 96 droplets

contained both green and red bacteria) (Figure 5.15A). At a slightly higher dilution ($10^3$X), there were fewer empty droplets (5/96, i.e. 5%). A small fraction of the occupied droplets were found to contain exclusively green (20/96, i.e. 21%) or red bacteria (17/96, i.e. 18%), while the majority of the occupied droplets contained a mix of both green and red bacteria (54/96, i.e. 56%) (Figure 5.15B). At even higher dilutions ($10^5$X), we needed to read more droplets (four 96-well plates, i.e. 384 droplets) as most of the droplets were devoid of cells (374/384, i.e. 97%). However, thedroplets which were occupied contained exclusively green (6/384, i.e.2%) or red bacteria (4/384, i.e. 1%) and no droplet was found to contain a mix of both bacteria (Figure 5.15C). We establish that, that was likely to be the concentration that resulted in single cell encapsulation in a 200nL droplet under our experimental conditions.

### 5.2.6 Plasmid for protein expression

As could be seen from single-cell experiments described above, most of the droplets (>90%) were empty. To overcome this problem, I cloned a reporter gene like EGFP in the same plasmid as the αHL, which will enable the selection of droplets expressing the αHL mutant of interest from the large pool of empty droplets. We did not intend to create a fusion protein of EGFP and αHL because that could result in αHL with altered behaviour in the bilayer. Instead, we wanted to co-express the reporter gene EGFP and the WT-αHL gene.

For this purpose we chose the pET-Duet-1 vector (Novagen). The Duet vectors are designed for the cloning and co-expression of two proteins. The Duet vector

contains two multiple cloning sites (MCS) each of which is preceded by a T7lac promoter and ribosome binding site (rbs). In this expression vector, I inserted the EGFP gene in MCS-1 and the αHL gene in MCS-2. This choice was based on the convenience and ease of cloning (see materials and methods, section 5.3.5).

After sequencing results showed successful cloning of both EGFP and αHL, IVTT was performed with the recombinant pETDuet1 vector, and the protein expression levels were analysed by SDS-PAGE (Figure 5.15). WTαHL-pT7 and EGFP-pET9d samples were used as controls. Both EGFP and αHL proteins were found to be successfully co-expressed.

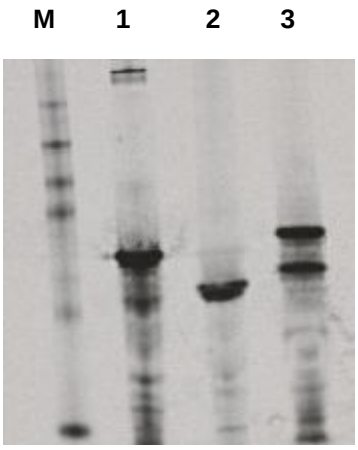


**Figure 5.16:** *Expression of proteins cloned in pETDuet1 by IVTT. 12% Bis-Tris precast XT-criterion gels. The gel was run at 200mV for 50min in XT-MOPS buffer. Left to right: Lane M: 14C marker, Lane 1: αHL-pT7 control (2µl). Lane 2: EGFP-PET9d control (2µl). Lane 3: EGFP- αHL-PETDuet1 (2µl).* Starting from the top, the molecular weight marker lane reads 97 kDa, 69 kDa, 55 kDa, 46 kDa, 30 kDa, and 12 kDa.

### 5.2.7 Conclusions

The work in this chapter looks at the possibility of using droplet interface bilayers to screen for membrane protein libraries. The screening of libraries in its entirety is quite detailed and would involve the development of microfluidics and imaging systems. Therefore, I have chosen to investigate certain important aspects of the screening process which lay the groundwork on which future work can be based. In particular, I established the various experimental conditions under which screening can be carried out. Bacterial growth in droplets was found to be compatible with conditions that are used for DIBs (hexadecane, lipids). Stable bilayers could be obtained in the presence of high densities of bacterial culture as well as in the presence of detergent lysis reagent. Dilution experiments were conducted to estimate the range of dilutions that would encapsulate a single cell in a 200nL droplet under our experimental conditions. Finally, I also successfully generated a plasmid containing the αHL gene and a reporter gene (EGFP) which can be used as the starting point for the generation of αHL mutant libraries.

To conclude, the groundwork seems promising and it does seem feasible to use droplets for a cell based screening assay for membrane proteins. Future directions of this project would be setting up of a microfluidic chip with an integrated microscope to enable both the monitoring of bacterial growth in the droplets and detection of protein expression in the droplets.

## 5.3 Materials and methods

### 5.3.1 Growing of bacterial culture in droplets

Competent cells of E. coli strain BL21 (DE3) (200ul) were transformed with wt-αHL DNA via a standard heat shock protocol (5 minutes on ice, 30s at 42°C, 2 minutes on ice). The cells were then allowed to recover in antibiotic-free SOC medium (800µL) at 37°C (200rpm shaking) for 2hrs. For experiments comparing bacterial growth in large volumes versus droplets (section 5.2.1.1), the transformed cells (1mL) were diluted into LB media with ampicillin (5mL). I then pipetted many droplets (5µL) of the diluted cell suspension under hexadecane. In control experiments (larger volume), the transformed culture (1mL) after dilution into LB media (5mL) with ampicillin (100µg/mL) was allowed to grow in falcon tubes.

Both cultures (in droplets and falcon tube) were allowed to grow at 37°C. Optical density (O.D) measurements were made at regular intervals using nanodrop spectrophotometer. For comparing bacterial growth under different oils (section 5.2.1.2), the transformed cells (1mL) were diluted into LB media with ampicillin (5mL) and droplets (5µL) were made under hexadecane, silicone oil (AR20), and squalene. The droplets were incubated on-chip at 37°C and O.D measurements were made at regular intervals using the nanodrop spectrophotometer. The effect of lipids on the growth of bacterial culture in droplets was investigated both by having the lipids inside the aqueous phase and outside in the oil phase. Two concentrations of lipid were investigated: (i) 0.2mg/mL (ii) 1mg/mL.

For the control experiments in the absence of lipids, droplets (5µL) were made from diluted transformed cells (1mL of transformed cells in 5mL of LB). For the lipid out experiments, droplets of the diluted transformed cells were overlaid with hexadecane containing DPhPC lipid at either 0.2mg/ml or 1mg/ml. For the 0.2mg/ml lipid in experiments, 2ul of 10mg/ml DPhPC liposomes in LB media were added to 98µL of thediluted transformed cells. For the 1mg/ml lipid in experiments, 10µL of 10mg/mL DPhPC liposomes in LB media were added to 90µL of the diluted transformed cells. The droplets were then overlaid with hexadecane. All the samples (control, lipid in, lipid out) were incubated at 37°C and their optical densities were measured at regular intervals using nanodrop spectrophotometer.

### 5.3.2 Isothermal cell lysis of bacteria in droplets

Isothermal lysis of the bacteria was attempted with detergents and UV light. The bacteria were transformed as mentioned above. Transformed cells (1mL) were diluted in LB with ampicillin (5mL). Made 5µL droplets and overlaid them with oil (hexadecane unless specified otherwise). The bacteria encapsulated in droplets were allowed to grow at 37°C. As a proof of concept, both lysis experiments (detergent and UV) were carried out when the culture was moderately dense (O.D600 = ~0.15).

Detergent lysis was carried out using popculture lysis reagent from Novagen. The lysis reagent is sold as a 10X concentrate which needs to be diluted to 1X in the culture. As

detergents cause bilayer instability, the aim was to find the lowest dilution of lysis reagent which could cause lysis and be compatible with bilayer measurements. For this purpose, the ability of popculture to lyse the cells was studied at varying dilutions (1X, 0.1X, 0.01X). As we were trying dilutions of the lysis reagent well below the optimal concentration of 1X we decided to try a longer incubation times of 20 minutes as against the recommended time of 10 minutes. Lysis was carried out by manually adding 0.5ul of the popculture reagent at the appropriate dilution to a 5ul droplet with the bacterial culture and then incubating it at RT for 20 minutes. For experiments with UV lysis, the droplets (O.D600 = ~0.15) were exposed to UV light (254nm) for exposure times of 1 min, 5 min and 10 minutes. In both experiments, the extent of lysis was determined by measuring the optical density at 600nm.

Post lysis, the samples were then run on a hemolytic assay to determine extent of protein release after lysis. The lysed samples (5 μL) were diluted into MBSA [10mM MOPS and 150mM NaCl (pH 7.4) containing 1 mg/mL bovine serum albumin] in the first well of a microtiter plate (final volume of 100 μL). The lysed cells were then subjected to serial 2-fold dilution in MBSA over the remaining 11 wells of the plate row (final volumes of 50 μL). An equal volume of 1% washed rabbit erythrocytes (rRBC) in MBSA was then added to each well, beginning with the most diluted lane. Hemolysis was followed for 1.5 h at 24°C by monitoring the decrease in light scattering at 595 nm with a Bio-Rad microplate reader (model 3550-UV) running MicroplateManager version 4.0.

### 5.3.3 Droplet bilayer stability in presence of bacteria

Competent cells of E. coli strain BL21 (DE3) (200 µL) were transformed with wt-αHL DNA via a standard heat shock protocol (5 minutes on ice, 30s at 42°C, 2 minutes on ice). The cells were then allowed to recover in antibiotic-free SOC medium (800ul) at 37°C (200rpm shaking) for 2hrs. The transformed cells (1mL) were diluted into LB media with ampicillin (5mL). DPhPC liposomes in LB media (2µL of 10mg/mL) were added to the diluted transformed cells (98ul) and many droplets were pipetted under hexadecane. All the droplets were incubated at 37°C and their optical densities were measured at regular intervals using nanodrop spectrophotometer. The stability of bilayer was tested at three different culture densities: (i) low densities ($OD_{600}$ = 0.5), (ii) moderate ($OD_{600}$ = 1.4) and, (iii) high ($OD_{600}$ = 3.0). At these ODs, the droplet was removed from the incubator and suspended on an electrode under an oil-lipid mix (5mg/mL DPhPC in hexadecane). Another LB-droplet was suspended on the other electrode. After the droplets had incubated, they were brought together to initiate bilayer formation. The stability of the droplet was studied at +50mV.

### 5.3.4 Single cell encapsulation in droplets

To encapsulate single cell in 200nL droplets, the transformed cells need to be diluted further. To determine the range of dilution that was likely to result in a single cell per drop, we used two plasmids: EGFP and mCherry. Studies with single cells were carried out using the E.coli strain JM109 (DE3) instead of BL21 (DE3) as mcherry plasmid was not expressing in the BL21 (DE3). Competent cells of E. coli strain JM109 (DE3)

(200µL) were co-transformed with equal amounts of both EGFP and mCherry DNA via a standard heat shock protocol (5 minutes on ice, 30s at 42°C, 2 minutes on ice). The cells were then allowed to recover in antibiotic-free SOC medium (800ul) at 37°C (200rpm shaking) for 2hrs. Post recovery, the transformed cells were diluted (10X to $10^6$X) in kanamycin containing LB medium. For each dilution, I pipetted 2µL droplets into the 96 wells of the microplate. Each well was overlaid with hexadecane to prevent evaporation of the droplets. The plates were incubated at 37°C until they were ready to be read using the microplate reader. The excitation wavelength was 490nm and 580nm for EGFP and m-Cherry respectively. The emission wavelength was 520nm and 640nm for EGFP and m-Cherry respectively. The plates at every dilution were read at both green and red wavelengths.

### 5.3.5 Cloning of EGFP and aHL into pETDuet1

Restriction enzymes for molecular biology were obtained from New England Biolabs (Ipswich, MA, U.S.A.) and the pETDuet-1 vector was obtained from Novagen (Darmstadt, Germany). The α-hemolysin gene cloned in the pT7 plasmid was already available in the Bayley lab. The EGFP gene cloned in pET-9d was a kind gift from Dr. David Dreschel (MPI-CBG, Dresden).

Cloning of EGFP into MCS1: EGFP fragment flanked by BamH1 and SacI was generated by PCR using EGFP-pET9d as the template. The PCR was performed using the Phusion® High-Fidelity PCR Master Mix with HF Buffer (New England Biolabs) as follows:

| | |
|---|---|
| Template EGFP-pET9d DNA | 2.5ul (10ng) |
| PCR Forward Primer EGFP | 1ul of a 50uM stock |
| PCR Reverse Primer EGFP | 1ul of a 50uM stock |
| PCR master mix | 25ul |
| Water | 20.5ul |
| **Total:** | **50ul** |

The thermocycling conditions were:

Initial denaturation: 98°C (10 seconds); 30 cycles: 98°C (1 second), 50°C (5 seconds), 72°C (15 seconds); Extension: 72°C (1 minute).

An overnight ligation reaction between the gel purified BamH1-EGFP-SacI insert and the doubly-cut pETDuet1 vector was set up at 4°C. The ligation reaction was transformed into Novablue cells (50μg/mL ampicillin) and the colonies sequenced.

| | |
|---|---|
| Vector | 9ul |
| Insert | 25ul |
| Ligase buffer(10x) | 5ul |
| T4 ligase | 5ul |
| H20 | 6ul |
| **Total** | **50ul** |

Cloning of αHL into MCS2: αHL gene flanked by Nde1 and XhoI was generated by PCR using WTαHL-pT7 as the template. The PCR was performed using the Phusion® High-Fidelity PCR Master Mix with HF Buffer (New England Biolabs) as follows:

| | |
|---|---|
| Template WTαHL-pT7 DNA | 2.5ul (10ng) |
| PCR Forward Primer αHL | 1ul of a 50uM stock |
| PCR Reverse Primer αHL | 1ul of a 50uM stock |
| PCR master mix | 25ul |
| Water | 20.5ul |
| **Total:** | **50ul** |

The thermocycling conditions were:

Initial denaturation: 98°C (10 seconds); 30 cycles: 98°C (1 second), 50°C (5 seconds), 72°C (15 seconds); Extension: 72°C (1 minute).

An overnight ligation reaction between the gel purified NdeI-αHL-XhoI insert and the doubly-cut EGFP-pETDuet1 vector was set up at 4°C. The ligation reaction was transformed into Novablue cells (50μg/mL ampicillin) and incubated at 37°C till colonies appeared. DNA samples obtained from QIAGEN Plasmid Mini Kit preparations from the colonies were sequenced at the Source BioScience LifeSciences centre, located in the Department of Biochemistry, at the University of Oxford.

| | |
|---|---|
| Vector | 9ul |
| Insert | 25ul |
| Ligase buffer(10x) | 5ul |
| T4 ligase | 5ul |
| H20 | 6ul |
| **Total** | **50ul** |

The αHL-EGFP-pETDuet1 plasmid was sequenced using the recommended primers for pETDuet1. The sequence of the EGFP-αHL-pETDuet1 vector, the primers used for cloning and the primers used for sequencing can be found in the appendix.

### 5.3.6 Cell-Free Coupled in vitro Transcription and Translation (IVTT) of pETDuet1

As a quick test, the EGFP and αHL proteins cloned in the pETDuet1 plasmid were expressed using a cell-free coupled in vitro transcription and translation system (IVTT), using an E. coli T7-S30 extract optimised for circular DNA (Promega no. L1130). The complete 1 mM amino acid mixture (2.5 μL) and premix solution (10 μL) provided with the kit, were mixed with [L-35S] methionine, plasmid DNA (4 μL, 400 ng/μL) and T7-S30 extract (7.5 μL) supplemented with rifampicin and incubated at 37°C for 1 hour. Expressed protein was analysed by SDS PAGE and visualised by exposure to film (Kodak BioMax MR-1).

## 5.4 Bibliography

[1] J. P. John P. Overington, B. Al-Lazikani, and A. L. Hopkins, "How many drug targets are there?," *Nature Reviews Drug Discovery*, vol. 5, pp. 993-996, 2006.

[2] M. E.A., R. R., and B. R.R, "High-Throughput Screening: The Hits and Leads of Drug Discovery- An Overview " *Journal of Applied Pharmaceutical Science*, vol. 01, pp. 02-10, 2011.

[3] G. Maglia, A. J. Heron, W. L. Hwang, M. A. Holden, E. Mikhailova, Q. H. Li, *et al.*, "Droplet networks with incorporated protein diodes show collective properties," *Nature Nanotechnology*, vol. 4, pp. 437-440, Jul 2009.

[4] Y. Astier, D. E. Kainov, H. Bayley, R. Tuma, and S. Howorka, "Stochastic detection of motor protein-RNA complexes by single-channel current recording," *Chemphyschem*, vol. 8, pp. 2189-2194, Oct 2007.

[5] X. F. Kang, S. Cheley, X. Y. Guan, and H. Bayley, "Stochastic detection of enantiomers," *Journal of the American Chemical Society*, vol. 128, pp. 10684-10685, Aug 2006.

[6] O. Braha, B. Walker, S. Cheley, J. J. Kasianowicz, L. Z. Song, J. E. Gouaux, *et al.*, "Designed protein pores as components for biosensors," *Chemistry & Biology*, vol. 4, pp. 497-505, Jul 1997.

[7] L. Q. Gu and H. Bayley, "Interaction of the noncovalent molecular adapter, beta-cyclodextrin, with the staphylococcal alpha-hemolysin pore," *Biophysical Journal*, vol. 79, pp. 1967-1975, Oct 2000.

[8] A. Banerjee, E. Mikhailova, S. Cheley, L. Q. Gu, M. Montoya, Y. Nagaoka, *et al.*, "Molecular bases of cyclodextrin adapter interactions with engineered protein nanopores," *Proceedings of the National Academy of Sciences of the United States of America*, vol. 107, pp. 8165-8170, May 2010.

[9] S. Cheley, L. Q. Gu, and H. Bayley, "Stochastic sensing of nanomolar inositol 1,4,5-trisphosphate with an engineered pore," *Chemistry & Biology*, vol. 9, pp. 829-838, Jul 2002.

[10] S. Cheley, H. Z. Xie, and H. Bayley, "A genetically encoded pore for the stochastic detection of a protein kinase," *Chembiochem*, vol. 7, pp. 1923-1927, Dec 2006.

[11] D. Stoddart, "Progress Towards Ultra-rapid DNA Sequencing with Protein Nanopores," PhD, Chemistry Research Laboratory, University of oxford, Oxford, 2011.

[12] D. Stoddart, A. J. Heron, J. Klingelhoefer, E. Mikhailova, G. Maglia, and H. Bayley, "Nucleobase Recognition in ssDNA at the Central Constriction of the alpha-Hemolysin Pore," *Nano Letters*, vol. 10, pp. 3633-3637, Sep 2010.

[13] D. Stoddart, A. J. Heron, E. Mikhailova, G. Maglia, and H. Bayley, "Single-nucleotide discrimination in immobilized DNA oligonucleotides with a biological nanopore," *PNAS*, vol. 106, pp. 7702-7707, May 2009.

[14] J. Clarke, H. C. Wu, L. Jayasinghe, A. Patel, S. Reid, and H. Bayley, "Continuous base identification for single-molecule nanopore DNA sequencing," *Nature Nanotechnology*, vol. 4, pp. 265-270, Apr 2009.

[15] A. F. Hammerstein, S. H. Shin, and H. Bayley, "Single-Molecule Kinetics of Two-Step Divalent Cation Chelation," *Angewandte Chemie-International Edition*, vol. 49, pp. 5085-5090, 2010.

[16] S. H. Shin, M. B. Steffensen, T. D. W. Claridge, and H. Bayley, "Formation of a chiral center and pyrimidal inversion at the single-molecule level," *Angewandte Chemie-International Edition*, vol. 46, pp. 7412-7416, 2007.

[17] S. R. Lu, W. W. Li, D. Rotem, E. Mikhailova, and H. Bayley, "A primary hydrogen-deuterium isotope effect observed at the single-molecule level," *Nature Chemistry*, vol. 2, pp. 921-928, Nov 2010.

[18] S. H. Shin, T. Luchian, S. Cheley, O. Braha, and H. Bayley, "Kinetics of a reversible covalent-bond-forming reaction observed at the single-molecule level," *Angewandte Chemie-International Edition*, vol. 41, pp. 3707-3709, 2002.

[19] T. Luchian, S. H. Shin, and H. Bayley, "Kinetics of a three-step reaction observed at the single-molecule level," *Angewandte Chemie-International Edition*, vol. 42, pp. 1925-1929, 2003.

[20] J. Dunlop, M. Bowlby, R. Peri, D. Vasilyev, and R. Arias, "High-throughput electrophysiology: an emerging paradigm for ion-channel screening and physiology," *Nature Reviews Drug Discovery*, vol. 7, pp. 358-368, Apr 2008.

[21] K. H. Choi, C. Song, C. S. Cheong, and H. Rhim, "Pharmacological studies of Ca(v)3.1 T-type calcium channels using automated patch-clamp techniques," *General Physiology and Biophysics*, vol. 30, pp. 100-105, Mar 2011.

[22] M. Falconer, F. Smith, S. Surah-Narwal, G. Congrave, Z. Liu, P. Hayter, *et al.*, "High-throughput screening for ion channel modulators," *Journal of Biomolecular Screening*, vol. 7, pp. 460-465, Oct 2002.

[23] I. Kariv, M. E. Stevens, D. L. Behrens, and K. R. Oldenburg, "High throughput quantitation of cAMP production mediated by activation of seven transmembrane domain receptors," Journal of Biomolecular Screening, vol. 4, pp. 27-32, Feb 1999.

[24] J. P. Felix, B. S. Williams, B. T. Priest, R. M. Brochu, I. E. Dick, V. A. Warren, *et al.*, "Functional assay of voltage-gated sodium channels using membrane potential-sensitive dyes," *Assay and Drug Development Technologies*, vol. 2,pp. 260-268, Jun 2004.

[25] C. Joesch, E. Guevarra, S. P. Parel, A. Bergner, P. Zbinden, D. Konrad, *et al.*, "Use of FLIPR membrane potential dyes for validation of high-throughput screening with the FLIPR and mu ARCS technologies: Identification of ion channel modulators acting on the GABA(A) receptor," *Journal of Biomolecular Screening*, vol. 13, pp. 218-228, Mar 2008.

[26] C. D. Weaver, D. Harden, S. I. Dworetzky, B. Robertson, and R. J. Knox, "A thallium-sensitive, fluorescence-based assay for detecting and characterizing potassium channel modulators in mammalian cells," *Journal of Biomolecular Screening*, vol. 9, pp. 671-677, Dec 2004. 198

[27] F. Belardetti, E. Tringham, C. Eduljee, X. P. Jiang, H. H. Dong, A. Hendricson, *et al.*, "A Fluorescence-Based High-Throughput Screening Assay for the Identification of T-Type Calcium Channel Blockers," *Assay and Drug Development Technologies*, vol. 7, pp. 266-280, Jun 2009.

[28] S. Gill, R. Gill, D. Wicks, and D. Liang, "A cell-based Rb+-flux assay of the Kv1.3 potassium channel," *Assay and Drug Development Technologies*, vol. 5, pp. 373-380, Jun 2007.

[29] S. Gill, R. Gill, S. Sen Lee, J. C. Hesketh, D. Fedida, S. Rezazadeh, *et al.*, "Flux assays in high throughput screening of ion channels in drug discovery," *Assay and Drug Development Technologies*, vol. 1, pp. 709-717, Oct 2003.

[30] X. Su, E. W. K. Young, H. A. S. Underkofler, T. J. Kamp, C. T. January, and D. J. Beebe, "Microfluidic Cell Culture and Its Application in High-Throughput Drug Screening: Cardiotoxicity Assay for hERG Channels," *Journal of Biomolecular Screening*, vol. 16, pp. 101-111, Jan 2011.

[31] R. Syeda, M. A. Holden, W. L. Hwang, and H. Bayley, "Screening Blockers Against a Potassium Channel with a Droplet Interface Bilayer Array," *Journal of the American Chemical Society*, vol. 130, pp. 15543-15548, Nov 2008.

[32] M. Kreir, C. Farre, M. Beckler, M. George, and N. Fertig, "Rapid screening of membrane protein activity: electrophysiological analysis of OmpF reconstituted in proteoliposomes," *Lab on a Chip*, vol. 8, pp. 587-595, 2008.

[33] S. Leptihn, J. R. Thompson, J. C. Ellory, S. J. Tucker, and M. I. Wallace, "In Vitro Reconstitution of Eukaryotic Ion Channels Using Droplet Interface

Bilayers," *Journal of the American Chemical Society*, vol. 133, pp. 9370-9375, Jun 2011.

[34] X. Z. Lu, B. Hora, F. P. Cai, and F. Gao, "Generation of random mutant libraries with multiple primers in a single reaction," *Journal of Virological Methods*, vol. 167, pp. 146-151, Aug 2010.

[35] T. W. Wang, H. Zhu, X. Y. Ma, T. Zhang, Y. S. Ma, and D. Z. Wei, "Mutant library construction in directed molecular evolution," *Molecular Biotechnology*, vol. 34, pp. 55-68, Sep 2006.

[36] Y. Yawata, K. Toda, E. Setoyama, J. Fukuda, H. Suzuki, H. Uchiyama, *et al.*, "Bacterial growth monitoring in a microfluidic device by confocal reflection microscopy," *Journal of Bioscience and Bioengineering*, vol. 110, pp. 130-133, Jul 2010.

[37] J. Q. Boedicker, M. E. Vincent, and R. F. Ismagilov, "Microfluidic Confinement of Single Cells of Bacteria in Small Volumes Initiates High-Density Behavior of Quorum Sensing and Growth and Reveals Its Variability," *Angewandte Chemie-International Edition*, vol. 48, pp. 5908-5911, 2009.

[38] S. Moon, E. Ceyhan, U. A. Gurkan, and U. Demirci, "Statistical Modeling of Single Target Cell Encapsulation," *Plos One*, vol. 6, Jul 2011.

[39] S. Koster, F. E. Angile, H. Duan, J. J. Agresti, A. Wintner, C. Schmitz, *et al.*, "Drop-based microfluidic devices for encapsulation of single cells," *Lab on a Chip*, vol. 8, pp. 1110-1115, 2008.

[40] Y. C. Tan, K. Hettiarachchi, M. Siu, and Y. P. Pan, "Controlled microfluidic encapsulation of cells, proteins, and microbeads in lipid vesicles," *Journal of the American Chemical Society*, vol. 128, pp. 5656-5658, May 2006.

[41] E. Um, S. G. Lee, and J. K. Park, "Random breakup of microdroplets for single-cell encapsulation," *Applied Physics Letters*, vol. 97, Oct 2010.

[42] J. F. Edd, D. Di Carlo, K. J. Humphry, S. Koster, D. Irimia, D. A. Weitz, *et al.*, "Controlled encapsulation of single-cells into monodisperse picolitre drops," *Lab on a Chip*, vol. 8, pp. 1262-1264, Aug 2008.

[43] Y. J. Eun, A. S. Utada, M. F. Copeland, S. Takeuchi, and D. B. Weibel, "Encapsulating Bacteria in Agarose Microparticles Using Microfluidics for High-Throughput Cell Analysis and Isolation," *Acs Chemical Biology*, vol. 6, pp. 260-266, Mar 2011.

[44] A. Huebner, M. Srisa-Art, D. Holt, C. Abell, F. Hollfelder, A. J. Demello, *et al.*, "Quantitative detection of protein expression in single cells using droplet microfluidics," *Chemical Communications*, pp. 1218-1220, 2007.

[45] J. U. Shim, L. F. Olguin, G. Whyte, D. Scott, A. Babtie, C. Abell, *et al.*, "Simultaneous Determination of Gene Expression and Enzymatic Activity in Individual Bacterial Cells in Microdroplet Compartments," *Journal of the American Chemical Society*, vol. 131, pp. 15251-15256, Oct 2009.

[46] A. Huebner, D. Bratton, G. Whyte, M. Yang, A. J. deMello, C. Abell, *et al.*, "Static microdroplet arrays: a microfluidic device for droplet trapping, incubation and release for enzymatic and cell-based assays," *Lab on a Chip*, vol. 9, pp. 692-698, 2009.

[47] J. Q. Boedicker, L. Li, T. R. Kline, and R. F. Ismagilov, "Detecting bacteria and determining their susceptibility to antibiotics by stochastic confinement in nanoliter droplets using plug-based microfluidics," *Lab on a Chip*, vol. 8, pp. 1265-1272, Aug 2008.

[48] E. Brouzes, M. Medkova, N. Savenelli, D. Marran, M. Twardowski, J. B. Hutchison, *et al.*, "Droplet microfluidic technology for single-cell high-throughput screening," *Proceedings of the National Academy of Sciences of the United States of America*, vol. 106, pp. 14195-14200, Aug 2009.

[49] M. A. Holden, D. Needham, and H. Bayley, "Functional bionetworks from nanoliter water droplets," *Journal of the American Chemical Society*, vol. 129, pp. 8650-8655, Jul 2007.

[50] B. Cronin, A. Heron, M. A. Holden, W. L. Hwang, R. Syeda, and H. Bayley, "Droplet interface bilayers," *Molecular biosystems*, vol. 4, pp. 1191-208, 2008.

[51] M. A. Borden and M. L. Longo, "Oxygen permeability of fully condensed lipid monolayers," *Journal of Physical Chemistry B*, vol. 108, pp. 6009-6016, May 2004.

[52] G. Pu, M. L. Longo, and M. A. Borden, "Effect of microstructure on molecular oxygen permeation through condensed phospholipid monolayers," *Journal of the American Chemical Society*, vol. 127, pp. 6524-6525, May 2005.

[53] F. A. Henn and T. E. Thompson, "Synthetic lipid bilayer membranes," *Annual Review of Biochemistry*, vol. 38, pp. 241-&, 1969.

[54] S. Kjelleberg and T. A. Stenstrom, "Lipid surface-films - interaction of bacteria with free fatty-acids and phospholipids at the air-water-interface," *Journal of General Microbiology*, vol. 116, pp. 417-423, 1980.

[55] T. C. Marentis, B. Kusler, G. G. Yaralioglu, S. J. Liu, E. O. Haeggstrom, and B. T. Khuri-Yakub, "Microfluidic sonicator for real-time disruption of eukaryotic cells and bacterial spores for DNA analysis," *Ultrasound in Medicine and Biology*, vol. 31, pp. 1265-1277, Sep 2005.

[56] T. Tandiono, D. S. W. Ow, L. Driessen, C. S. H. Chin, E. Klaseboer, A. B. H. Choo, *et al*., "Sonolysis of Escherichia coli and Pichia pastoris in microfluidics," *Lab on a Chip*, vol. 12, pp. 780-786, 2012.

[57] S. S. Yun, S. Y. Yoon, M. K. Song, S. H. Im, S. Kim, J. H. Lee, *et al*., "Handheld mechanical cell lysis chip with ultra-sharp silicon nano-blade arrays for rapid intracellular protein extraction," *Lab on a Chip*, vol. 10, pp. 1442-1446, 2010.

[58] C. Y. Lee, G. B. Lee, J. L. Lin, F. C. Huang, and C. S. Liao, "Integrated microfluidic systems for cell lysis, mixing/pumping and DNA amplification," *Journal of Micromechanics and Microengineering*, vol. 15, pp. 1215-1223, Jun 2005.

[59] L. F. Yu, H. Q. Huang, X. L. Dong, D. P. Wu, J. H. Qin, and B. C. Lin, "Simple, fast and high-throughput single-cell analysis on PDMS microfluidic chips," *Electrophoresis*, vol. 29, pp. 5055-5060, Dec 2008.

[60] S. Movahed and D. Q. Li, "Microfluidics cell electroporation," *Microfluidics and Nanofluidics*, vol. 10, pp. 703-734, Apr 2011.

[61] S. Li, L. H. Xu, H. Hua, C. A. Ren, and Z. L. Lin, "A set of UV-inducible autolytic vectors for high throughput screening," *Journal of Biotechnology*, vol. 127, pp. 647-652, Jan 2007.

[62] Y. A. Vladimirov, T. V. Puchkova, A. V. Putvinsky, and O. M. Parnev, "Electrical stability of artificial membranes," *General Physiology and Biophysics*, vol. 5, pp. 231-242, 1986.

[63] A. Hildebrand, M. Pohl, and S. Bhakdi, "Staphylococcus-aureus alpha-toxin - dual mechanism of binding to target-cells," *Journal of Biological Chemistry*, vol. 266, pp. 17195-17200, Sep 1991.

# Chapter 6

# Final conclusions and future directions

## 6.1 Final conclusions

The work in this thesis was started with the aim to diversify the scope of droplet interface bilayers in studying membrane proteins. The major part of the thesis (Chapters 1-4) focuses on the novel uses of fluorinated amphiphiles in membrane protein studies. Work in these chapters was based on the results of a study carried out by Krafft et al. [1, 2] wherein they showed that due to the enhanced hydrophobicity of fluorinated amphiphiles, even short single chain F-amphiphiles could form lamellar structures (vesicles to extended bilayers) in solution. This led to two very interesting findings of the thesis.

In planar lipid bilayer experiments, the addition of F-amphiphiles above the CMC, led to the arrest in protein insertion into DPhPC bilayers. We found both classes of protein to be similarly affected in presence of F-amphiphiles. We propose that the protein gets sequestered in bilayer aggregates formed by F-amphiphiles, therefore being unavailable for insertion in DPhPC bilayers. This method could prove to be useful in controlling the number of channels in the bilayer in single-molecule experiments.

# CHAPTER 6

Chapter four looked at bilayers formed from F-amphiphiles. Both symmetric fluorinated bilayers and asymmetric fluorinated - DPhPC bilayers could be successfully formed. Due to the instability of symmetric fluorinated bilayers, further studies such as characterization of electrical properties and protein behaviour were carried out with the asymmetric fluorinated – DPhPC bilayers. The asymmetric bilayers showed very interesting properties vis-à-vis asymmetric I-V curves, lower specific capacitances and different behaviour of the truncated α-haemolysin TBMΔ4NN in the bilayer depending on the side of insertion.

Chapter five assessed the feasibility of using DIBs in screening membrane protein libraries and lays the groundwork towards achieving this aim. Results showed that bacterial growth in droplets was compatible with conditions used in droplet bilayer experiments (hexadecane, lipids). We studied bilayer stability in presence of varying densities of bacterial culture and at varying dilutions of detergent lysis reagent. Encapsulating single cells in droplets requires that drops contain at most one cell , so the majority of drops contain no cell at all. This results in a large pool of empty droplets with a few droplets containing the cells expressing the protein of interest. We then generated a plasmid to co-express αHL and the reporter gene EGFP which will enable the selection of occupied droplets from a background of empty droplets. This plasmid containing the EGFP gene can be a good starting point for generating mutants of α-haemolysin for the library.

## 6.2 Future directions

Compared to amphiphiles made from hydrocarbons, fluorinated amphiphiles are relatively new with little known about them. Studies with fluorinated bilayers in this thesis have come up with interesting results, which opens up many interesting avenues to take the project forward. Future work includes more experiments with varied types of F-amphiphiles (longer chain length, double chain, etc.) and validation of experimental results by molecular dynamics and X-ray diffraction. Molecular dynamics simulation of lipid bilayers provides an atomic-level picture of membrane structure and dynamics, and the information from simulation results can be utilized in the interpretation of laboratory experiments. Results from X-ray diffraction and simulation would be able to provide information on the bilayer structure (thickness, packing etc.), the bilayer electrostatic potential, and interactions between protein residues and the fluorocarbon chains of the F-amphiphiles.

Work done in chapter five on single-cell based screening of libraries using droplets can be extended by generating the library containing the mutants and screening it using a microfluidic chip integrated with a microscope. This would allow us to monitor bacterial cell growth in the droplets as well to detect fluorescence from droplets containing expressing cells. It can be hoped that the screening assay will provide a quicker method to identify mutants of interest.

## 6.3 References

[1] M. P. Krafft, F. Giulieri, and J. G. Riess, "Can single-chain perfluoroalkylated amphiphiles alone form vesicles and other organized supramolecular systems," *Angewandte Chemie-International Edition in English*, vol. 32, pp. 741-743, May 1993.

[2] F. Giulieri, M. P. Krafft, and J. G. Riess, "Stable flexible fibers and rigid tubules made from single-chain perfluoroalkylated amphiphiles," *Angewandte Chemie-International Edition in English*, vol. 33, pp. 1514-1515, Aug 1994.

# APPENDIX: Gene Sequences

## 1. EGFP-αHL in pETDuet1 vector

GGGGAATTGTGAGCGGATAACAATTCCCCTCTAGAAATAATTTTGTTTAACTTTAAGAAGGAGATATACCATGGGCA

GCAGCCATCACCATCATCACCACAGCCA**GGATCC**CATGGTGAGCAAGGGCGAGGAGCTGTTCACCGGGGTGGTGCC

CATCCTGGTCGAGCTGGACGGCGACGTAAACGGCCACAAGTTCAGCGTGTCCGGCGAGGGCGAGGGCGATGCCACC

TACGGCAAGCTGACCCTGAAGTTCATCTGCACCACCGGCAAGCTGCCCGTGCCCTGGCCCACCCTCGTGACCACCCT

GACCTACGGCGTGCAGTGCTTCAGCCGCTACCCCGACCACATGAAGCAGCACGACTTCTTCAAGTCCGCCATGCCCG

AAGGCTACGTCCAGGAGCGCACCATCTTCTTCAAGGACGACGGCAACTACAAGACCCGCGCCGAGGTGAAGTTCGA

GGGCGACACCCTGGTGAACCGCATCGAGCTGAAGGGCATCGACTTCAAGGAGGACGGCAACATCCTGGGGCACAAG

CTGGAGTACAACTACAACAGCCACAACGTCTATATCATGGCCGACAAGCAGAAGAACGGCATCAAGGTGAACTTCA

AGATCCGCCACAACATCGAGGACGGCAGCGTGCAGCTCGCCGACCACTACCAGCAGAACACCCCCATCGGCGACGG

CCCCGTGCTGCTGCCCGACAACCACTACCTGAGCACCCAGTCCGCCCTGAGCAAAGACCCCAACGAGAAGCGCGATC

ACATGGTCCTGCTGGAGTTCGTGACCGCCGCCGGGATCACTCTCGGCATGGACGAGCTGTACAAGTAAA**GAGCTC**G

GCGCGCCTGCAGGTCGACAAGCTTGCGGCCGCATAATGCTTAAGTCGAACAGAAAGTAATCGTATTGTACACGGCCG

CATAATCGAAATTAATACGACTCACTATAGGGGAATTGTGAGCGGATAACAATTCCCCATCTTAGTATATTAGTTAA

GTATAAGAAGGAGATATA**CATATG**GCAGATTCTGATATTAATATTAAAACCGGTACTACAGATATTGGAAGCAATAC

TACAGTAAAAACAGGTGATTTAGTCACTTATGATAAAGAAAATGGCATGCACAAAAAAGTATTTTATAGTTTTATCG

ATGATAAAAATCACAATAAAAAACTGCTAGTTATTAGAACAAAAGGTACCATTGCTGGTCAATATAGAGTTTATAGC

GAAGAAGGTGCTAACAAAAGTGGTTTAGCCTGGCCTTCAGCCTTTAAGGTACAGTTGCAACTACCTGATAATGAAGT

AGCTCAAATATCTGATTACTATCCAAGAAATTCGATTGATACAAAAGAGTATATGAGTACTTTAACTTATGGATTCAA

CGGTAATGTTACTGGTGATGATACAGGAAAAATTGGCGGCCTTATTGGTGCAAATGTTTCGATTGGTCATACACTGA

AATATGTTCAACCTGATTTCAAAACAATTTTAGAGAGCCCAACTGATAAAAAAGTAGGCTGGAAAGTGATATTTAAC

AATATGGTGAATCAAAATTGGGGACCATACGATCGAGATTCTTGGAACCCGGTATATGGCAATCAACTTTTCATGAA

AACTAGAAATGGTTCTATGAAAGCAGCAGATAACTTCCTTGATCCTAACAAAGCAAGTTCTCTATTATCTTCAGGGTT

TTCACCAGACTTCGCTACAGTTATTACTATGGATAGAAAAGCATCCAAACAACAAACAAATATAGATGTAATATACG

AACGAGTTCGTGATGATTACCAATTGCATTGGACTTCAACAAATTGGAAAGGTACCAATACTAAAGATAAATGGACA

GATCGTTCTTCAGAAAGATATAAAATCGATTGGGAAAAAGAAGAAATGACAAATTAA**CTCGAG**TCTGGTAAAGAAA

CCGCTGCTGCGAAATTTGAACGCCAGCACATGGACTCGTCTACTAGCGCAGCTTAATTAACCTAGGCTGCTGCCACC

GCTGAGCAATAACTAGCATAACCCCTTGGGGCCTCTAAACGGGTCTTGAGGGGTTTTTTGCTGAAAGGAGGAACTAT

ATCCGGATTGGCGAATGGGACGCGCCCTGTAGCGGCGCATTAAGCGCGGCGGGTGTGGTGGTTACGCGCAGCGTGAC

# APPENDIX

CGCTACACTTGCCAGCGCCCTAGCGCCCGCTCCTTTCGCTTTCTTCCCTTCCTTTCTCGCCACGTTCGCCGGCTTTCCCC

GTCAAGCTCTAAATCGGGGGCTCCCTTTAGGGTTCCGATTTAGTGCTTTACGGCACCTCGACCCCAAAAAACTTGATT

AGGGTGATGGTTCACGTAGTGGGCCATCGCCCTGATAGACGGTTTTTCGCCCTTTGACGTTGGAGTCCACGTTCTTTA

ATAGTGGACTCTTGTTCCAAACTGGAACAACACTCAACCCTATCTCGGTCTATTCTTTTGATTTATAAGGGATTTTGCC

GATTTCGGCCTATTGGTTAAAAAATGAGCTGATTTAACAAAAATTTAACGCGAATTTTAACAAAATATTAACGTTTAC

AATTTCTGGCGGCACGATGGCATGAGATTATCAAAAAGGATCTTCACCTAGATCCTTTTAAATTAAAAATGAAGTTTT

AAATCAATCTAAAGTATATATGAGTAAACTTGGTCTGACAGTTACCAATGCTTAATCAGTGAGGCACCTATCTCAGC

GATCTGTCTATTTCGTTCATCCATAGTTGCCTGACTCCCCGTCGTGTAGATAACTACGATACGGGAGGGCTTACCATC

TGGCCCCAGTGCTGCAATGATACCGCGAGACCCACGCTCACCGGCTCCAGATTTATCAGCAATAAACCAGCCAGCCG

GAAGGGCCGAGCGCAGAAGTGGTCCTGCAACTTTATCCGCCTCCATCCAGTCTATTAATTGTTGCCGGGAAGCTAGA

GTAAGTAGTTCGCCAGTTAATAGTTTGCGCAACGTTGTTGCCATTGCTACAGGCATCGTGGTGTCACGCTCGTCGTTT

GGTATGGCTTCATTCAGCTCCGGTTCCCAACGATCAAGGCGAGTTACATGATCCCCCATGTTGTGCAAAAAAGCGGTT

AGCTCCTTCGGTCCTCCGATCGTTGTCAGAAGTAAGTTGGCCGCAGTGTTATCACTCATGGTTATGGCAGCACTGCAT

AATTCTCTTACTGTCATGCCATCCGTAAGATGCTTTTCTGTGACTGGTGAGTACTCAACCAAGTCATTCTGAGAATAG

TGTATGCGGCGACCGAGTTGCTCTTGCCCGGCGTCAATACGGGATAATACCGCGCCACATAGCAGAACTTTAAAAGT

GCTCATCATTGGAAAACGTTCTTCGGGGCGAAAACTCTCAAGGATCTTACCGCTGTTGAGATCCAGTTCGATGTAACC

CACTCGTGCACCCAACTGATCTTCAGCATCTTTTACTTTCACCAGCGTTTCTGGGTGAGCAAAAACAGGAAGGCAAA

ATGCCGCAAAAAAGGGAATAAGGGCGACACGGAAATGTTGAATACTCATACTCTTCCTTTTTCAATCATGATTGAAG

CATTTATCAGGGTTATTGTCTCATGAGCGGATACATATTTGAATGTATTTAGAAAAATAAACAAATAGGTCATGACCA

AAATCCCTTAACGTGAGTTTTCGTTCCACTGAGCGTCAGACCCCGTAGAAAAGATCAAAGGATCTTCTTGAGATCCTT

TTTTTCTGCGCGTAATCTGCTGCTTGCAAACAAAAAAACCACCGCTACCAGCGGTGGTTTGTTTGCCGGATCAAGAGC

TACCAACTCTTTTTCCGAAGGTAACTGGCTTCAGCAGAGCGCAGATACCAAATACTGTCCTTCTAGTGTAGCCGTAGT

TAGGCCACCACTTCAAGAACTCTGTAGCACCGCCTACATACCTCGCTCTGCTAATCCTGTTACCAGTGGCTGCTGCCA

GTGGCGATAAGTCGTGTCTTACCGGGTTGGACTCAAGACGATAGTTACCGGATAAGGCGCAGCGGTCGGGCTGAACG

GGGGGTTCGTGCACACAGCCCAGCTTGGAGCGAACGACCTACACCGAACTGAGATACCTACAGCGTGAGCTATGAG

AAAGCGCCACGCTTCCCGAAGGGAGAAAGGCGGACAGGTATCCGGTAAGCGGCAGGGTCGGAACAGGAGAGCGCA

CGAGGGAGCTTCCAGGGGGAAACGCCTGGTATCTTTATAGTCCTGTCGGGTTTCGCCACCTCTGACTTGAGCGTCGAT

TTTTGTGATGCTCGTCAGGGGGGCGGAGCCTATGGAAAAACGCCAGCAACGCGGCCTTTTTACGGTTCCTGGCCTTTT

GCTGGCCTTTTGCTCACATGTTCTTTCCTGCGTTATCCCCTGATTCTGTGGATAACCGTATTACCGCCTTTGAGTGAGC

TGATACCGCTCGCCGCAGCCGAACGACCGAGCGCAGCGAGTCAGTGAGCGAGGAAGCGGAAGAGCGCCTGATGCGG

TATTTTCTCCTTACGCATCTGTGCGGTATTTCACACCGCATATATGGTGCACTCTCAGTACAATCTGCTCTGATGCCGC

ATAGTTAAGCCAGTATACACTCCGCTATCGCTACGTGACTGGGTCATGGCTGCGCCCCGACACCCGCCAACACCCGC

TGACGCGCCCTGACGGGCTTGTCTGCTCCCGGCATCCGCTTACAGACAAGCTGTGACCGTCTCCGGGAGCTGCATGTG

TCAGAGGTTTTCACCGTCATCACCGAAACGCGCGAGGCAGCTGCGGTAAAGCTCATCAGCGTGGTCGTGAAGCGATT

CACAGATGTCTGCCTGTTCATCCGCGTCCAGCTCGTTGAGTTTCTCCAGAAGCGTTAATGTCTGGCTTCTGATAAAGC
GGGCCATGTTAAGGGCGGTTTTTTCCTGTTTGGTCACTGATGCCTCCGTGTAAGGGGGATTTCTGTTCATGGGGGTAA
TGATACCGATGAAACGAGAGAGGATGCTCACGATACGGGTTACTGATGATGAACATGCCCGGTTACTGGAACGTTGT
GAGGGTAAACAACTGGCGGTATGGATGCGGCGGGACCAGAGAAAAATCACTCAGGGTCAATGCCAGCGCTTCGTTA
ATACAGATGTAGGTGTTCCACAGGGTAGCCAGCAGCATCCTGCGATGCAGATCCGGAACATAATGGTGCAGGGCGCT
GACTTCCGCGTTTCCAGACTTTACGAAACACGGAAACCGAAGACCATTCATGTTGTTGCTCAGGTCGCAGACGTTTTG
CAGCAGCAGTCGCTTCACGTTCGCTCGCGTATCGGTGATTCATTCTGCTAACCAGTAAGGCAACCCCGCCAGCCTAGC
CGGGTCCTCAACGACAGGAGCACGATCATGCTAGTCATGCCCCGCGCCCACCGGAAGGAGCTGACTGGGTTGAAGG
CTCTCAAGGGCATCGGTCGAGATCCCGGTGCCTAATGAGTGAGCTAACTTACATTAATTGCGTTGCGCTCACTGCCCG
CTTTCCAGTCGGGAAACCTGTCGTGCCAGCTGCATTAATGAATCGGCCAACGCGCGGGGAGAGGCGGTTTGCGTATT
GGGCGCCAGGGTGGTTTTTCTTTTCACCAGTGAGACGGGCAACAGCTGATTGCCCTTCACCGCCTGGCCCTGAGAGA
GTTGCAGCAAGCGGTCCACGCTGGTTTGCCCCAGCAGGCGAAAATCCTGTTTGATGGTGGTTAACGGCGGGATATAA
CATGAGCTGTCTTCGGTATCGTCGTATCCCACTACCGAGATGTCCGCACCAACGCGCAGCCCGGACTCGGTAATGGC
GCGCATTGCGCCCAGCGCCATCTGATCGTTGGCAACCAGCATCGCAGTGGGAACGATGCCCTCATTCAGCATTTGCA
TGGTTTGTTGAAAACCGGACATGGCACTCCAGTCGCCTTCCCGTTCCGCTATCGGCTGAATTTGATTGCGAGTGAGAT
ATTTATGCCAGCCAGCCAGACGCAGACGCGCCGAGACAGAACTTAATGGGCCCGCTAACAGCGCGATTTGCTGGTGA
CCCAATGCGACCAGATGCTCCACGCCCAGTCGCGTACCGTCTTCATGGGAGAAAATAATACTGTTGATGGGTGTCTG
GTCAGAGACATCAAGAAATAACGCCGGAACATTAGTGCAGGCAGCTTCCACAGCAATGGCATCCTGGTCATCCAGCG
GATAGTTAATGATCAGCCCACTGACGCGTTGCGCGAGAAGATTGTGCACCGCCGCTTTACAGGCTTCGACGCCGCTT
CGTTCTACCATCGACACCACCACGCTGGCACCCAGTTGATCGGCGCGAGATTTAATCGCCGCGACAATTTGCGACGG
CGCGTGCAGGGCCAGACTGGAGGTGGCAACGCCAATCAGCAACGACTGTTTGCCCGCCAGTTGTTGTGCCACGCGGT
TGGGAATGTAATTCAGCTCCGCCATCGCCGCTTCCACTTTTTCCCGCGTTTTCGCAGAAACGTGGCTGGCCTGGTTCA
CCACGCGGGAAACGGTCTGATAAGAGACACCGGCATACTCTGCGACATCGTATAACGTTACTGGTTTCACATTCACC
ACCCTGAATTGACTCTCTTCCGGGCGCTATCATGCCATACCGCGAAAGGTTTTGCGCCATTCGATGGTGTCCGGGATC
TCGACGCTCTCCCTTATGCGACTCCTGCATTAGGAAGCAGCCCAGTAGTAGGTTGAGGCCGTTGAGCACCGCCGCCG
CAAGGAATGGTGCATGCAAGGAGATGGCGCCCAACAGTCCCCCGGCCACGGGGCCTGCCACCATACCCACGCCGAA
ACAAGCGCTCATGAGCCCGAAGTGGCGAGCCCGATCTTCCCCATCGGTGATGTCGGCGATATAGGCGCCAGCAACCG
CACCTGTGGCGCCGGTGATGCCGGCCACGATGCGTCCGGCGTAGAGGATCGAGATCGATCTCGATCCCGCGAAATTA
ATACGACTCACTATA

**Note:** EGFP is cloned in MCS1 between BamH1 and SacI sites. WT-αHL is cloned in MCS2 between NdeI and XhoI sites. The cloning sites of MCS1, BamH1 and SacI, are

in red bold type and underlined. The EGFP gene cloned in between these two restriction sites is in green. The cloning sites of MCS2, NdeI and XhoI, are in blue bold type and underlined. The wt-αHL gene cloned in between these two restriction sites is in yellow.

**2. Cloning primers:**

**(i)** PCR Forward Primer EGFP:

5’ –GCGCCGGAGCTCTTTACTTGTACAGCTCG —3’

**(ii)** PCR Reverse Primer EGFP:

5’—ATAATTGGATCCCATGGTGAGCAAGGGCG –3’

**(iii)** PCR Forward Primer αHL:

5’—GCGCCGCATATGGCAGATTCTGATATTAAT—3’

**(iv)** PCR Reverse Primer αHL:

5’— GCCGGCCTCGAGTTAATTTGTCATTTCTTC –3’

**3. Sequencing primers for pETDuet-1**

**(i)** MCS1 Forward Primer:

5'-ATGCGTCCGGCGTAGA-3'

**(ii)** MCS1 Reverse Primer:

5'-GATTATGCGGCCGTGTACAA-3'

**(iii)** MCS2 Forward Primer:

5'-TTGTACACGGCCGCATAATC-3'

**(iv)** MCS2 Reverse Primer:

5'-GCTAGTTATTGCTCAGCGG-3'